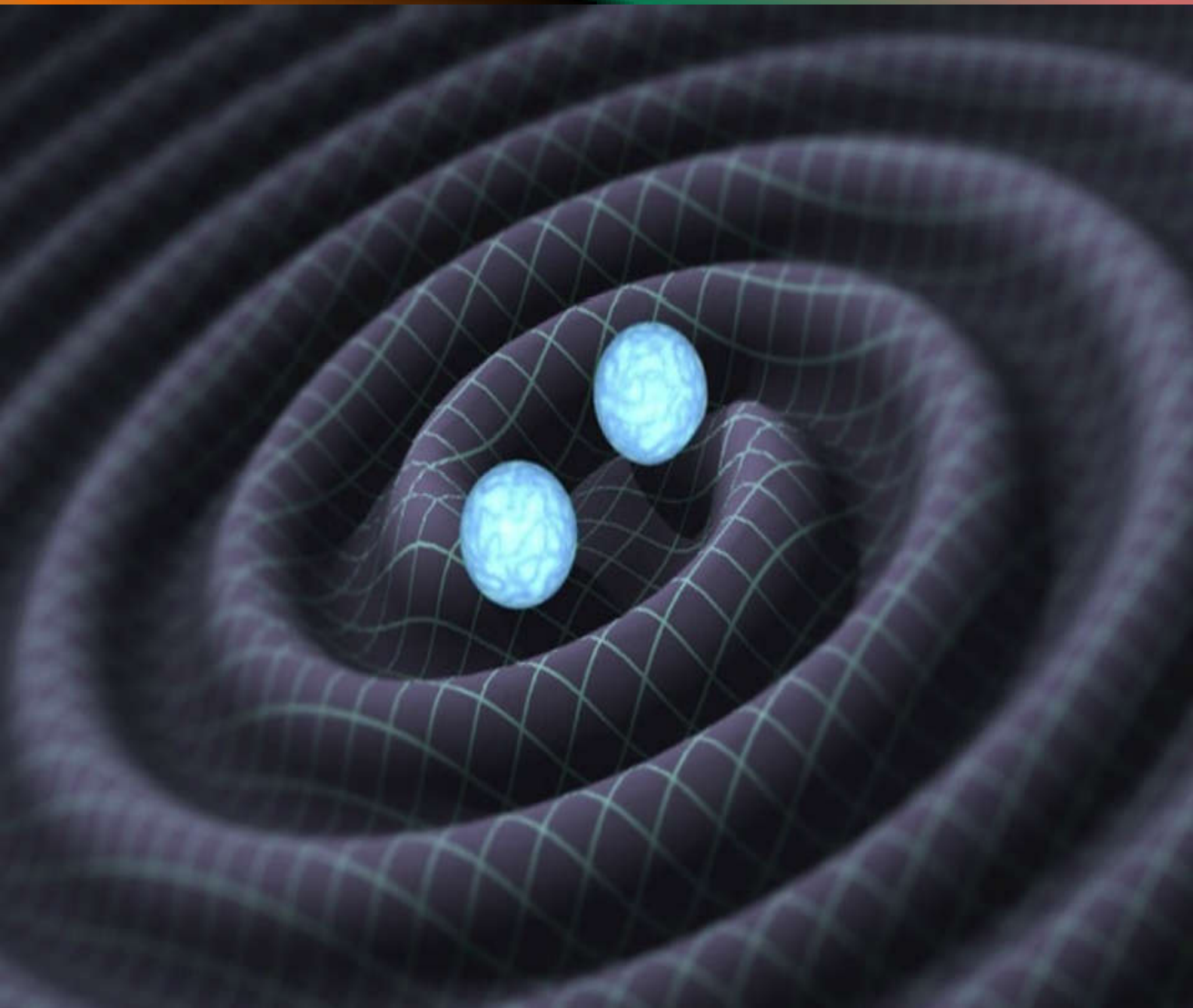


Vol 32 No. 1 Jan - Mar 2016 ISSN 0970-5953



PHYSICS EDUCATION



Gravitational Waves – GW150914

www.physedu.in

Volume 32, Number 1
In this Issue

- **Editorial** 01 page
M. S. Santhanam
- **Scaling Analysis: Size of Lilliputs, Giants and Normal Humans** 08 pages
Debnarayan Jana
- **Graphical Vector Method for Solving Relative Velocity & Dynamics Problems with Causality Visualization** 07 pages
V. Shekoyan, S. Dehipawala, T. Holden, D. Lieberman, and T. Cheung
- **Alternative method for introducing torque and angular momentum** 10 pages
Yukio Kobayashi
- **Rotational motion of a rigid body with the system IP–Coach** 07 pages
Z. Gibová, O. Fričová, M. Kládiová, J. Kecer, M. Hutníková, M. Kovaľáková
- **Reinforcing Harmonic Oscillators in Electrostatics** 04 pages
Michael A. Waxman
- **The Electrodynamics of Charges in Capacitors-Pulley System & Teaching Physics Discovery Lessons** 06 pages
G. Tremberger, Jr., V. Shekoyan, S. Dehipawala, T. Holden, D. Lieberman, and T. Cheung
- **Rutherford's Scattering: A Fortran Simulation** 08 Pages
Antonio Ortiz Castro
- **Nature of Legendre foretold by Pascal** 13 Pages
P. R. Subramanian, B. V. Jenisha, and A. Jestin Lenus
- **Comparative Analysis of M 3 and NGC 2420 using SDSS Data** 15 Pages
Shishir Khandelwal, Saurabh Nangia
- **NIM based muon Telescope – An Educational Experiment for Post Graduate Students** 17 Pages
SNL Sirisha, Kajal Garg, Sonali Bhatnagar
- **Functional differential equations. 6: Quantum Mechanics** 14 Pages
C. K. Raju
- **ANNOUNCEMENT: Gravitational Waves Detected -Laser Interferometric Gravitational Observatory GW150914 Event** 02 Pages
Arvind Gupta

EDITORIAL

From this issue onwards, *Physics Education* will be administered from Indian Institute of Science Education and Research (IISER) Pune. I take this opportunity to thank the preceding editor Prof. Pramod Joag and all the earlier editors who have worked hard to make this journal what it is today. In particular, the enthusiasm shown by Prof. R. Ramachandran, Consulting Editor, in maintaining this journal is noteworthy. I must also thank Savitribhai Phule Pune University for hosting *Physics Education* since its inception. As part of impending changes to be implemented in the next few months, we hope to improve the visibility of the journal by including more sections, more dynamic content that is of interest to physics teachers and students and possibly multimedia content as well.

As always, physics is in for exciting times. The ground breaking observation of gravitational waves reported last month is not really the end of

a rather long search but a beginning of a new tool to observe the universe. We hope ultimately exciting new physics will emerge out of this new tool. The cover page of this issue carries an artist's impression of colliding massive bodies that generated the gravitational waves. We have also provided a pointer to an interesting and simple introduction to gravitational waves through animations by Arvind Gupta and his team from IUCAA Pune. We thank him for the permission to use this material.

We hope you will enjoy reading this issue and count on your continued support.

M. S. Santhanam
Chief Editor
Physics Education

Scaling Analysis: Size of Lilliputs, Giants and Normal Humans

Debnarayan Jana¹

¹Department of Physics
University of Calcutta, 92 A P C Road
Kolkata 700 009, India.
E-mail: djphy@caluniv.ac.in

(Submitted 29-2-2015)

Abstract

In this paper, we would like to illustrate the power of scaling analysis to estimate the order of magnitude of the size of Lilliputs, Giants and Normal humans. We further extend this scaling approach to estimate the typical life span of human being in terms of natural fundamental constants of physics.

1. Introduction

Scaling laws [1-9] are observed in all over science. The simplest is the Kepler's third law seen in the planetary motion governed by Newton's law of gravitation. The square of the time period of revolution of the planets is proportional to the cube of the distance between the planets and the Sun. In fact, there is indeed a deep symmetry between space and time for this particular power law. Considering Newton's inverse square law, we can write down the force equation

$$m \frac{d^2 r}{dt^2} = -\frac{GMm}{r^2} \quad (1)$$

A quick look between the power of space and time ensures that $t^2 \propto r^3$. However, instead of inverse square, for inverse cube law (arises when general theory of relativity is taken into account) gives us $t \propto r^2$.

Assuming earth to be homogeneous sphere of radius R and density ρ , it is easy to notice that the acceleration due to gravity g varies with the variables as

$$g \propto \rho R \quad (2)$$

The important point of the above scaling relation is that it is free from the universal gravitational constant G and can be used in other astrophysical object such as moon. In fact, if we assume further that both earth and moon have the same density, then the ratio of acceleration due to earth's gravity is 3 times larger that due to moon. However, a correct factor of 6 can be visualized if one takes into the correct numerical value of the densities of moon and earth.

Simple spring also satisfies a scaling relation between the time-period T and the mass of the spring m as

$$T \propto \sqrt{\frac{m}{k}} \quad (3)$$

where k is the stiffness constant, The famous Richter scale (1-10) or Marshili scale (1-12) used in the earthquake [9] follows the power law. The probability p for quake releasing energy E due to generation of shock wave is seen to proportional to $E^{-\beta}$, where β is the relevant exponent. It is evident that the above two scales are based on the logarithm of the

energy. Even the recession of speed v of the galaxy at a distance R away from the observer was given by Hubble as $v \propto R^{-1}$.

Mathematically, all these power laws [4,5] can be expressed as

$$Y = f(x) = Cx^\alpha \quad (4)$$

If we scale $x \rightarrow bx$, we get from the above equation that

$$Y(bx) = f(bx) = Cb^\alpha x^\alpha = b^\alpha f(x) \quad (5)$$

The above equation indicates that if we measure x in meters or inches, the form of Y - x relationship remains unchanged. This invariance of scale change justifies the name of scaling relation. In fact, taking the logarithm of both sides of equation (4), we can easily obtain the exponent α from the slope the straight line with log-log axis. Moreover, if the two functions $f(x)$ and $f(y)$ satisfy the following relation

$$f(x)f(y) = f(xy) \quad (6)$$

one can show that the function must be $f(x) \sim x^\lambda$. It is easy to note from equation (6) that

$$y \frac{f'(y)}{f(y)} = x \frac{f'(x)}{f(x)} = \lambda \quad (7)$$

Here, λ is a constant because the LHS is a function of y while the RHS is a function of x only. Naturally, the solution of equation (7) can be easily guessed as $f(x) \sim x^\lambda$. In non-equilibrium as well as equilibrium statistical mechanics, the scaling relation [6-8] can be of the form

$$Y(x, w) = x^\alpha g\left(\frac{w}{x^\beta}\right) \quad (8)$$

Here, the observables Y depends on two parameters x and w . In such a case, one understands the scaling regime $Y \sim x^\alpha$ in the range w is sufficiently small so that $g\left(\frac{w}{x^\beta}\right) \sim g(0)$, a constant. In critical phenomena, the physical quantity at the critical point scales with a power law with anomalous rational exponent [7].

Sometimes, pure dimensional analysis can help one to deduce the scaling relation. For example, the typical phase velocity v of water waves in

shallow water depends on the acceleration due to gravity g , and water depth h . Here, the surface tension and the viscous effects are neglected. A quick straightforward calculation reveals that

$$v = \sqrt{gh} f\left(\frac{h}{\lambda}\right) \quad (9)$$

where λ is the wavelength of the water wave. In the limit, $h \ll \lambda$, $f\left(\frac{h}{\lambda}\right) \rightarrow f(0)$, we find in a

place that the velocity $v \propto \sqrt{h}$, the well-known scaling relation in fluid dynamics.

Even when x is independent of Y , we can regard that as a power law of exponent being zero. In fact from biology, it has been seen that the maximum height of animals scales with size (L) as L^0 . This surprising result [10-13] can be understood physically as follows. The maximum height that an animal can achieve must be proportional to the achievable potential energy divided by its weight. The maximum applied force or the strength of the muscle of animal scale with the characteristic length/ size L of an animal body as L^2 . Therefore, the achievable potential energy will scale as L^3 (Force \times distance). However, the weight of the animal (assuming the density of body remains constant) is proportional to its volume, L^3 . Hence, the height to which an animal can jump turns out to be independent of the size L .

The above scaling behavior can be used in another way. A bone's strength increases as its cross-sectional area while an animal's weight is proportional to its volume, so that to support its own weight an elephant's legs need to be relatively stouter than a dog's. The scaling law is that $w \propto L^{3/2}$, where w is the leg width and L its length.

It is known from biological scaling [13] analysis that the strength of a muscle is proportional to L^2 while the weight of the muscle varies as L^3 . Therefore, the ratio of the strength to weight is

proportional to $\frac{1}{L}$. This result has a remarkable consequence as follows. For example, an elephant bears the ratio as 1 m^{-1} while a tiny flea 1000 m^{-1} . This indicates the impossibility of jumping of an elephant over a flea. Moreover, a flea can support almost 100 times of its body weight while an elephant can something of $\frac{1}{10}$ of its body weight. This is in accord with the fact that the characteristic dimension of an elephant is 1000 times that of a flea.

Scaling analysis along with dimensional analysis can be used to estimate the maximum height [14] of a tree. Each tree is characterized by two different length scales namely the radius and its length or height. In this case one has to compare the two energy scales – namely gravity energy and the elastic one. We know that the typical potential energy of a tree of mass m and height h is simply $E_{grav} \sim mgh = \rho g r^2 h^2$ with r being the radius of the tree. But the elastic energy E_{elast} stored in a tree can be written in terms of elastic modulus as $\frac{Yr^4}{h}$, where Y is the Young's modulus of the material of the tree. Now, for the stability of a tree i.e. no buckling, the condition is $E_{grav} \leq E_{elast}$. Thus, for a given region with the same type of tree, we must have scaling relation with the radius r and the height h as $r^2 \propto h^3$. Thus, for a given radius r , the maximum height of a tree can be estimated as

$$h_{\max} \leq \left(\frac{Y}{\rho g} \right) r^{\frac{2}{3}} \quad (10)$$

In case of a typical length L of an animal, the relation is modified as $r^2 \propto L^3$. Moreover, the mass of an animal scales $M \sim \rho L r^2 = \frac{\rho^2 g}{Y} L^4 \sim L^4$. This eventually gives an important scaling between the mass and length of an animal as $L \sim M^{\frac{1}{4}}$, which is known

as Kleiber's law [13]. Hence, the radius scales simply $r \propto L^{\frac{3}{2}} \propto M^{\frac{3}{8}}$. It is interesting to note that this scaling is quite different from the isometric one where $L \sim M^{\frac{1}{3}}, r \sim M^{\frac{1}{3}}$. This scaling can also be applied to the situation of exhausting to animals for climbing a hill. This is related to the metabolic rate of a typical animal. However, the metabolic rate essentially depends on the flow rate of oxygen. Note that the flow rate of O_2 scales as the surface area of the lungs $\sim M^{\frac{3}{4}}$. Now the comparison of the two energy scales indicates that $Mgh \sim M^{\frac{3}{4}}$ or $h \sim M^{\frac{1}{4}}$. Estimation reveals that it is almost 13 times exhausting for a 1 ton horse than for 30 gm mouse to climb a hill.

The paper is organized as follows. With the brief introduction, we would like to use the scaling analysis for the existence of Lilliput and Giants as depicted in Gullivers' travel book. Finally, in section 3, we point out the order of magnitude of height and life-span of common man in terms of fundamental constants of physics. In section 4, we give our conclusions.

2. Scaling Analysis of Lilliput

To introduce the topic of scaling analysis, let us look at a classical example of the romantic literature, in which Dean Swift, in "The Adventures of Gulliver" describes the imaginary voyages of Lemuel Gulliver to the kingdoms of Lilliput and Brobdingnag. In these two places life was identical to that of normal humans; their geometric dimensions were, however, different. In Lilliput, man, houses, dogs, trees were twelve times smaller than in the country of Gulliver, and in Brobdingnag, everything was twelve times taller. The man of Lilliput was a geometric model of Gulliver in a scale 1:12, and that of Brobdingnag a model in a scale of 12:1.

One can come to interesting observations of these two kingdoms through dimensional analysis. Much time before Dean Swift, Galileus already found out that amplified or reduced models of man could not be like we are. The human body is built of columns, stretchers, bones and muscles. The weight of the body that the structure has to support is proportional to its volume, that is, L^3 , and the resistance of a bone to compression or of a muscle for fraction, is proportional to L^2 .

Let's compare Gulliver with the giant of Brobdingnag, which has all of his linear dimensions twelve times larger.

It is known that a person's food intake capacity is related to his mass (volume). Gulliver was 12 times taller than Lilliputians. Let us assume that the linear dimension of Gulliver be L_G with the volume V_G . Similarly for the Lilliputian, the volume is V_L with L_L be the linear dimension. Then, we can write simply $V_G/V_L=(L_G/L_L)^3=12^3=1728$. Therefore, Gulliver needs the food of 1728 times the amount of food of each as the Lilliputians. This simple problem has a quite good impact in modern days in drug dosage in humans.

The resistance of his legs would be 144 times larger than that of Gulliver, and his weight 1728 times larger. The ratio resistance/weight of the giant would be 12 times less than ours. In order to sustain its own weight, he would have to make an equivalent effort to that we would have to make to carry eleven other men.

Galileus treated this subject very clearly, using arguments that deny the possibility of the existence [6] of giants of normal aspect. If we wanted to have a giant with the same leg/arm proportions of a normal human, we would have to use a stronger and harder material to make the bones, or we would have to admit a lower resistance in comparison to a man of normal stature. On the other hand, if the size of the body would be diminished, the resistance would not diminish in the same proportion. The smaller the body, the greater is its relative resistance. In this way, a very small dog could, probably, carry two

or three other small dogs of his size on his back; on the other hand, an elephant could not carry even another elephant of his own size.

In figure 1, we show the schematic picture from Gullivers' book to compare the typical length scales of a normal human being with Lilliput.

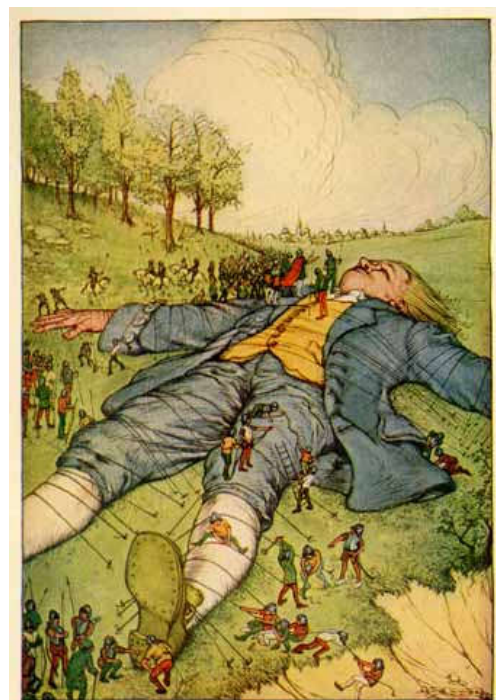


Figure 1: A picture from Gullivers' book

Let's analyze the problem of the Lilliputians from the idea of heat loss. The heat that a body loses to the environment goes through the skin, being proportional to the area covered by the skin, that is, L^2 , maintaining constant the body temperature and skin characteristics. The food taken in must supply this amount of heat. Therefore the minimum food needs should scale as L^2 .

If Gulliver would be happy with a broiler, a bread and a fruit per day, a Lilliputian would need a $(1/12)^2$ smaller food volume. But a broiler, a bread, a fruit when reduced to the scale of his world, would have volumes $(1/12)^3$ smaller. He would, therefore, need twelve broilers, twelve breads and twelve fruits to be as happy as Gulliver. Besides Lilliputians must be hungry enough, famine, restless, active and can become easily water-logged. It is easy to recognize that these properties with many small mammals such as mouse for example. It is interesting to note that there are not many warm-blooded animals smaller than mouse, probably in light of the scale laws discussed above. Notice that in nature, fish, frogs and insects can have much smaller size because of the fact that this digested over a feasible time. Thus, it is clear that

the agriculture of the Lilliputians could not have supported a kingdom like described by Gulliver.

We also illustrate the scale factor from the famous book in Fig.2.

It is also evident from the above scaling arguments that the heat loss/mass is proportional to L^{-1} . In other words, small animals will lose more heat compared to bigger one and naturally, they will not survive in the polar region at that cold atmosphere. Let us give some numerical estimation on mouse and polar bear. Considering a small mouse of length 5 cm, heat loss is of the order of $20 m^{-1}$.

However, polar bear of length 2 m, the heat loss is $0.5 m^{-1}$. Therefore, the ratio of heat loss of mouse to polar bear is $20:0.5=40:1$.

From all the above observations, we come to the following conclusions that, although being geometric models of our world, Brobdingnag and Lilliput could never exist in our physical models, since they would not have the necessary physical similarity which is found in natural phenomena. In the case of Brobdingnag, for example, the giant

body temperature is not higher than their surroundings. As a consequence, large animals by the above scaling law require relatively a good deal of food in compared to smaller creatures to maintain a relatively higher body temperature. In fact, it is indeed very difficult for small animals to gather such an enormous amount of food. Not only that if the foods were collected, that could not be

Therefore, in our earth it is thus impossible for Lilliput to survive with giants as compared to them.

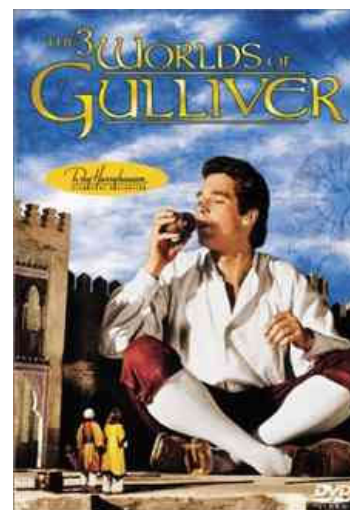


Fig 2. A Picture from the famous book

would be able to support his own weight having the stature of humans, only if he would be living on a planet having a gravitational force of $(1/12)g$.

2.1 Absence of giants of normal size

To argue this, we know that the human body is built of columns, stretchers, bones and muscles. Naturally, the weight [1, 10-12] of the body that the structure has to support is proportional to its volume, L^3 . However, the resistance of a bone to compression or of a muscle for fraction is proportional to L^2 . Therefore, if we wanted to have a giant with the same leg/arm proportions of a normal human being, we would have two options. Either, we must have to use a stronger and harder material to make the bones, or we would have to admit a lower resistance in comparison to a man of

normal stature. If his/her height is proportionally increased, naturally he/she will fall and be crushed completely under his/her own weight. In fact, smaller is the body; greater is its relative strength. On the other hand, if the size of the body is diminished, then, the resistance will not diminish in the same proportion. Therefore, the smaller is the body, the greater its relative resistance. In this way, a very small dog could, probably, carry [2, 10-12] two or three other small dogs of his size on his back. But, an elephant will never be able to carry even another elephant of his own size.

3. Size and life span of a normal man

It is known [10-13] that smaller animals have quick pulse rate and short lives while larger animals have slow pulse rates and long lives. The biological scaling analysis suggests that

$$\begin{aligned} LS &\propto m^{1/4} \propto L^{3/4} \\ HR &\propto m^{-1/4} \propto L^{-3/4} \\ BMR &\propto m^{3/4} \propto L^{9/4} \end{aligned} \quad (11)$$

where LS, HR and BMR refer to life span, heart rate and Basal metabolic rate respectively.

Below we follow an order of magnitude estimation of the size and life span of normal human being in accord with the model developed by William H. Press [15]. In brief, we attempt here to express the characteristic size L_H and life span t_H in terms of natural fundamental constants such as e, \hbar, c, G etc.

It is important to note that this simple estimation however, cannot distinguish between male and female; moreover, since it is based on the scaling arguments, the accuracy level is unable to distinguish between the size of elephant and human being. More, sophisticated model calculations are welcome to match with the experimental data. The model computation however, is based on three fundamental assumptions [15].

- (i) Human being is composed of very complicated molecules.
- (ii) For the survival of human race, it is desirable that the atmosphere should not be primordial or cosmological in nature. This excludes eventually the presence of hydrogen and helium in the atmosphere.
- (iii) Lastly, it is supposed that the height will be sufficiently large to carry its huge (heavy) brain. The person, however, can stumble or fall, but should not break at all by doing so.

With these three assumptions, let us look into the characteristic sizes of atoms, density and the binding energy. We choose the characteristic size

$$\text{of the atom as Bohr's length } a_0 = \frac{\hbar^2}{m_e e^2} = 0.52 \text{ \AA}.$$

This can be justified from simple dimensional analysis and uncertainty principle [14, 16]. If we assume that one proton in a cube of 1 Bohr diameter, the relevant density scale turns out to

$$\text{be } \rho_0 = \frac{m_p}{(2a_0)^3} = 1.44 \text{ g/cc}. \text{ Now, the scale of all}$$

molecular binding energy can be measured in terms of the hydrogen binding energy fixed at

$$E_B = \frac{e^2}{2a_0} = 13.6 \text{ eV}.$$

Now, according to the first assumption, since the involved chemistry of the molecules in human being is complex in nature, we can take the binding energy of these molecules to be a small fraction ($\varepsilon \approx 0.003$) of E_B . This eventually gives an order of magnitude of the environment around the human being as

$$T_{env} = \frac{0.003 \times 13.6}{k_B} \text{ eV} \quad (12)$$

This temperature will naturally provide the perfect environment for continuing the internal chemical processes and hence the survival.

Considering the second assumption, we know that the atmosphere of the human race is neither hydrogen or helium nor vacuum. This is possible if the escape velocity from the surface of the earth is greater than the thermal velocity of hydrogen at T_{env} . Therefore, we must have

$$\frac{GM_E}{R_E} \approx \frac{0.003 \times 13.6}{m_p} \quad (13)$$

and again from density consideration,

$$\frac{M_E}{R_E^3} \approx \frac{m_p}{(2a_0)^3} \quad (14)$$

These two simple equations (13) and (14) can be used to estimate the radius R_E and mass M_E of the earth as

$$\begin{aligned} R_E &= \sqrt{\varepsilon}(2a_0) \sqrt{\frac{e^2}{Gm_p^2}} \\ M_E &= \varepsilon^{3/2} m_p \left(\frac{e^2}{Gm_p^2} \right)^{3/2} \end{aligned} \quad (15)$$

The equation (15) also points out the emergence of a dimensionless constant $\left(\frac{e^2}{Gm_p^2} \right)$ formed from the natural fundamental constants.

Now, if the characteristic size of human being is L_H , then we can estimate its order of magnitude from the mass M_H as

$$M_H \approx \rho_0 L_H^3 \quad (16)$$

The characteristic energy scale of the potential energy of the fall of human being is fixed as

$M_H L_H g = M_H L_H \left(\frac{GM_E}{R_E^2} \right)$. The typical number of atoms N_H in a human being is of the order

$\left(\frac{M_H}{m_p} \right)$. The breaking energy can be fixed at the

scale $\varepsilon \left(\frac{e^2}{2a_0} \right) \left(\frac{M_H}{m_p} \right)^{2/3}$, the last factor originates from the two dimensional surface. Now, considering the third and final assumption, we can write an equation

$$M_H L_H \left(\frac{GM_E}{R_E^2} \right) \approx \varepsilon \left(\frac{e^2}{2a_0} \right) \left(\frac{M_H}{m_p} \right)^{2/3} \quad (17)$$

which after simplification, we obtain the size of the human being as

$$L_H \approx \varepsilon^{1/4} (2a_0) \left(\frac{e^2}{Gm_p^2} \right)^{1/4} \quad (18)$$

The estimated height (2.6 cm) of the human being turns out to be 10^2 smaller than the actual data (180-212 cm) because of the assumption (iii). If one equates the excess breaking energy (which is 10^4 - 10^5 times that used above) to the number of atoms in a protein, one gets a reasonable estimation of the length of the human being.

The life span t_H of a human being can be estimated [15] from the solar radiation in an environment temperature T_{env} in terms of Stefan-Boltzmann

constant $\sigma = \frac{\pi^2 k_B^2}{60 \hbar^2 c^3}$. The life-span or shelter-seeking time can be set if one equates the total energy of chemical bond in human being to the solar flux radiation on human's surface area L_H^2

multiplied by t_H . Thus, we get the desired equation as

$$\begin{aligned} \varepsilon \left(\frac{e^2}{2a_0} \right) &= \sigma \left(\frac{\varepsilon \times e^2}{2a_0 k_B} \right)^4 L_H^2 \times t_H \\ t_H &= \left(\frac{k_B^4}{\sigma} \right) \left(\frac{\rho_0}{m_p} \right) \frac{L_H}{\left(\varepsilon \frac{e^2}{2a_0} \right)^3} \end{aligned} \quad (19)$$

The estimated value (5×10^4 sec) however does not match with the observed data (2.2×10^9 sec).

4. Conclusions

Even within the cutting edge support from the technology, the scaling arguments presented above are quite important. Sometimes, we design a new large object on the basis of knowledge gathered from the small one, we are warned that the new effects may become a serious issue to consider. One cannot just scale up and down blindly, geometrically; but by scaling in the light of physical reasoning, one can predict some new things about the unknown system. Like any other order of magnitude estimation, they are extremely important and helpful to study any physical system. This can in fact serve as a best guide to a detailed analysis of the physical system.

Acknowledgements

The author would like to thank all his undergraduate and postgraduate students for asking several questions during past few years. This article is dedicated to those students who have prompted me to write this work.

References:

- [1] K. Wiesenfeld, *Am. J. Phys.*, **69**, 938 (2001).
- [2] *Physics*, Published by Physical Science Study Committee under NCERT, New Delhi, 1962.
- [3] L. C. Timm, K. Reichardt1 and O. O. S. Bacchi, *Dimensional Analysis, Scaling and Fractals*, (Lecture given at the College on Soil Physics Trieste, 3-21 March 2003, LNS0418035).
- [4] G. I. Barenblatt, *Scaling, Self-Similarity and Intermediate Asymptotics* (Cambridge Press, 1996).
- [5] G. I. Barenblatt, *Scaling* (Cambridge Press, 2003).
- [6] L. P. Kadanoff, *Physica A*, **163**, 1 (1990).
- [7] L. P. Kadanoff, *Scaling and Multiscaling: Fractals and Multifractals in Non-linear Phenomena in Fluids, Solids and other complex systems* edited by P. Cordero and B. Nachtergaele (Elsevier, Amsterdam, 1991).
- [8] M. A. Continentino, *Phys. Rep.*, **239**, 179 (1994).
- [9] T. Nishimura and H. Hamaguchi, *Geophys. Res. Lett.*, **20**, 2479 (1993).
- [10] K. Schmidt-Nielsen, *Scaling: Why is Animal Size So Important?* (Cambridge University Press, Cambridge, 1984).
- [11] R. H. Stinson, *Am. J. Phys.*, **45**, 498 (1977).
- [12] J. Maynard Smith, *Mathematical Ideas in Biology* (Cambridge University Press, Cambridge, 1968).
- [13] G. B. West and J. H. Brow, *Phys Today*, **57**, 36 (2004)
- [14] D. Jana, *Dimensional Analysis: Modern Perspectives* (Lambert Academic Publishing, Germany, 2011).
- [15] W. H. Press, *Am. J. Phys.*, **48**, 597 (1980).
- [16] D. Jana, *Physics Education*, **25**, 35 (2008).

Graphical Vector Method for Solving Relative Velocity & Dynamics Problems with Causality Visualization

V. Shekoyan, S. Dehipawala, T. Holden, D. Lieberman, and T. Cheung

Department of Physics
CUNY Queensborough Community College
Bayside NY 11364, USA.

(Submitted 24-10-2015)

Abstract

A novel graphical vector method in the solving of the standard 2-object with pulley on an incline problem was devised and has been taught in the classroom setting. The case of pulley with inertia would not hinder the presented vector methodology in solving vector equations of motion in dynamics. The delivery plan would first prepare the class to use graphical vector method in solving relative velocity problems without the 90-degree velocity diagram convenience; and the visualization of causality through vector drawing has been emphasized. Good Physics Education delivery would be vital for doing Physics Education Research on the collected student performance data to assess student learning. Physics Education materials in spatial thinking training in relationship to the neuro-science learning research findings is discussed.

1. Introduction

Vector is a capstone concept in Mechanics and is usually taught in a College Physics I course. On the other hand, the 2-object incline plane problem is usually taught using the scalar equations in the x and y coordinates associated with Newton's 2nd Law of motion $F = ma$, which was taught with force and acceleration as vectors. We have developed a set of graphical vector methods for solving these problems and they are presented in this report. The discussed topics include walking map, projectile velocity with gravity puling, relative velocity, forces in equilibrium, 2-object incline problem, rotational problem, and momentum. The goal is to merge vector into a student's mindset and reinforce the causality

relationship. Like most college physics textbooks, the kinematics is a precursor to dynamics with newton's Law of Motion; we have used walking map and velocity vector diagram as preparatory materials for the full use of vector method in dynamics.

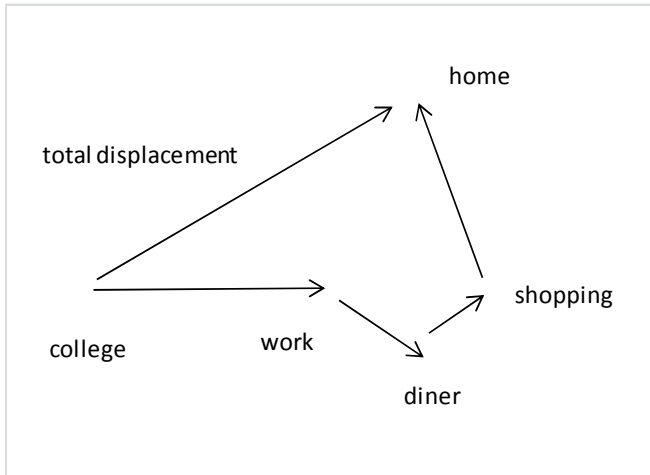


FIG. 1: A schematic view of the walking vectors.

The walking map in Figure 1 is usually a good introduction to the displacement vector concept without much demand on the math pre-requisite. A student would recognize the general polygon with its sides as vectors. The starting point connection to the final destination with an arrow-drawing would be the total displacement vector. When the teaching continues to projectile motion, the Figure 2 illustration could build on Figure 1 visualization with the realization that acceleration*time ($9.8 \text{ m/s}^2 * \text{time}$) is a vector for gravity pulling, which is the cause for the initial velocity v_0 vector to become the final velocity v_f vector.

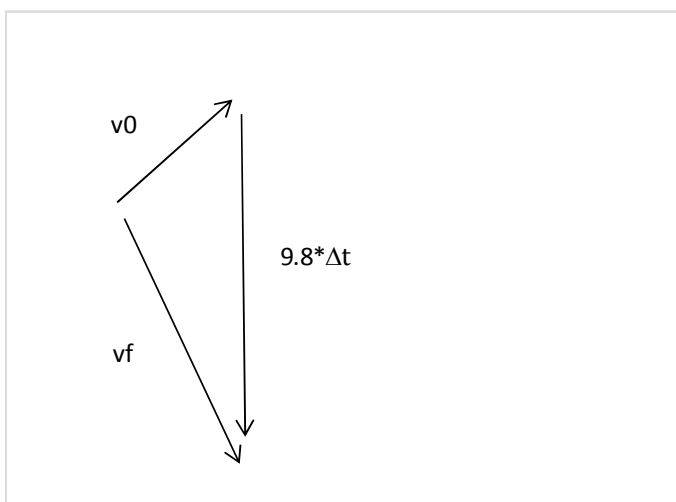


FIG. 2: A schematic view of the projectile velocity vectors.

The use of vector addition in relative velocity problems without the 90-degree velocity diagram convenience would follow, as illustrated in Figure 3. The water current would push the boat off course such that the arrival would be the targeted destination when the boat direction is set properly.

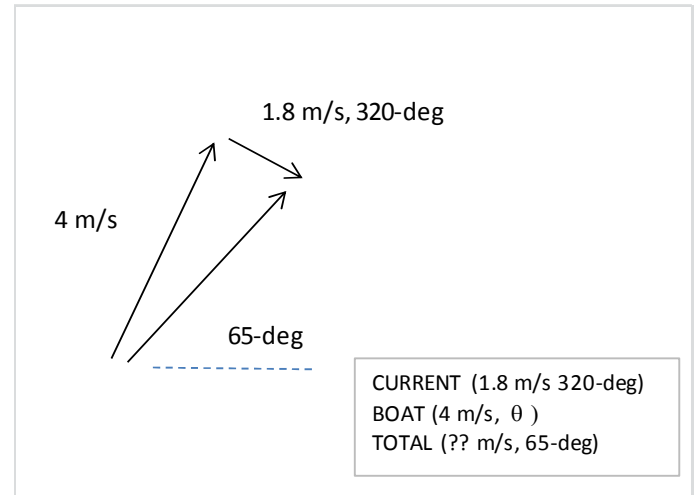


FIG. 3: A schematic view of the velocity vectors.

The graphical vector method would offer not only an easy visualization, but a guaranteed answer within drawing accuracy. The algebra method is not easy for every student as the steps involve trigonometry. In fact our experience showed that only about 30% students in a calculus physics class could solve the associated scalar equations in x and y coordinates within 30 minutes. As for our college physics class designed for the health sciences and pre-med majors, only about 10% could solve the scalar equations involving trigonometry terms. As for our technology physics class designed for students aiming for technician jobs, the percentage would drop to about 2%. But every student would understand the graphical vector solution presented in Figure 4. Here the concept of causality is reinforced because the sketch in Figure 3 dictates that the Boat vector must be drawn from the start-point of Current vector.

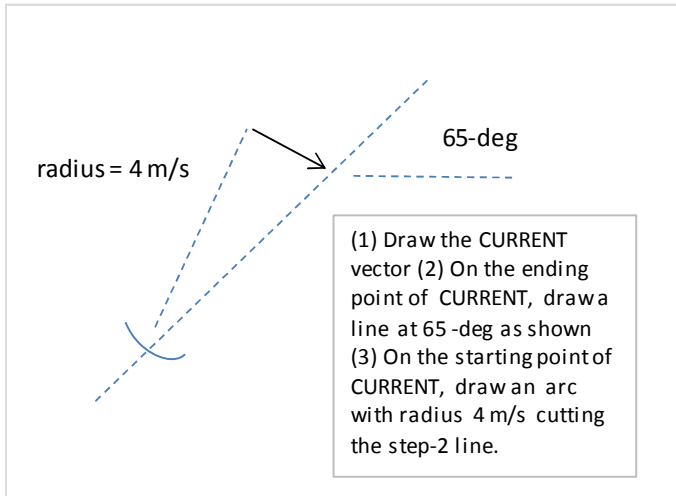


FIG. 4: An illustration of the construction of the velocity vectors in Figure 3..

2. Force Related Problems

The equilibrium condition is a typical problem in Mechanics. Figure 5 displays a situation where a horizontal force is keeping an object at rest on a rough incline plane. The friction could be any value below the maximum allowed by μ , the coefficient of static friction.. There is more than one answer and the problem can be considered as ill-posed. Nevertheless physics is about concept learning, and the fact that there could be several answers would not mean poor teaching technique.

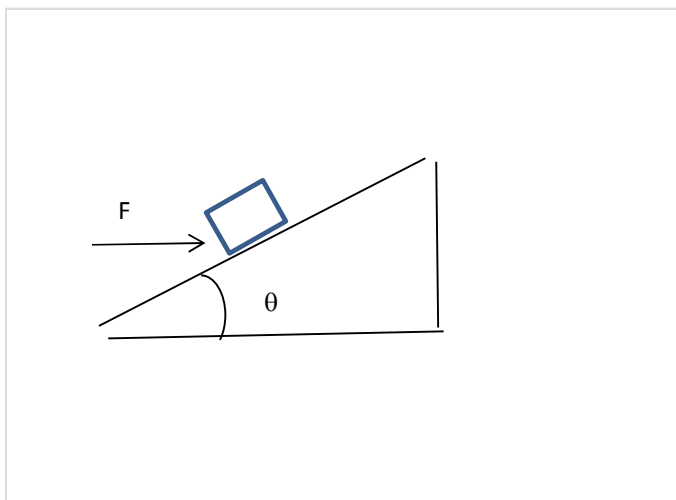


FIG. 5: A schematic view of the applied force.

The forces are shown in Figure 6 and the solution is shown in Figure 7 for the case of maximum horizontal force.

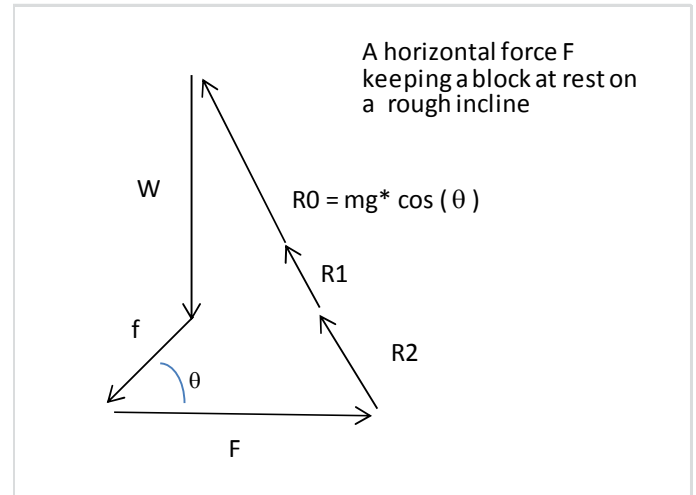


FIG. 6: A schematic view of the force vectors in Figure 5

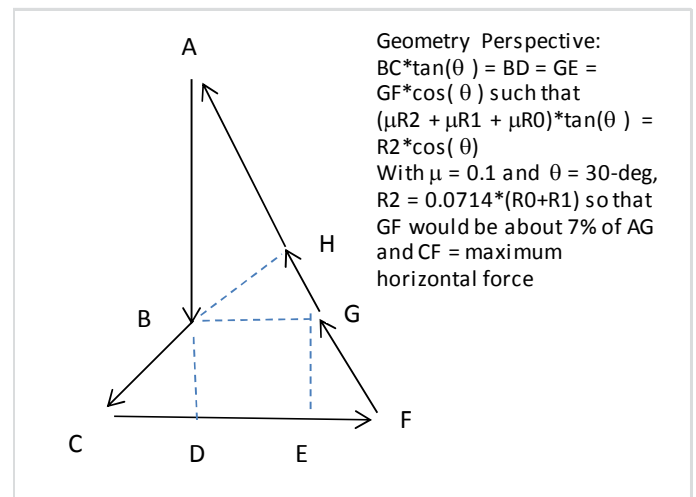


FIG. 7: An illustration of the construction of the force vectors in Figure 6.

The corresponding minimum force situation is shown in Figure 8.

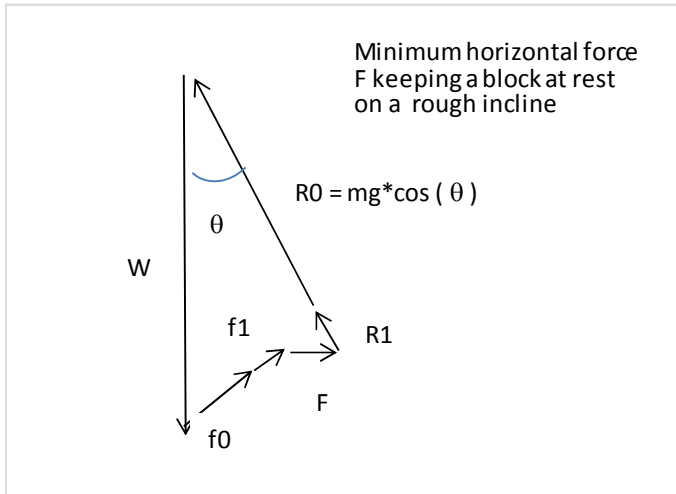


FIG. 8: A schematic view of the force vectors for the minimum horizontal force case where $f_0 = \mu * R_0$ and $f_1 = \mu * R_1$.

The graphical vector method is shown in Figure 9.

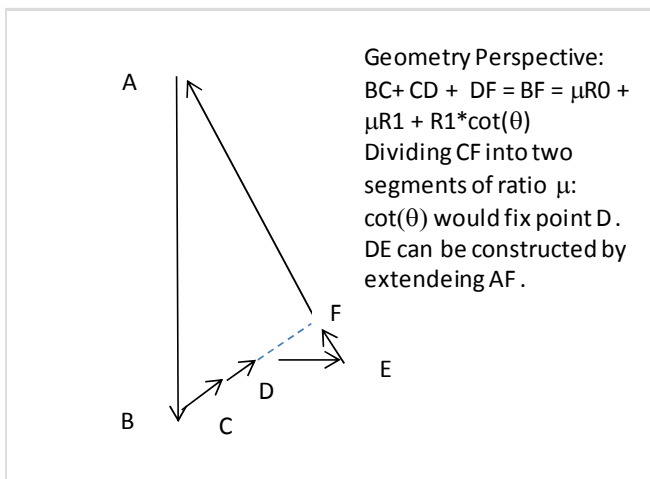


FIG. 9: An illustration of the construction of the force vectors in Figure 8

A standard 2-object on incline problem is shown in Figure 10.

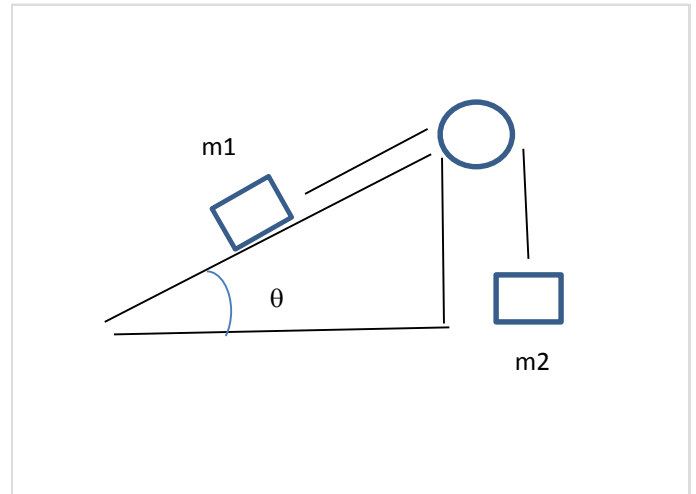


FIG. 10: A schematic view of the 2-object on an incline problem.

The free body force diagrams for the m_2 object driving the acceleration are displayed in Figure 11.

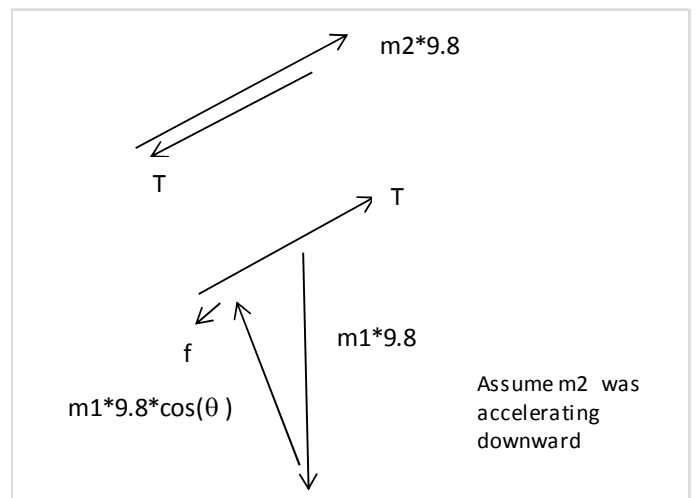


FIG. 11: A schematic view of the force vectors in Figure 10 when the vertically hanging object is dropping..

The graphical solution is displayed in Figure 12. The Segment AC would need to be divided into two portions in a ratio of m_1 to m_2 .

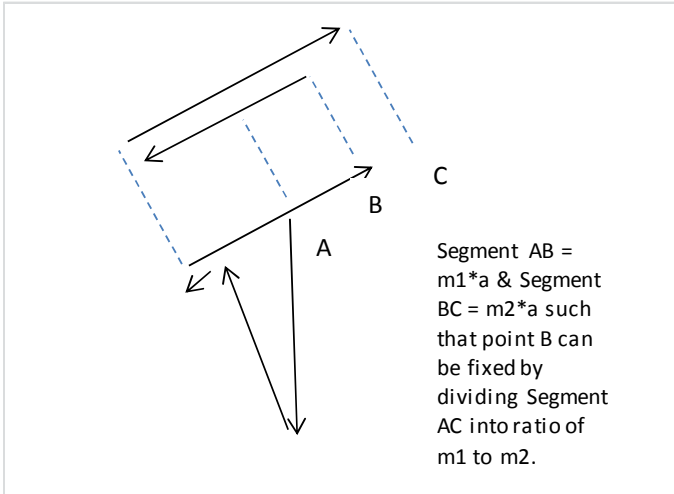


FIG. 12: An illustration of the construction of the force vectors in Figure 11 when the vertically hanging object is dropping.

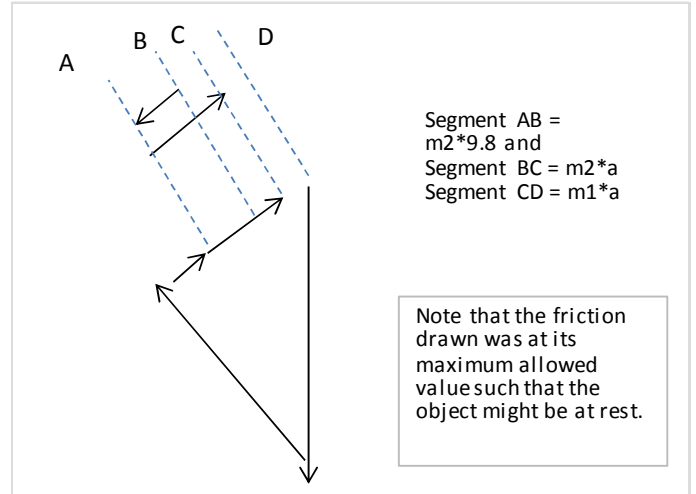


FIG. 14: A An illustration of the construction of the force vectors in Figure 12 when the inclined object is sliding downward..

The free body force diagrams for the m1 object driving the acceleration are displayed in Figure 13.

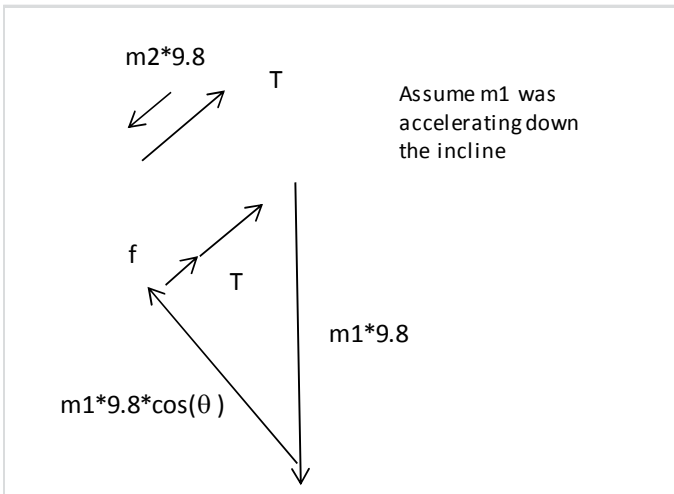


FIG. 13: A schematic view of force vector in Figure 10 when the inclined object is sliding downward.

The graphical solution is displayed in Figure 12. The Segment BD would need to be divided into two portions in a ratio of m2 to m1.

When the pulley has inertia, the free body force diagrams for m1 and m2 is shown in Figure 15, assuming that m2 falling s driving the acceleration. Note that the T1 pulling up the m1 object would be different from the T2 preventing m2 going a free fall.

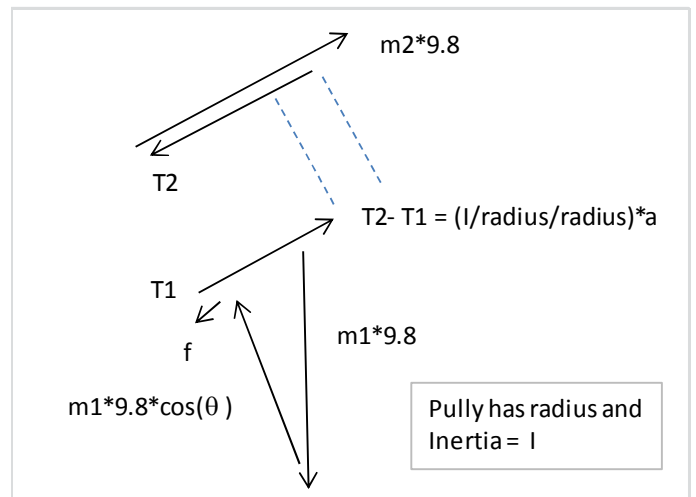


FIG. 15: A schematic view of the force vectors when the pulley has an inertia value.

The graphical solution is displayed in Figure 16. The Segment AD would need to be divided into three portions in the ratio proportion of m1: I/radius/radius: m2.

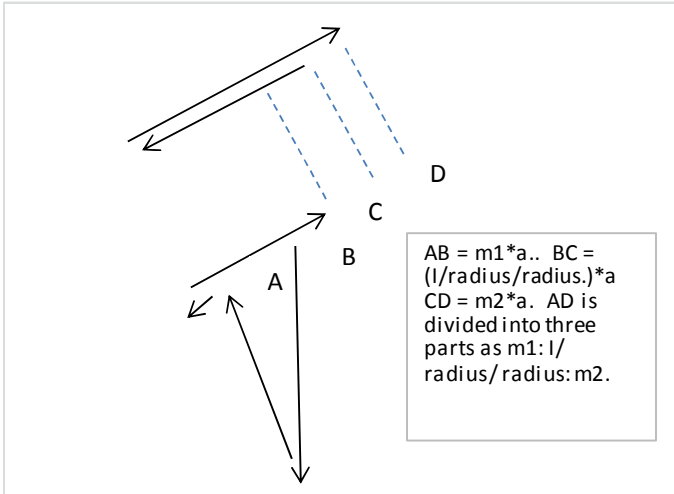


FIG. 16: An illustration of the construction of the force vector when the pulley has an inertia value in Figure 15..

It is interesting to point out that the graphical vector method can also be employed when the torque equation has two different moment-arm distances. A double-pulley with two hanging masses is shown in Figure 17. The torque equation has two forces with two different moment-arm distances.

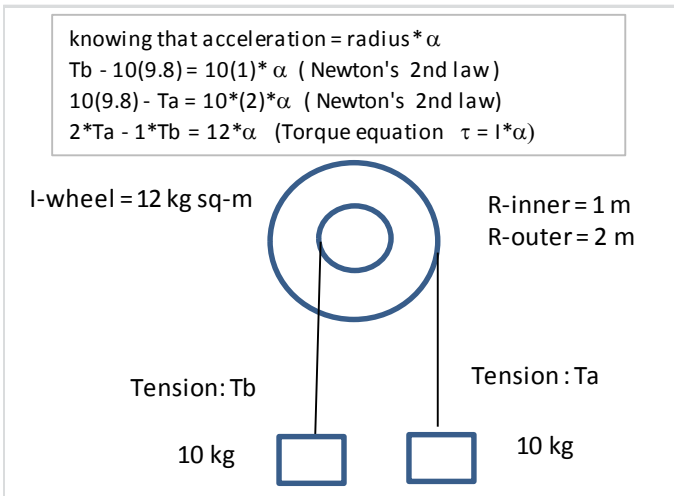


FIG. 17: A schematic view of applied weights on a double-pulley system.

The graphical solution is displayed in Figure 18. Note that the m_2 equation of motion is multiplied by a factor of 2 to facilitate the vector drawing solution.

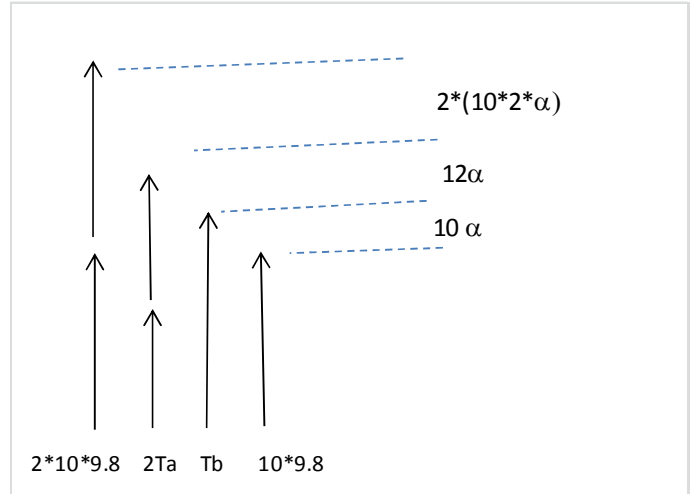


FIG. 18: An illustration of the construction of the force vectors in Figure 17.

The standard two-car intersection collision problem would also carry a graphical vector solution. The total momentum P_{total} would equal to the wreckage momentum $P_{wreckage}$, with no external force or impulse. The students would recognize that each momentum vector has different mass value. This momentum vector diagram echoes the projectile velocity vector diagram shown in Figure 2 where each vector can be multiplied by the projectile mass resulting in a momentum vector diagram. The $mass * 9.8 * \Delta t$ would be the external impulse induced by gravity pulling.

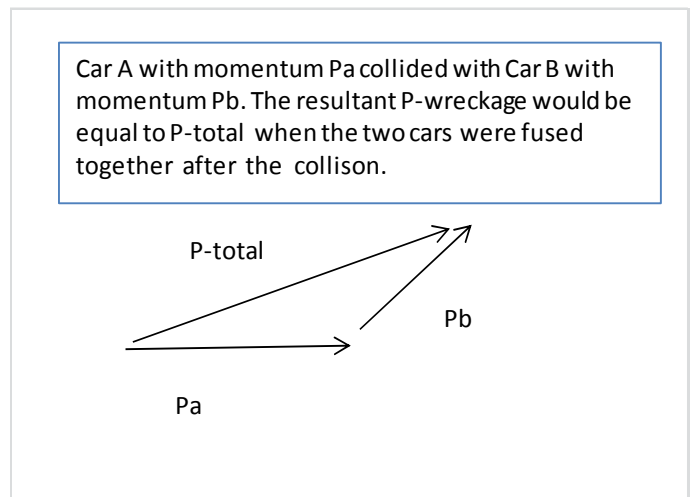


FIG. 19: A schematic view of the momentum vectors in a collision.

3. Discussion

A literature search on vector teaching showed a few references where vectors crossing each other in drawing [1] and would create confusion for below average students in our teaching experience, or no graphical construction method was presented in the writing [2], or the published numerical examples are on single-object situations [3]. Our above examples are aimed to improve vector teaching without lowering the syllabus.

Good Physics Education delivery would be vital for doing productive Physics Education Research with the collected student performance data to assess student learning. The inclusion of the graphical vector methods presented above would be consistent with the vector nature of force as put forward by Newton. A directional change can be visualized easily unlike scalar equation approach in the solving of the vector $F = ma$ equation. Force is the cause and the observed acceleration is the effect. Extension to the impulse vector concept with the knowledge of time duration would help the teaching of momentum as a vector concept in dynamics. In fact, in the teaching of Schrödinger equation in modern physics, a typical course after the first year calculus physics course, the momentum operator is taught readily without any mathematical expression of a quantum force.

A sound collection of physics education materials should also be consistent with neuro-science findings. Handwriting where the letters must be free-form creations of the child herself/himself is an important tool to train a child's brain reading circuit [4], and that motor execution would play an essential part, not perceptual feedback [5]. By the same token, graphical vector drawing could strengthen that part of the brain neural circuit responsible for spatial thinking, a vital aspect of understanding vector in physics. Taking notes on laptops rather than in longhand has been reported as a less efficient method in classroom learning

[6], and the graphical vector method would reinforce learning through tactile practice of drawing and longhand.

4. Conclusions

We have presented a novel graphical vector method in the solving of the standard 2-object on an incline problem. The case of pulley with inertia would not hinder the presented vector methodology in solving vector equations of motion. The graphical vector materials would serve as a platform for physics education research and neuro-science learning research in future studies.

Acknowledgements

The authors thank all those who put their research results on the web for open access. The project was partially supported by several CUNY internal funding sources.

References:

- [1] Alexander S. Kondratyev and Willard Sperry (1994) Direct use of vectors in mechanics problems. *The Physics Teacher* 32, 416
- [2] David Wheeler and Niran Charoenkul (1998). Whole vectors. *The Physics Teacher* 36, 274.
- [3] David Wheeler (2001). Calculations with whole vectors: a really easy alternative to components. *Phys. Educ.* 36 406
- [4] James KH, Engelhardt L, *Trends Neurosci Educ.* 1 (2012) 32-42.
<http://www.ncbi.nlm.nih.gov/pubmed/25541600>
- [5] Kersey AJ, James KH. *Front Psychol.* 4 (2013) Article 567, 1- 16.
<http://www.ncbi.nlm.nih.gov/pubmed/24069007>
- [6] Mueller PA, Oppenheimer DM. *Psychol Sci.* 25 (2014) 1159-1168.
<http://www.ncbi.nlm.nih.gov/pubmed/24760141>

Alternative method for introducing torque and angular momentum

Yukio Kobayashi

Department of Information Systems Science
Faculty of Science and Engineering
Soka University
Tokyo 192 - 8577, Japan.
koba@t.soka.ac.jp

(Submitted 24-10-2015)

Abstract

An alternative method is presented for introducing the physical quantities that are represented by vector products, namely, torque and angular momentum. The basis of the definitions of these quantities becomes evident through this approach. The reason that the position vector of a particle appears in these definitions is also clarified. The present approach can be smoothly integrated into the concepts of generalized forces and coordinates in analytical mechanics.

1 Introduction

Torque is an important physical quantity that arises in regard to the circular motion of a particle and the motion of rigid bodies. Even today, the derivation of the rotational form of Newton's second law from the translational form is discussed in the field of physics edu-

cation [1]. In standard textbooks on classical mechanics [2, 3], however, a convenient vector expression for torque is introduced without explaining the basis of the definition, although the idea of torque is familiar at the undergraduate level. There are two questions that should be addressed from a pedagogical standpoint. Why is the torque vector defined using a position vector that has its origin at

the fulcrum and that points towards the location where the force is applied? How do we understand the circumstances that result in the torque vector being defined as a vector that is orthogonal to both the position and force vectors?

An example [4] of the way in which the concepts of torque and angular momentum are commonly introduced is as follows. First, the torque and angular momentum vectors are defined as the vector products of the position, force, and linear momentum vectors. Suppose a force \mathbf{F} acts on a particle whose position with respect to the origin is the position vector \mathbf{r} . Then, the torque acting on the particle with respect to the origin located at the fulcrum is defined as

$$\mathbf{T} = \mathbf{r} \times \mathbf{F}. \quad (1)$$

Suppose the particle has a linear momentum \mathbf{p} relative to the origin. Then, the angular momentum of the particle is defined as

$$\mathbf{L} = \mathbf{r} \times \mathbf{p}. \quad (2)$$

Using the definitions of torque and angular momentum, the relationship between them can be derived. Starting from the equation of motion

$$\frac{d\mathbf{p}}{dt} = \mathbf{F}, \quad (3)$$

the torque is

$$\mathbf{T} = \mathbf{r} \times \frac{d\mathbf{p}}{dt}. \quad (4)$$

By slightly rearranging this expression, the torque can be expressed as

$$\mathbf{T} = \frac{d\mathbf{L}}{dt}. \quad (5)$$

This method of explaining the relationship between the torque and angular momentum is clear, but no basis is given for why we consider the vector products of the position, force, and linear momentum.

In the present article, we propose an alternative method for introducing torque by letting it develop smoothly from the relationship between the work done by a force and the kinetic energy; this is done by clarifying the basis of the definition of the angular velocity vector. The rate of change of the kinetic energy is familiar to beginning students, although the mathematical treatment of the transformation of the equations is not necessarily simple. The mathematical notes necessary to derive the expressions for torque and angular momentum are good examples for introducing students in advanced classes to vector analysis. Misconceptions about the dynamics of rigid bodies are also discussed using the definition of torque expressed with the position vector.

2 Introducing torque and angular momentum using the relationship between work and kinetic energy

2.1. Basis of vector representation of angular velocity

Suppose the time rate of change of the position vector of a particle is restricted to pure

rotation. The position of the particle is

$$\mathbf{r} = \mathbf{i}x + \mathbf{j}y + \mathbf{k}z$$

in the frame in which the particle is at rest, where x , y , and z are the coordinates of the particle and \mathbf{i} , \mathbf{j} , and \mathbf{k} are the three corresponding orthogonal unit vectors that define the Cartesian coordinate system. These coordinates do not change with time; that is, $dx/dt = 0$, $dy/dt = 0$, and $dz/dt = 0$, and thus

$$\mathbf{v} \equiv \frac{d\mathbf{r}}{dt} = \frac{d\mathbf{i}}{dt}x + \frac{d\mathbf{j}}{dt}y + \frac{d\mathbf{k}}{dt}z.$$

Following a textbook on mechanics [5], $d\mathbf{i}/dt$, $d\mathbf{j}/dt$, and $d\mathbf{k}/dt$ are expressed with the given Cartesian unit vectors. We recall that $\mathbf{i} \cdot \mathbf{i} = 1$, $\mathbf{j} \cdot \mathbf{j} = 1$, and $\mathbf{k} \cdot \mathbf{k} = 1$, and thus

$$\begin{aligned} \mathbf{i} \cdot \frac{d\mathbf{i}}{dt} &= 0, \\ \mathbf{j} \cdot \frac{d\mathbf{j}}{dt} &= 0, \\ \mathbf{k} \cdot \frac{d\mathbf{k}}{dt} &= 0. \end{aligned} \quad (6)$$

These inner products imply

$$\mathbf{i} \perp \frac{d\mathbf{i}}{dt}, \quad \mathbf{j} \perp \frac{d\mathbf{j}}{dt}, \quad \mathbf{k} \perp \frac{d\mathbf{k}}{dt}.$$

Thus, $d\mathbf{i}/dt$, $d\mathbf{j}/dt$, and $d\mathbf{k}/dt$ are in the yz , zx , and xy planes, respectively. We also recall that $\mathbf{i} \cdot \mathbf{j} = 0$, $\mathbf{j} \cdot \mathbf{k} = 0$, and $\mathbf{k} \cdot \mathbf{i} = 0$, and thus

$$\begin{aligned} \frac{d\mathbf{i}}{dt} \cdot \mathbf{j} + \mathbf{i} \cdot \frac{d\mathbf{j}}{dt} &= 0, \\ \frac{d\mathbf{j}}{dt} \cdot \mathbf{k} + \mathbf{j} \cdot \frac{d\mathbf{k}}{dt} &= 0, \\ \frac{d\mathbf{k}}{dt} \cdot \mathbf{i} + \mathbf{k} \cdot \frac{d\mathbf{i}}{dt} &= 0. \end{aligned} \quad (7)$$

Let $d\mathbf{i}/dt$, $d\mathbf{j}/dt$, and $d\mathbf{k}/dt$ be expressed as $\mathbf{j}c_1 + \mathbf{k}c_2$, $\mathbf{k}c_3 + \mathbf{i}c_4$, and $\mathbf{i}c_5 + \mathbf{j}c_6$, respectively, where c_i ($i = 1, 2, \dots, 6$) are undetermined coefficients. Note that these six coefficients are not independent. From

$$\frac{d\mathbf{i}}{dt} \cdot \mathbf{j} = c_1$$

and

$$\mathbf{i} \cdot \frac{d\mathbf{j}}{dt} = c_4,$$

we obtain

$$c_4 = -c_1,$$

because we have

$$\frac{d\mathbf{i}}{dt} \cdot \mathbf{j} = -\mathbf{i} \cdot \frac{d\mathbf{j}}{dt}$$

from Eqs. (7). Similarly,

$$c_5 = -c_2, \quad c_6 = -c_3.$$

We represent c_1 , c_2 , and c_3 as ω_z , $-\omega_y$, and ω_x , respectively, giving

$$\begin{aligned} \frac{d\mathbf{i}}{dt} &= \mathbf{j}\omega_z - \mathbf{k}\omega_y, \\ \frac{d\mathbf{j}}{dt} &= \mathbf{k}\omega_x - \mathbf{i}\omega_z, \\ \frac{d\mathbf{k}}{dt} &= \mathbf{i}\omega_y - \mathbf{j}\omega_x, \end{aligned} \quad (8)$$

and thus we can represent the velocity vector in the form of the vector product

$$\begin{aligned} \mathbf{v} &= \mathbf{i}(\omega_y z - \omega_z y) + \mathbf{j}(\omega_z x - \omega_x z) \\ &\quad + \mathbf{k}(\omega_x y - \omega_y x). \end{aligned} \quad (9)$$

Here, we define a vector $\boldsymbol{\omega}$ whose three components are ω_x , ω_y , and ω_z and call it the angular velocity vector from the standpoint of

its physical meaning. This idea is the basis of the vector product $\mathbf{v} = \boldsymbol{\omega} \times \mathbf{r}$, as follows. The magnitude of the velocity vector $|\mathbf{v}|$ is the product of $|\boldsymbol{\omega}|$ and $|\mathbf{r}|\sin\theta$, where θ is the angle between $\boldsymbol{\omega}$ and \mathbf{r} . The direction of the vector $\boldsymbol{\omega}$ is along the instantaneous axis of rotation, and $|\mathbf{r}|\sin\theta$ is the radius of a circle in the plane perpendicular to $\boldsymbol{\omega}$ (see Appendix).

2.2. Basis of definitions of torque and angular momentum

Based on the above preliminaries, we can consider the rate of change of the kinetic energy for a particle. Differentiating the kinetic energy gives

$$\begin{aligned} \frac{d}{dt} \left(\frac{1}{2} m |\mathbf{v}|^2 \right) &= \frac{d}{dt} \left(\frac{1}{2} m \mathbf{v} \cdot \mathbf{v} \right) \\ &= \mathbf{v} \cdot m \frac{d\mathbf{v}}{dt}, \end{aligned}$$

where m is the mass of the particle. Suppose a net external force \mathbf{F} acts on the particle. From Newton's second law, the equation of motion is

$$m \frac{d\mathbf{v}}{dt} = \mathbf{F},$$

where $\mathbf{F} = iF_x + jF_y + kF_z$. From Eqs. (8), we have

$$\begin{aligned} \frac{d\mathbf{i}}{dt} \cdot \mathbf{j} &= \omega_z, \\ \frac{d\mathbf{j}}{dt} \cdot \mathbf{k} &= \omega_x, \\ \frac{d\mathbf{k}}{dt} \cdot \mathbf{i} &= \omega_y, \end{aligned}$$

and thus we can write

$$\mathbf{v} \cdot m \frac{d\mathbf{v}}{dt}$$

$$\begin{aligned} &= \left(\frac{d\mathbf{i}}{dt} x + \frac{d\mathbf{j}}{dt} y + \frac{d\mathbf{k}}{dt} z \right) \cdot (iF_x + jF_y + kF_z) \\ &= \frac{d\mathbf{i}}{dt} \cdot \mathbf{i} xF_x + \frac{d\mathbf{i}}{dt} \cdot \mathbf{j} xF_y + \frac{d\mathbf{i}}{dt} \cdot \mathbf{k} xF_z \\ &\quad + \frac{d\mathbf{j}}{dt} \cdot \mathbf{i} yF_x + \frac{d\mathbf{j}}{dt} \cdot \mathbf{j} yF_y + \frac{d\mathbf{j}}{dt} \cdot \mathbf{k} yF_z \\ &\quad + \frac{d\mathbf{k}}{dt} \cdot \mathbf{i} zF_x + \frac{d\mathbf{k}}{dt} \cdot \mathbf{j} zF_y + \frac{d\mathbf{k}}{dt} \cdot \mathbf{k} zF_z \\ &= \frac{d\mathbf{i}}{dt} \cdot \mathbf{j} (xF_y - yF_x) + \frac{d\mathbf{j}}{dt} \cdot \mathbf{k} (yF_z - zF_y) \\ &\quad + \frac{d\mathbf{k}}{dt} \cdot \mathbf{i} (zF_x - xF_z) \\ &= (yF_z - zF_y) \omega_x + (zF_x - xF_z) \omega_y \\ &\quad + (xF_y - yF_x) \omega_z \\ &= (\mathbf{r} \times \mathbf{F}) \cdot \boldsymbol{\omega}. \end{aligned} \tag{10}$$

This result means that the change in kinetic energy, $\frac{d}{dt} \left(\frac{1}{2} m |\mathbf{v}|^2 \right)$, is caused by $(\mathbf{r} \times \mathbf{F}) \cdot \boldsymbol{\omega}$, and thus this inner product indicates the work done on the particle. The vector product $\mathbf{r} \times \mathbf{F}$ is a measure of how much a net external force acting on a particle causes that particle to rotate, so we call this vector product the torque.

The same result can also be confirmed in the following way. For simplicity, we assume that $\boldsymbol{\omega}$ is constant. Differentiating the kinetic energy yields

$$\begin{aligned} \frac{d}{dt} \left(\frac{1}{2} m |\mathbf{v}|^2 \right) &= \frac{d}{dt} \left(\frac{1}{2} m \mathbf{v} \cdot \mathbf{v} \right) \\ &= \frac{d}{dt} \left[\frac{1}{2} m (\boldsymbol{\omega} \times \mathbf{r}) \cdot \mathbf{v} \right] \\ &= \frac{d}{dt} \frac{1}{2} m [(\omega_y z - \omega_z y) v_x + (\omega_z x - \omega_x z) v_y \\ &\quad + (\omega_x y - \omega_y x) v_z] \\ &= (\omega_y v_z - \omega_z v_y) m v_x + (\omega_z v_x - \omega_x v_z) m v_y \end{aligned}$$

$$\begin{aligned}
& + (\omega_x v_y - \omega_y v_x) m v_z \\
& + (\omega_y z - \omega_z y) m \frac{dv_x}{dt} \\
& + (\omega_z x - \omega_x z) m \frac{dv_y}{dt} \\
& + (\omega_x y - \omega_y x) m \frac{dv_z}{dt} \\
= & (\omega_y z - \omega_z y) F_x + (\omega_z x - \omega_x z) F_y \\
& + (\omega_x y - \omega_y x) F_z, \\
= & (\boldsymbol{\omega} \times \mathbf{r}) \cdot \mathbf{F} \\
= & \mathbf{v} \cdot \mathbf{F},
\end{aligned}
\tag{11}$$

$$\begin{aligned}
& = \left[\frac{d}{dt} (y p_z - z p_y) \right] \omega_x \\
& + \left[\frac{d}{dt} (z p_x - x p_z) \right] \omega_y \\
& + \left[\frac{d}{dt} (x p_y - y p_x) \right] \omega_z \\
= & \left[\frac{d}{dt} (\mathbf{r} \times \mathbf{p}) \right] \cdot \boldsymbol{\omega}.
\end{aligned}
\tag{12}$$

By comparing $[d(\mathbf{r} \times \mathbf{p})/dt] \cdot \boldsymbol{\omega}$ in Eq. (12) with $(\mathbf{r} \times \mathbf{F}) \cdot \boldsymbol{\omega}$ transformed from Eq. (11), we obtain

$$\frac{d}{dt}(\mathbf{r} \times \mathbf{p}) = \mathbf{r} \times \mathbf{F},$$

which indicates the rate at which work is done. To express a measure of the amount of rotation and the tendency of a force to rotate a particle about an axis, the power expressed by Eq. (11) can be transformed into

$$\begin{aligned}
& (y F_z - z F_y) \omega_x + (z F_x - x F_z) \omega_y \\
& + (x F_y - y F_x) \omega_z \\
= & (\mathbf{r} \times \mathbf{F}) \cdot \boldsymbol{\omega}.
\end{aligned}$$

We recall that $p_x = m v_x$, $p_y = m v_y$, and $p_z = m v_z$, so the rate of change of kinetic energy can be expressed as

$$\begin{aligned}
& (\omega_y z - \omega_z y) m \frac{dv_x}{dt} \\
& + (\omega_z x - \omega_x z) m \frac{dv_y}{dt} \\
& + (\omega_x y - \omega_y x) m \frac{dv_z}{dt} \\
= & \left(y \frac{dp_z}{dt} - z \frac{dp_y}{dt} \right) \omega_x \\
& + \left(z \frac{dp_x}{dt} - x \frac{dp_z}{dt} \right) \omega_y \\
& + \left(x \frac{dp_y}{dt} - y \frac{dp_x}{dt} \right) \omega_z
\end{aligned}$$

which is the same as Eq. (5). The physical quantity $\mathbf{r} \times \mathbf{p}$ is a measure of the amount of rotation, so we call this vector product the angular momentum. This relationship indicates that the rate of change of the angular momentum is equal to the torque.

If students are familiar with the scalar triple product, the above results can be derived from $(\mathbf{r} \times \mathbf{F}) \cdot \boldsymbol{\omega} = (\boldsymbol{\omega} \times \mathbf{r}) \cdot \mathbf{F}$ and $(\mathbf{r} \times \mathbf{p}) \cdot \boldsymbol{\omega} = (\boldsymbol{\omega} \times \mathbf{r}) \cdot \mathbf{p}$, which means that the dot and cross products in the scalar triple product may be interchanged without altering the value of the product. Pedagogically, it is important for beginning students to rearrange the equation without relying on the formulae.

From the point of view of analytical mechanics, we can understand the introductory remarks by Feynman [7], which are based on an analogy between linear and angular quantities. The definition of work as the force times the displacement is thus readily converted to the torque times the rotational an-

gle. Suppose that a force is applied to a particle at a certain point (x, y) in the xy plane, and the particle rotates by a very small angle $\Delta\theta$ in this plane. Slightly rearranging the expression of the work $F_x\Delta x + F_y\Delta y$ yields $(xF_y - yF_x)\Delta\theta$, where Δx and Δy are the change in x and y , respectively, because $\Delta x = -y\Delta\theta$ and $\Delta y = +x\Delta\theta$ [7] by reference to the kinematics of two-dimensional rotation. The generalized force is the coefficient of the variation of a generalized coordinate in the formulation of virtual work. By replacing the changes Δx , Δy , and $\Delta\theta$ by the virtual displacements, δx , δy , and $\delta\theta$, $xF_y - yF_x$ and θ can be regarded as the generalized force and the generalized coordinate, respectively. The generalized force in this motion is a kind of rotational force called torque.

The main results of the process described above are summarized as follows. A pedagogical framework of elementary mechanics can be developed from temporal and spatial viewpoints [6].

1. From a spatial viewpoint, the change in the kinetic energy of a rotating particle is caused by the total work done on that particle by all the torques that act on it during the process of rotation. In the simple case of rotation in the xy plane, this theorem can be expressed as

$$d\left(\frac{1}{2}m|\mathbf{v}|^2\right) = \mathbf{T} \cdot \mathbf{k}d\theta,$$

where $\boldsymbol{\omega}$ is along the z -axis and can be represented as $(d\theta/dt)\mathbf{k}$.

2. From a temporal viewpoint, the change in the angular momentum of a rotating particle is caused by the total impulse of all the

torques that act on it during the process of rotation:

$$d(\mathbf{r} \times \mathbf{p}) = \mathbf{T}dt,$$

where $\mathbf{T}dt$ is the vector product of \mathbf{r} and $\mathbf{F}dt$.

We can develop a framework of elementary mechanics from these temporal and spatial viewpoints [6]. There are three alternatives to the equation of motion that can act as starting points for elucidating mechanical phenomena: (1) The change in the linear momentum of a particle is caused by an impulse. (2) The change in the kinetic energy of a particle is caused by the work done on that particle by an applied force. (3) The change in the angular momentum of a particle is caused by torque. Of these three propositions, (2) is a theorem common to both translational and rotational motion. We can consider that these three propositions result in the equation of motion. From this standpoint, we have introduced the concept of torque to describe rotational motion by (2) in the present article. Temporal and spatial viewpoints are two perspectives on the same physical phenomenon. Thus, we can translate between (1) and (3) for translational motion and between (2) and (3) for rotational motion. In this sense, we can say that (3) has been translated from (2) in the present article.

3 Misconceptions about the dynamics of rigid bodies

Unexpectedly, in the field of mechanical engineering, there are misconceptions about the

definitions of torque and angular momentum. From this fact, we expect similar misconceptions are found in college physics, and thus we consider the following example. By gaining an understanding of this issue, beginning students can improve their ability to find misconceptions and to correct them.

According to commentary [8] on the free rotation of rigid bodies, the definitions of torque and angular momentum as the vector products of the position vector of the particle relative to the origin, the net external force on that particle, and the linear momentum vector of the particle are not correct, because the origin is considered, but the axis of rotation is not. This commentary claims that the definitions of torque and angular momentum are the distance from the axis of rotation times the transverse components of force and linear momentum, respectively.

The above interpretation contains a misunderstanding. The commentary [8] confuses the definitions of torque and moment of inertia. Beginning students may also share this misunderstanding. We can explain the circumstances through a simple example. Suppose that a thin slab lies in the xy plane and rotates about the z -axis with an angular velocity vector ω in the z -direction (Figure 1). For the present purpose, it is convenient to use a cylindrical coordinate system (Figure 2). The position vector r_i for the mass element m_i can be expressed as

$$\mathbf{r}_i = \hat{\rho}_i \rho_i + \mathbf{k} z_i, \quad (13)$$

where $\hat{\rho}_i$ is a unit vector perpendicular to the z -axis and defined by coordinates ρ_i and φ_i ,

and the relationships between the cylindrical coordinates ρ_i , φ_i , and z_i , and the Cartesian coordinates are given by $x_i = \rho_i \cos \varphi_i$, $y_i = \rho_i \sin \varphi_i$, and $z_i = z_i$.

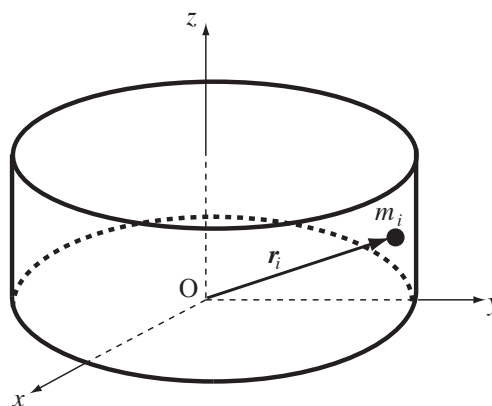


Figure 1. Mass element of a slab.

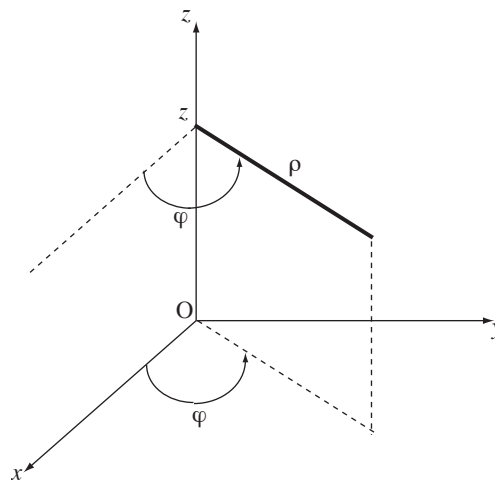


Figure 2. Cylindrical coordinate system.

For the relationships between the Cartesian and cylindrical unit vectors, we have

$$\hat{\rho}_i = \mathbf{i} \cos \varphi_i + \mathbf{j} \sin \varphi_i, \quad (14)$$

$$\begin{aligned} \hat{\varphi}_i &= \mathbf{i} \cos \left(\varphi_i + \frac{\pi}{2} \right) + \mathbf{j} \sin \left(\varphi_i + \frac{\pi}{2} \right) \\ &= -\mathbf{i} \sin \varphi_i + \mathbf{j} \cos \varphi_i, \end{aligned} \quad (15)$$

and thus

$$\begin{aligned} \frac{d\hat{\rho}_i}{dt} &= (-\mathbf{i} \sin \varphi_i + \mathbf{j} \cos \varphi_i) \frac{d\varphi_i}{dt} \\ &= \hat{\varphi}_i \frac{d\varphi_i}{dt}. \end{aligned} \quad (16)$$

The height of the slab is constant, because the slab lies in the xy plane, and thus $dz_i/dt = 0$ for mass element m_i . The radius of rotation ρ_i is also constant, because the slab is a rigid body in which deformation is neglected, and thus the distance between any two points on the slab remains constant in time regardless of the external forces exerted on the slab. The angular velocity is common for all mass elements, so $d\varphi_i/dt = \omega$, where ω is the magnitude of $\boldsymbol{\omega}$. From Eq. (16), the velocity vector of mass element m_i is

$$\begin{aligned} \mathbf{v}_i &\equiv \frac{d\mathbf{r}_i}{dt} \\ &= \rho_i \frac{d\hat{\rho}_i}{dt} \\ &= \hat{\varphi}_i \rho_i \frac{d\varphi_i}{dt} \\ &= \hat{\varphi}_i \rho_i \omega, \end{aligned} \quad (17)$$

where $\hat{\varphi}_i$ is a unit vector perpendicular to $\hat{\rho}_i$. By reference to $\hat{\rho}_i \times \hat{\varphi}_i = \mathbf{k}$ and $\mathbf{k} \times \hat{\varphi}_i = -\hat{\rho}_i$ obtained from Eqs. (14) and (15), we can calculate the angular momentum \mathbf{L}_i for mass

element m_i . Thus, from Eqs. (13) and (17), we have

$$\begin{aligned} \mathbf{L}_i &\equiv \mathbf{r}_i \times m_i \mathbf{v}_i \\ &= (\hat{\rho}_i \rho_i + \mathbf{k} z_i) \times \hat{\varphi}_i m_i \rho_i \omega \\ &= \mathbf{k} m_i \rho_i^2 \omega - \hat{\varphi}_i m_i \rho_i z_i \omega. \end{aligned}$$

We sum over all elements, and the angular momentum for the slab is then

$$\begin{aligned} \mathbf{L} &= \sum_i \mathbf{L}_i \\ &= \mathbf{k} \left(\sum_i m_i \rho_i^2 \right) \omega \\ &\quad - \left(\sum_i \hat{\varphi}_i m_i \rho_i z_i \right) \omega \\ &= \mathbf{k} I_z \omega, \end{aligned}$$

where, in the first term, we have defined the physical quantity I_z , called the moment of inertia, for the slab with respect to the z -axis as $I_z \equiv \sum_i m_i \rho_i^2$. The physical quantity of the second term is zero, because the slab is symmetric with respect to the xy plane, as shown in Figure 1. This result indicates that the angular momentum is expressed as a vector in the direction of the rotational axis. The moment of inertia is determined by ρ_i^2 , the square of the distance from the z -axis to the mass element m_i , instead of by $|\mathbf{r}_i|^2$, the square of the distance from the origin to that element.

Therefore, the angular momentum is properly defined as the vector product of the position vector of a particle relative to the origin and the linear momentum vector of that particle. As a result, we can say that a net exter-

nal torque is needed for the angular acceleration of the particle about the axis of rotation. The angular momentum with respect to the rotational axis described in the commentary [8] is exactly the z -component of \mathbf{L} expressed as $\mathbf{L} \cdot \mathbf{k}$, which is $I_z \omega$. The moment of inertia I_z is determined by the distance from the axis of rotation. Similarly, the net external torque giving rise to the changing angular momentum vector is exactly the z -component of \mathbf{T} expressed as $\mathbf{T} \cdot \mathbf{k}$, where \mathbf{T} includes the sum of the interactions between particles [9].

4 Concluding remarks

A physical law is extended by defining new physical quantities such that the elementary principles can be maintained. An extension of a physical law to include a fundamental law is similar to the mathematical principle of the permanence of form and its transition [10].

For the present subject, two approaches can be used to introduce the concept of torque through the kinetic energy and work theorem. One is to maintain the analogy between linear and angular quantities through the corresponding arrangement of the expression of work [7]. The amount of work is expressed as the rotational angle multiplied by a combination of the force and the distance. The other is to arrange the expression of the kinetic energy of a rotating particle as shown in Section 2.2.

Understanding the relationships between physical quantities is essential to learning the meaning of physical laws. It is pedagogically

important to explore the basis of the definitions of physical quantities.

Appendix: Direction of vector obtained by vector product

For each direction, a line segment has two senses, a positive and a negative sense. Similarly, a plane has two sides. A directed area element corresponds to the length of the directed line segment. Given two vectors \mathbf{a} and \mathbf{b} , the area of the plane determined by these vectors is expressed as the exterior product $\mathbf{a} \wedge \mathbf{b}$. When the vector \mathbf{a} in the first position in the expression is rotated by the smallest angle that will cause it to coincide with the direction of \mathbf{b} , the area of the plane is defined as positive.

The vector product $\mathbf{a} \times \mathbf{b}$ is defined by a vector perpendicular to \mathbf{a} and \mathbf{b} and has a magnitude of $|\mathbf{a} \wedge \mathbf{b}|$. The sense of the plane determined by \mathbf{a} and \mathbf{b} is that of the motion of a right-handed screw. Thus, $\mathbf{a} \times \mathbf{b} = (\mathbf{a} \wedge \mathbf{b}) \mathbf{n}$, where \mathbf{n} is a unit vector with a positive sense.

Following this rule, the senses of \mathbf{T} , \mathbf{L} , and \mathbf{v} are defined, and thus \mathbf{T} is perpendicular to \mathbf{r} and \mathbf{F} , and so on. When a particle rotates in a plane, the direction of \mathbf{n} is that of the axis of rotation. The direction of $\boldsymbol{\omega}$ is defined as that of the axis of rotation, and thus the velocity of a particle \mathbf{v} is perpendicular to the plane determined by $\boldsymbol{\omega}$ and \mathbf{r} .

References

- [1] D. J. Cross (2015). *Am. J. Phys.* 83, 121-125
- [2] C. Kittel, W. D. Knight, and M. A. Ruderman. *Berkeley Physics Course Volume 1, Mechanics*, (New York: McGraw-Hill, 1973) pp. 102- 115, p. 185
- [3] H. Goldstein. *Classical Mechanics*, (Amsterdam: Addison-Wesley, 1978) pp. 24-25
- [4] K. Morgan. Torque and angular momentum in circular motion, (Project PHYS-NET, Physics Bldg, Michigan State University, 2002) p. 6
- [5] K. Husimi and S. Nakai. *Rikigaku*, (Tokyo: Kyoritsu Shuppan, 1959) pp. 3-4 (in Japanese)
- [6] Y. Kobayashi (2012). *Phys. Educ.* 28, 6
- [7] R. P. Feynman, R. B. Leighton, and M. Sands. *The Feynman Lectures on Physics*, (Amsterdam: Addison-Wesley, 1970) 18-2
- [8] Y. Yamada (2000). *Gokiso* 370 (in Japanese)
- [9] T. Matsuda (1987). *J. Phys. Educ. Soc. Jpn.* 35, 262 (in Japanese)
- [10] Y. Kobayashi (2014). *Eur. J. Pure Appl. Math.* 7, 405-411

Rotational motion of a rigid body with the system IP–Coach

Z. Gibová, O. Fričová, M. Kladivová, J. Kecer, M. Hutníková, M. Kovaľaková

Department of Physics, Faculty of Electrical Engineering and Informatics,
Technical University of Košice
Park Komenského 2, 04200 Košice, Slovakia
maria.kovalakova@tuke.sk

(Submitted 30-07-2015)

Abstract

A correct understanding of basic physical quantities related to the rotational motion of a rigid body by undergraduates is important not only in mechanics but also for understanding of basic physical principles in other branches of physics. The rotational motion of a symmetric rigid body about an axis through its centre of mass and perpendicular to the Earth's surface can be examined in the experiment which is presented in this paper. An optical gate connected to the system IP-Coach makes it possible to record the angular displacement as a function of time from which the angular velocity and angular acceleration can be calculated at any instant of time. Using these kinematic dependences, the influence of the moment of inertia as well as the influence of resistance forces on the rotational motion of a rigid body can be evaluated. The proposed experiment can be included as a demonstration or laboratory experiment in the basic physics course in technical bachelor's degree programmes.

1. Introduction

Rotational motion of a rigid body about a fixed axis is difficult for students to grasp mainly from the point of view of understanding the quantities which are used to describe this motion. This can be improved by the demonstration of this motion using apparatus which makes it possible to record simultaneously the values of angular displacement and time. The apparatus consists of the rotation apparatus and the system IP-Coach (optical gate, CoachLab panel and computer with IP-Coach program). The advantage of using the system IP-

Coach is immediate display of the measured kinematic quantities – angular displacement (φ) and derived quantities – angular velocity (ω) and angular acceleration (α) as a functions of time (t). These quantities are then used for elucidation of basic dynamic characteristics of rotational motion of a rigid body – torque (moment of force) (M) and moment of inertia (I). Moreover, the system IP-Coach when used in laboratory practicals makes it more effective and faster to process the measured data.

The above-mentioned apparatus can be also used in the laboratory practicals in the specialized

technical study programmes since it enables to study the influence of frictional forces as well as to observe subtle effects of viscous resistance forces of surroundings (air) on the motion.

2. Experimental

Rotation apparatus (3B Scientific) used in experiments is shown in Fig. 1. It consists of plastic weight fastener (1), 100 g weight discs (2), 10 g slotted weights (3), string (4), 20 g slotted weight (5), hanger for slotted weights (6), 200 g weight discs (7), spindle (8), base and mount (9) and hollow aluminium rod (10).

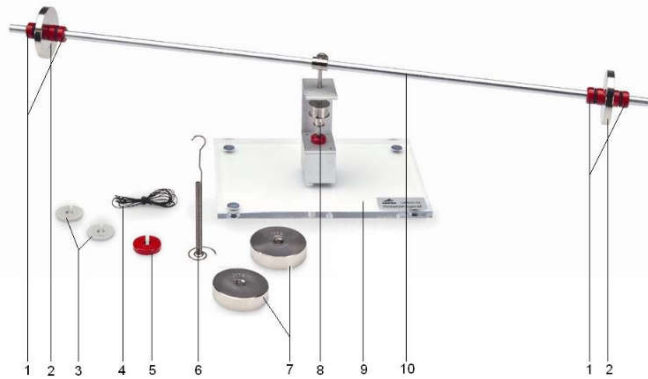


FIG. 1: Rotation apparatus.

[https://www.3bscientific.com/rotation-apparatus-u8405715,p_853_18606.html]

The apparatus is set into motion by the weight of slotted weights (3,5) placed on a hanger (Fig. 2) fixed at the end of the string (4) wound around a spindle (8) with diameter of 1.8 cm. The string runs over the deflection pulley of negligible mass (Fig. 2). The weight discs (2,7) can be placed on the crossbar in various positions using weight fasteners (1) changing the moment of inertia of the crossbar and in this way also the characteristics of the rotational motion [1].



FIG. 2: Rotation apparatus with a weight placed on a weight hanger.

The CoachLab panel (Fig. 3) with the optical gate connected (CMA Photogate code 06621) makes it possible to record the dependence of the number of half-revolutions on time during the rotational motion and to display the data simultaneously on the screen as a graph and as a table [2].



FIG. 3: Rotation apparatus with the system IP – Coach: 1 – CoachLab panel (interface), 2 - optical gate.

3. Results and discussion

3.1 Uniformly accelerated rotational motion – kinematics

Generally, if a rotational motion takes place in plane, the following equations hold

$$\omega = \frac{d\varphi}{dt} \quad (1)$$

$$\alpha = \frac{d\omega}{dt} \tag{2}$$

Uniformly accelerated rotational motion is performed by the body rotating about fixed axis with constant angular acceleration α . Angular velocity ω and angular displacement φ as functions of time can be expressed by the following equations

$$\omega = \omega_0 + \alpha t \tag{3}$$

$$\varphi = \varphi_0 + \omega_0 t + \frac{1}{2} \alpha t^2 \tag{4}$$

where ω_0 is initial angular velocity and φ_0 is initial angular displacement.

The measured experimental dependence of angular displacement on time is depicted in Fig. 4. In our experiment, the weight discs with mass of 200 g were placed symmetrically at the distance of 15 cm from the axis of rotation (labelling I2 in graphs) and apparatus was set into motion by the slotted weights with mass $m = 30$ g.

The IP-Coach programme makes it possible to record and to analyse the measured dependence of angular displacement on time. Using the option “Analyse” the function $y = ax^2 + bx + c$ can be fitted to the data. As can be seen, this function describes the measured dependence satisfactorily. Based on the comparison with the theoretical function (4) it can be assumed that the apparatus performed uniformly accelerated motion and the values of parameters a, b, c correspond to the values of angular acceleration $\alpha = 2a$, initial angular velocity $\omega_0 = b$ and initial angular displacement $\varphi_0 = c$. The values of $\alpha, \omega_0, \varphi_0$ obtained from the fitting procedure are listed in the inset in Fig. 4.

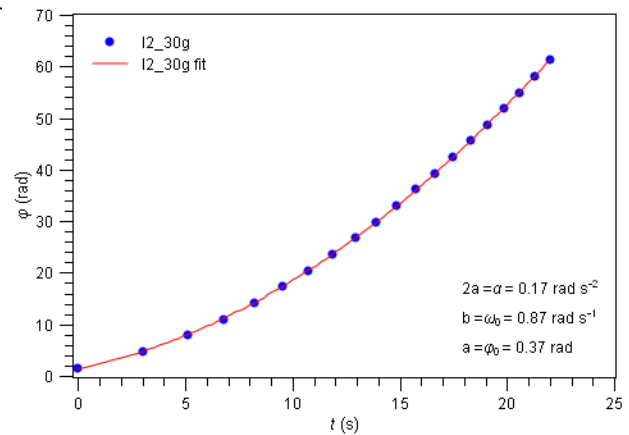


FIG. 4: Angular displacement φ as a function of time t for uniformly accelerated rotational motion: blue dots – experimental data, red line – fitted function (Eq.(4))

Derivative of the experimental dependence of angular displacement with respect to time calculated using the option “Processing” in the IP-Coach programme provides the dependence of angular velocity on time (Fig. 5). It can be seen that angular velocity increases nearly linearly with time which is in agreement with the assumption of uniformly accelerated rotational motion for which equation (3) holds.

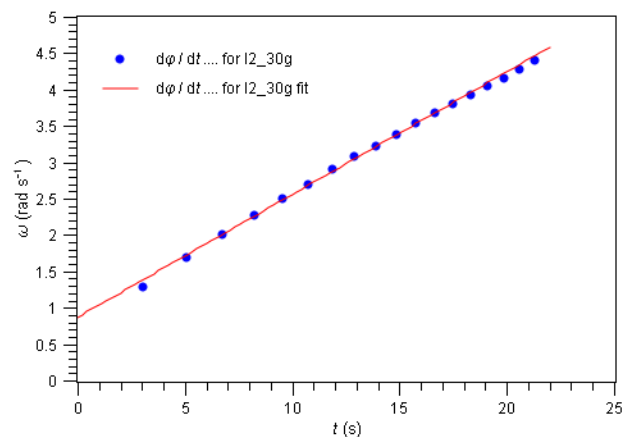


FIG. 5: Angular velocity ω as a function of time for uniformly accelerated rotational motion obtained by numerical calculation of the first derivative of angular displacement with respect to time: blue dots – values from experimental data, red line – Eq. (3)

The first derivative of angular velocity (Fig. 5), i.e. the second derivative of angular

displacement, with respect to time provides constant angular acceleration as was already assumed (red line in Fig. 6, i.e., $\alpha = 2a = 0.17 \text{ rad.s}^{-2}$), the obtained dependence is displayed in Fig. 6. However, the first derivative of the experimental data of angular velocity with respect to time results in a more complex dependence of angular acceleration on time with the values whose dispersion is approximately 20 % with respect to the above-mentioned value of angular acceleration α . This dispersion is brought about by repeated calculations of the derivatives of experimental dependences since they increase uncertainties of calculated values. A slight deviation of the values of the first derivative of experimental dependence of angular displacement with respect to time from a straight line (Fig. 5) results in a small negative slope of a trend line of the second derivative of angular displacement with respect to time (green line in Fig. 6). The more detailed discussion concerning this issue will be presented in section 3.3.

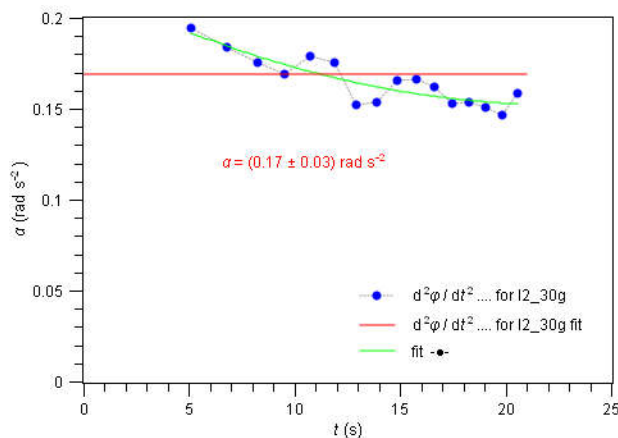


FIG. 6: Angular acceleration as a function of time for uniformly accelerated rotational motion obtained by the calculation of derivatives: blue dots –the second derivative of angular displacement with respect to time, green line –function polynomial fit (cubic) to the calculated values (to the set of blue dots in this graph), red line – $\alpha = 2a$.

3.2 Uniformly accelerated rotational motion – dynamics

Rotational motion of a rigid body about a fixed axis from the point of view of dynamics (acting forces) can be described by the following equation of motion

$$M = I\alpha \tag{5}$$

where M is torque (sum of acting moments of forces), I is moment of inertia of the body and α is angular acceleration. This equation says that the change in angular acceleration of rotational motion can be achieved by the change in torque M at constant moment of inertia I or by the change in moment of inertia I at a constant torque M [3].

It has to be noted that the equation of motion of the rotation apparatus is more complex than equation (5) because we deal with a system of rigid bodies in motion: rotating crossbar with weight discs (a rigid body with the moment of inertia I) and a ‘falling’ slotted weight of mass m . The equations of motion for this system of bodies provides the following equation

$$M = (I + mr^2)\alpha \tag{6}$$

where

$$M = mgr + M_{other} \tag{7}$$

where r is the radius of the spindle and torque M_{other} in our experiment comes from resistance forces acting on the rotating apparatus (M_{other} can be considered approximately constant for our equipment, see discussion in Sec. 3.3).

Since for the used rotation apparatus it holds $I \gg mr^2$, equation (5) can be considered to be correct.

Torque $M(t)$ in our experiment can be changed by placing the slotted weights with different masses m on a hanger fixed at the end of the string. The mass increase Δm leads to an Δmgr increase of M . The equation (5) implies that the increase in torque results in the increase in angular acceleration. The dependence of angular displacement on time will be steeper (Fig. 7).

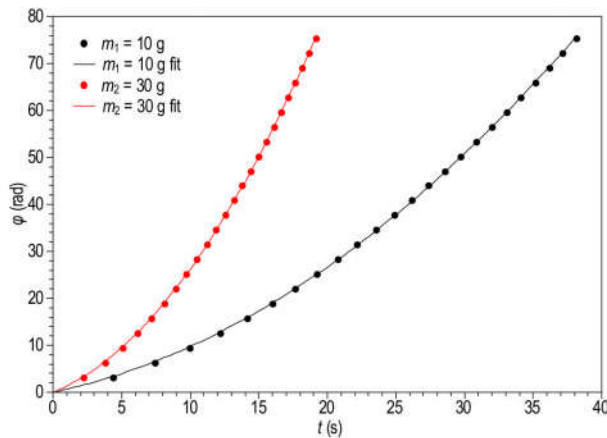


FIG. 7: Angular displacement as a function of time for two different values of torque at constant moment of inertia

Moment of inertia I can be markedly changed by changing the distance of weight discs placed on the crossbar from the axis of rotation. According to the equation (5) the increase in moment of inertia results in the decrease in angular acceleration and increase in angular displacement in time will be smaller. The smaller moment of inertia results in the steeper dependence of angular displacement on time. The plots of angular displacements versus time for two different moments of inertia $I_1 > I_3$ are displayed in Fig. 8, torque was produced by the weight of the slotted weight with mass of 30 g. Moment of inertia was changed by the changing the positions of weight discs on the crossbar, which were 21 cm and 11

cm from the axis of rotation for I_1 and I_3 , respectively.

As can be seen, the increase of angular displacement in time is slower for I_1 than for I_3 .

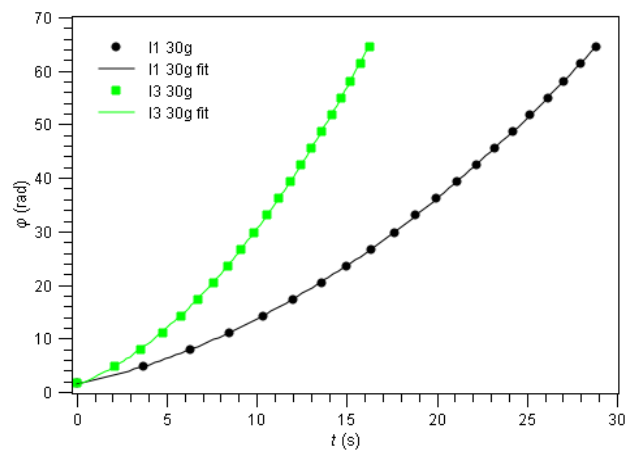


FIG. 8: Angular displacement as a function of time for two different values of moment of inertia ($I_1 > I_3$) and constant torque.

3.3. The influence of resistance forces on rotational motion

In sections 3.1 and 3.2 the influence of resistance forces on experimentally obtained data has not been discussed yet. The so far presented experimental procedure and data processing can be used in the basic physics course in which the knowledge of basic quantities and equations related to rotational motion should be deepened.

If this experiment is used in physics courses for specialized technical programmes, it is necessary to include the influence of resistance forces (frictional and viscous resistance forces) in the description of rotational motion in order to evaluate dynamic quantities in a correct way.

If frictional forces are taken into account then equation of motion of rotational motion of a rigid body (5) will have the following form

$$I\alpha = M - M_f \quad (8)$$

where the torque of frictional forces M_f is explicitly expressed now.

We will assume that torque of frictional forces is constant for our apparatus since the weight of slotted weights with m acts on the axle in perpendicular direction with respect to the axle axis and it does not increase the force which acts on the agate bearings and it does not increase the torque of frictional forces M_f . Its value can be determined in an experiment without driving weight: $m = 0, M = 0$. The crossbar will be set into motion manually by a stroke. The motion will be retarded due to the frictional forces between vertical axle and agate bearings. Torque of frictional forces M_f can be then determined from experimental dependence of the number of half-revolutions on time (Fig. 8).

Fitting function $y = ax^2 + bx + c$ to the experimental data and taking into account equation (4), the value of angular deceleration ($\alpha = \pi \cdot 2a$) can be obtained which is $\alpha = -0,0106 \text{ rad. s}^{-2}$ for the data plotted in Fig. 9. Moment of inertia can be calculated using the following expression

$$I = I_0 + 2m_d R^2 \quad (9)$$

where I_0 is moment of inertia of the crossbar ($I_0 = \frac{1}{12} ml^2$) and $2m_d R^2$ is moment of inertia of weight discs placed at distance R from the axis of rotation.

If the mass of weight discs is $m_d = 200 \text{ g}$ and their distance from axis of rotation is $R = 20 \text{ cm}$, the mass of the crossbar is $m = 0.0433 \text{ kg}$, its length is $l = 0.6 \text{ m}$, then moment of inertia of rotating apparatus can be calculated using (9) and it is $I = 0,0173 \text{ kgm}^2$.

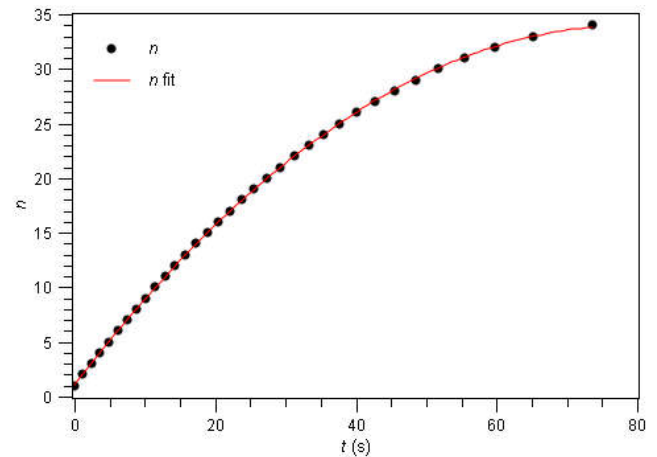


FIG. 9: Number of half-revolutions as a function of time for uniformly decelerated rotational motion: dots – experimental data, red line – correspond to function (Eq. (4)) divided by π fitted to the measured data.

Using experimental values for angular deceleration and moment of inertia, the moment of frictional forces can be calculated using equation (6) for $M = 0$ ($m = 0$)

$$M_f = -I\alpha \quad (7)$$

The experimental data provided the value $M_f = 1,834 \cdot 10^{-4} \text{ Nm}$.

It has to be noted that the rotational motion of rigid body is also slightly influenced by viscous resistance forces of the surrounding air which depends on the velocity of the body. This is the cause of slight deflection of the values of angular velocity from a straight line in Fig. 5. The dependence of angular acceleration on time (Fig. 6) is not constant but decreases in time (with increasing angular velocity). Decrease is

successively smaller since the torque of viscous resistance forces is function of velocity which increases in time and more and more compensates the torque of driving weight. The total torque which accelerates the apparatus is gradually smaller and smaller. We do not discuss frictional and viscous resistance forces acting on the other parts of the system (pulley, weights of mass m) since they can be considered negligibly small in comparison with resistance forces discussed above.

7. Conclusion

Rotational motion of a rigid body about a fixed axis can be easily demonstrated using the rotation apparatus and the system IP–Coach. The advantage of the proposed experimental setup is the possibility of immediate display of basic kinematic quantities – directly measured angular displacement, and derived quantities -angular velocity and angular acceleration as functions of time. These quantities can be related to basic dynamic characteristics of the rotational motion of a rigid body through the equation of motion for rotational motion. The influence of torque and

moment of inertia on kinematic quantities of rotational motion can also be demonstrated. The influence of frictional and viscous resistance forces can also be observed. The proposed experiment can be used not only in laboratory practicals but also as a video demonstration or live experiment during the lecture since students can observe directly uniformly accelerated and decelerated rotational motions and kinematic quantities related to this motion as functions of time.

Acknowledgements

This work was supported by the grant from the Cultural and Educational Grant Agency of the Ministry of Education of the Slovak Republic under the project KEGA Project No. 032TUKE-4/2014.

References:

- [1] <https://www.3bscientific.com/product-manual/U8405715.pdf>
- [2] <http://cma-science.nl/en/>
- [3] Halliday, D., Resnick, R., Walker, J. *Fundamentals of physics*. Sixth Edition (John Wiley & Sons, Inc., USA , 2001)

Reinforcing Harmonic Oscillators In Electrostatics

Michael A. Waxman

*Department of Natural Sciences,
University of Wisconsin-Superior,
Superior, WI 54880*

(Submitted 08-07-2015)

Abstract

We present a newly designed module for a General Physics course helping to reinforce the concept of harmonic motion through examples from electrostatics.

1. Introduction

Harmonic motion is one of the most important topics in general physics, particularly since understanding such motion is crucial for grasping a number of important processes in physical chemistry, such as absorption and emission of electromagnetic radiation, non-linear optics, or vibrotational molecular spectra [1]. Within the framework of a typical American university curriculum, harmonic oscillators are introduced in the first semester of a two-semester general physics sequence [2]. However, the amount of material and available choices for topics are so wide that occasionally introduction of the harmonic motion is delayed until the second semester of this sequence, the one traditionally devoted to electricity and magnetism. Below I describe a module (a series of activities and exercises) I designed for this specific purpose, namely for familiarizing students with harmonic motion through electrostatics-related problems and for reinforcing the relevant concepts.

Throughout this module I tried to keep the needed *mathematics* as simple as possible, thus allowing one to concentrate on the *physics* of things.

Less than a week into electrostatics [3], I start with a brief description of harmonic motion, both in terms of the definition and the transformations of energy during the oscillations of an object attached to a spring. I also present the main formula for the period of such oscillations,

$$\tau = 2\pi\sqrt{m/k}, \quad (1)$$

with m being the mass of the oscillator and k the spring constant. Then I assign, for the class work, the following problem:

Problem 1. A positively charged bead (charge q , mass m) is placed between two identical positive point charges Q which are separated by a fixed distance $2a$ (Figure 1). The bead, confined to move along the line connecting charges Q , is displaced a certain distance ϵ along the axis and released.

Determine the condition upon which the subsequent bead oscillations are simple harmonic motion and determine the frequency ν of these oscillations. What is the significance of this result with regard to the general features of harmonic vs. non-harmonic oscillations in the nature?

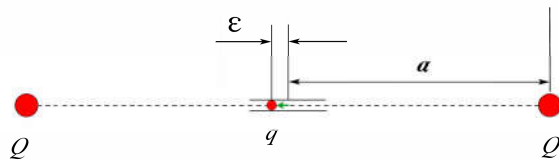


Figure 1. Geometry of Problem 1.

A number of students arrive at the solution successfully. The total force acting upon the bead is (see Fig. 1):

$$F_{tot} = F_{left} - F_{right} = k_e qQ \left[\frac{1}{(a - \epsilon)^2} - \frac{1}{(a + \epsilon)^2} \right] = 2k_e qQ a \frac{\epsilon}{(a - \epsilon)^2 (a + \epsilon)^2}, \quad (2)$$

where F_{right} , F_{left} are the magnitudes of the forces acting due to the right-hand-side and the left-hand-side point charges respectively. Clearly, when $\epsilon \ll a$, Eq. (2) yields

$$F_{tot} = \frac{2k_e qQ}{a^3} \epsilon \propto \epsilon,$$

thus the oscillations in this case are harmonic, and according to Eqs. (1), (3),

$$\nu = \frac{1}{2\pi} \sqrt{\frac{k}{m}} = \frac{1}{2\pi} \sqrt{\frac{2k_e qQ}{ma^3}}.$$

In order to solve this problem, students needed to figure out that the force acting upon the bead is, for $\epsilon \ll a$, directly proportional to its displacement

ϵ from the position in the center of the gap between the charges Q . And, as Richard Feynman once said (and an article on mechanical harmonic motion [4] reminded), “the same equations have the same solutions” – in other words, electric forces in our system work exactly like a spring with a spring constant of $\frac{2k_e qQ}{a^3}$, thus yielding the solution Eq. (4).

Discussing the answer to the latter part of Problem 1, I describe to the students the analogy with oscillations of electronic clouds in atoms under the action of ordinary light, when the magnitude of oscillations is small and thus the oscillations are harmonic. However, when a powerful enough laser is used for irradiating the medium, deviations from harmonic behavior become significant, which gives rise to the whole new class of phenomena of non-linear optics, particularly to frequency doubling (see, for example, Ref. [1], p. 776).

As a homework, I assign students a problem on determining the field of a semi-infinite charge line (problem 24 [3]), along with the following problem dealing with a similar system:

(3)

Problem 2. A positively charged bead (charge q , mass m) is placed between two identical semi-infinite line charges extending one from negative infinity to $x = -x_0$, and another one from $x = x_0$ to positive infinity as shown in Figure 2. The lines carry positive charges with uniform charge density λ_0 . The bead, confined to move along the x axis, is displaced by a small distance ϵ along the axis (where $\epsilon \ll x_0$) and released (Figure 2). Show that the particle oscillates in simple harmonic motion and determine the frequency of these oscillations.

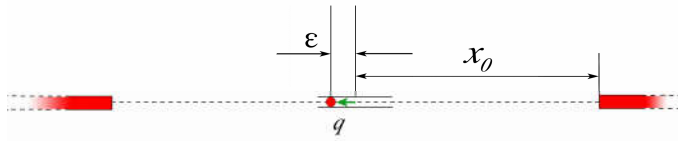


Figure 2. Geometry of Problem 2.

This latter problem is usually solved by a majority of students. They learn upon solving the (simultaneously assigned) problem 24 [3] that the magnitude of the force F_{right} acting due to the right-hand-side line charge is

$$\begin{aligned}
 F_{right} &= k_e q \int_{x_a}^{\infty} \frac{\lambda_0 dx}{x^2} \\
 &= k_e q \frac{\lambda_0}{x_a} \qquad (5)
 \end{aligned}$$

where x_a is the distance between the particle and the edge of the line charge. Thus, for a bead deviated from $x=0$ by ϵ , the total force acting on it would be:

$$\begin{aligned}
 F_{tot} &= F_{left} - F_{right} \\
 &= k_e q \frac{\lambda_0}{x_0 - \epsilon} - k_e q \frac{\lambda_0}{x_0 + \epsilon} \\
 &= 2k_e q \lambda_0 \frac{\epsilon}{(x_0 - \epsilon)(x_0 + \epsilon)}, \qquad (6)
 \end{aligned}$$

and $F_{tot} \propto \epsilon$ for $\epsilon \ll x_0$. Therefore, as in Problem 1, electrical field acts as a spring with a constant of

$$k = \frac{2k_e q \lambda_0}{x_0^2}, \qquad (7)$$

and thus

$$\nu = \frac{1}{2\pi} \sqrt{\frac{k}{m}} = \frac{1}{2\pi} \sqrt{\frac{2k_e q \lambda_0}{m x_0^2}}. \qquad (8)$$

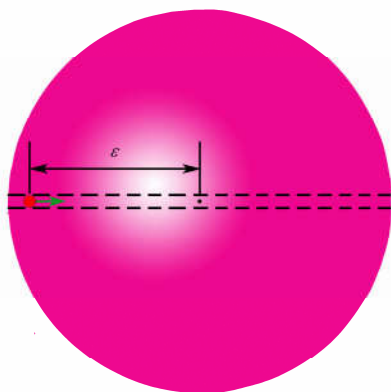
True to my usual routine [5,6], I assign a similar, but somewhat more open-ended, problem as a bonus problem for the test:

Problem 3. In a recent class we saw an example of an oscillator (pendulum) where the oscillations are harmonic only when their magnitude is small. Using the topics from electrostatics that we have just studied, design an oscillator for which the oscillations would remain harmonic for the finite, not just small, magnitude of oscillations. Express the frequency ν of these oscillations through the parameters of your designed system (size, etc).

Surprisingly, only very few students arrive at the correct solution this time – even though they all have studied the related system less than a week ago! In class, we consider the application of Gauss’s law to an insulating, uniformly charged solid sphere (Ref. [3], pp. 641-642). For $r < a$ (where r is the distance from the sphere’s center and a is its radius), it yields:

$$\begin{aligned}
 E &= \frac{k_e Q}{a^3} r, \qquad (9)
 \end{aligned}$$

where E is the electric field and Q is the total charge of this sphere. Thus, if we drill a narrow hole through the center of this sphere and let a small charged bead (with



a mass m and charge q opposite to Q) travel through that hole (see Figure 3), it will undergo harmonic oscillations for as long as their amplitude $\varepsilon < a$, i. e. for the finite ε . According to the above, the frequency of these oscillations is

$$\nu = \frac{1}{2\pi} \sqrt{\frac{k}{m}} = \frac{1}{2\pi} \sqrt{\frac{k_e q Q}{m a^3}} \quad .(10)$$

Figure 3. Geometry of Problem 3

In the author's opinion, the above activities/exercises allow one to "kill two rabbits with a single bullet", namely to reinforce the application of the principles of electrostatics in non-standard context and to teach students to recognize the harmonic motion in an unfamiliar setting, thereby providing the necessary reinforcement to the new concept. Besides, it allows for another reinforcement of the topic of frequency doubling ([1], p. 776), an example with which I always conclude the discussion of the solution to Problem 3 during the next class meeting, emphasizing the qualitative difference of the laser radiation's effect on the molecules from that of the traditional light source. Last, but not least, these exercises help the students to see one of the most beautiful aspects of physics – the

universality of the characteristics of seemingly unrelated effects [4].

Remarkably, even though the module is fairly brief, it appears to do the trick – now, when students come to my physical chemistry class next year, absolute majority of them clearly recognize the relevant concept and easily transition to the study of non-linear optical phenomena [1].

References

1. Peter Atkins and Julio de Paula, *Physical Chemistry*, 10th Edition (WH Freeman, New York, 2014), pp. 503-522.
2. Raymond A. Serway and John W. Jewett, Jr., *Principles of Physics. A Calculus-Based Text*, 5th ed. (Thomson, Brooks/Cole, 2013), volume 1, pp 1- 618.
3. *ibid.*, volume 2, Chapter 19 "Electric Forces and Electric Fields", pp. 619-655.
4. Iosif S. Bitensky, "Look at equations heedfully and you'll win," *Phys. Teach.***35**, 540-541 (1997).
5. Michael A.Waxman, "Exploring Rotations Due to Radiation Pressure: 2D to 3D Transition Is Interesting!" *Phys. Teach.***48**, 30-31 (2010).
6. Michael A.Waxman, "Using physics to investigate blood flow in arteries: A case study for pre-med students," *Am. J. Phys.***78**, no. 9, pp. 970-973 (2010).

ⁱ Another similar problem that could be assigned here is the one dealing with oscillations of a particle near the center of a ring (problem 76 [3]). Unfortunately, in order to solve that problem, greater sophistication in mathematics (particularly, vector analysis) is needed. As a result, students are unable to solve the problem on their own, and the physics of the solution (when presented to them) gets buried under the math.

The Electrodynamics of Charges in Capacitors-Pulley System & Teaching Physics Discovery Lessons

G. Tremberger, Jr., V. Shekoyan, S. Dehipawala, T. Holden, D. Lieberman, and T. Cheung

Department of Physics
CUNY Queensborough Community College
Bayside NY 11364, USA.

(Submitted 24-10-2015)

Abstract

A novel method in the solving of the College Physics II standard 2-capacitor parallel reconnection problem was presented with a focus on the motion of the transferred charges. The reduction in electrostatic field energy of the higher voltage capacitor would be equal to the work required to move the charges to the lower voltage capacitor. A spring with a movable gap capacitor model would connect the teaching of College Physics II field energy concept to College Physics I stored energy concept with some introduction to radiation. The addition of a pulley and mass to a movable gap capacitor in the Atwood machine configuration would serve as a numerical model for the teaching of oscillation, starting with an example of π computation using energy conservation principle in a spring-mass system with a simple period formula. The discovery spirit in electrodynamics development was modeled as extensions of mechanics topics in Physics I and was taught to the students in Physics II. Good Physics Education delivery would be vital for doing Physics Education Research on the collected student performance data to assess student learning in physics problem solving skill and discovery spirit.

1. Introduction

The College Physics standard 2-capacitor parallel reconnection problem is shown in Figure 1. The usual method have been focusing on the final charges on each capacitor with unknown charges as Q_1 and Q_2 respectively, coupled with the conservation of charge that Q_1 and Q_2 would be equal to the sum of the initial charges. Solving the simultaneous equations would give Q_1 and Q_2 .

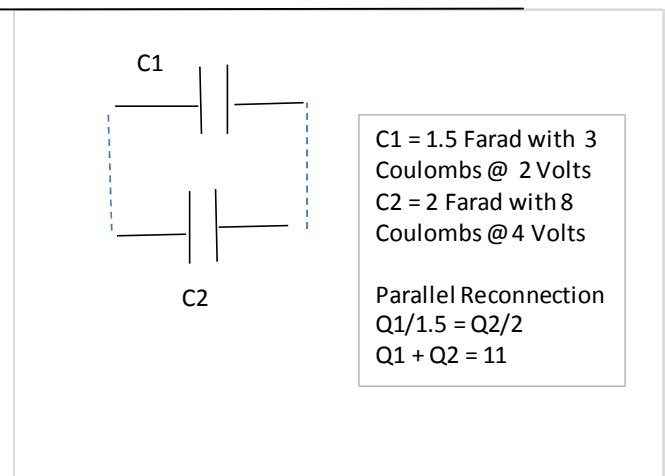


FIG. 1: A schematic view of connecting two capacitors in parallel.

The drawing in Figure 2 shows a solution method where the focus is on the transferred charge, Q_t . Setting up the voltage equality would immediately generate the numerical answer for Q_t in a single equation.

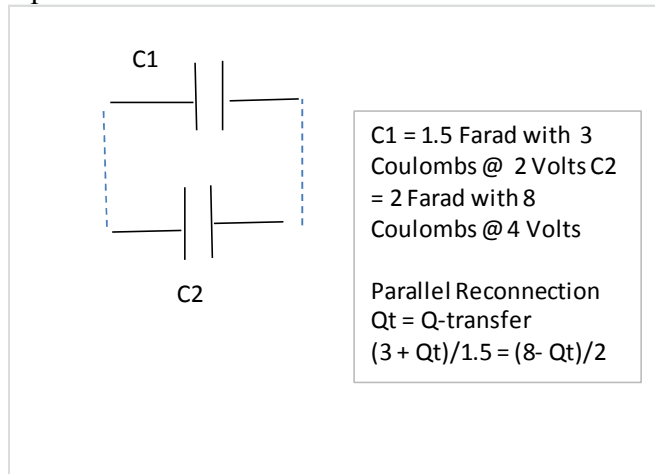


FIG. 2: An illustration of the Q-transfer relationship when two capacitors are connected in parallel.

2. Work-Energy Theorem

The energy used to transfer the charges can be calculated as the product of Q_t and voltage difference. However the numerical value for the voltage difference is not obvious since the voltage on either capacitor is changing until both capacitors reach the final voltage, 3.142857 Volts. The standard formulation of $\frac{1}{2}QV$ can still be used with the $\frac{1}{2}$ factor being explained in Figure 3. The area bounded by the triangle would be $\frac{1}{2} * \text{base} * \text{height} = \frac{1}{2} * (4-2) * 1.71 = 1.71$ Joules, with $Q_t = 1.71$ Coulomb.

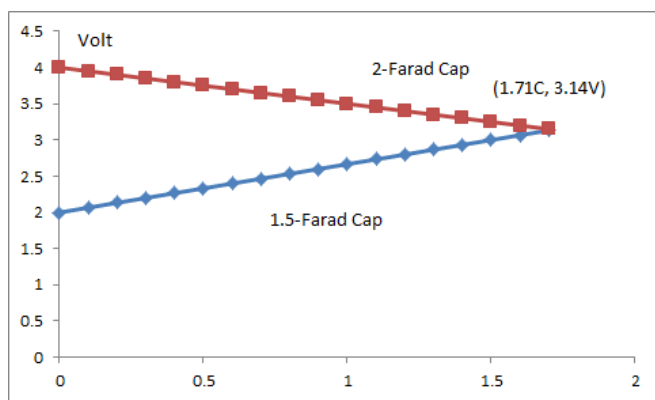


FIG. 3: Voltage (y-axis) versus Coulomb (x-axis)

The energy of the system can be computed using the expression $\frac{1}{2} * Q^2 / C$ or $\frac{1}{2} * \epsilon_0 * E^2 * \text{Volume}$ when focusing on the electric field energy in the gap space of a capacitor with ϵ_0 as the permittivity. The energy before reconnection would be 19 Joules ($3^2/2/1.5 + 8^2/2/2$ numerically). After reconnection, the energy would then become 17.29 Joules ($(3+1.71)^2/2/1.5 + (8-1.71)^2/2/2$ numerically) such that the loss energy 1.71 Joules is equal to the work which is illustrated in Figure 3, thus verify the Work-Energy Theorem. The work in Joules is also related to the voltage drop of C2 and the voltage increase in C1, as illustrated in Figure 3. In fact the voltage change concept can also be used to compute the transferred charge, as shown in Figure 4. In other words, the voltage difference of 2 Volts needs to be divided into the ratio of $1/C1$ to $1/C2$, that is, 0.67 to 0.5. Given a magnitude of 2, the division would be 1.15 to 0.85 such that C2 would have $(4 - 1.15) = 3.15$ Volt and C1 would have $(2 + 0.85) = 3.15$ Volt, with small round-off errors as shown in Figure 4.

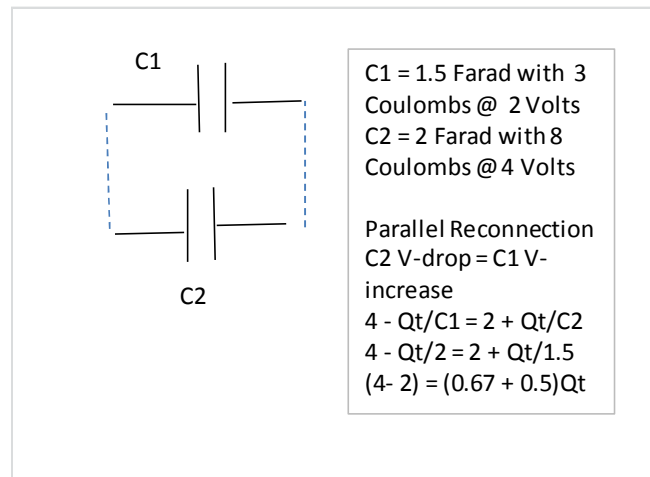


FIG. 4: An illustration of the voltage change relationship when two capacitors are connected in parallel

3. Capacitor-Pulley Problems

The case of a capacitor plate connected to a spring in a variable gap distance design has been worked out in open literature [1]. The electrostatic

attraction force between the capacitor plates would be $Q^2 / (2 \cdot A \cdot \epsilon_0)$ and the spring compression via Hooke's Law would be $Q^2 / (2kA\epsilon_0)$, with k represent the spring constant, and A represented the plate area. The electrostatic field energy is coupled with the stored mechanical spring energy. A small displacement with energy $\frac{1}{2} \cdot k \cdot \text{Amplitude} \cdot \text{Amplitude}$ would enable oscillation with damping governed by the dipole field radiation loss. Working on a simple postulation that an accelerated charge will radiate, the radiation should be proportional to acceleration-squared because the Cartesian representation of acceleration in the negative axis should not give different result from acceleration in the positive axis without symmetry breaking. Knowing that acceleration is proportional to frequency-squared in an oscillation, then the radiation of this capacitor-spring system should be proportional to frequency⁴, thus capturing an essential feature in the Rayleigh scattering model. When a variable gap capacitor is connected to another mass via a pulley as shown in Figure 5, the standard Atwood Machine configuration would become an oscillatory system when the capacitor charges are changing with time.

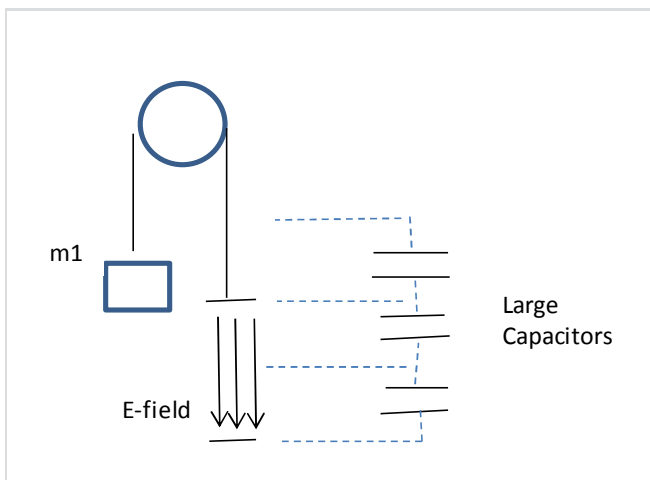


FIG. 5: A schematic view of the capacitor-pulley system.

The Figure 5 scenario can be illustrated with a numerical simulation using Microsoft Excel. The numerical simulation technique can be learned

with relative ease for the case of the simple harmonic motion as illustrated in Figure 6.

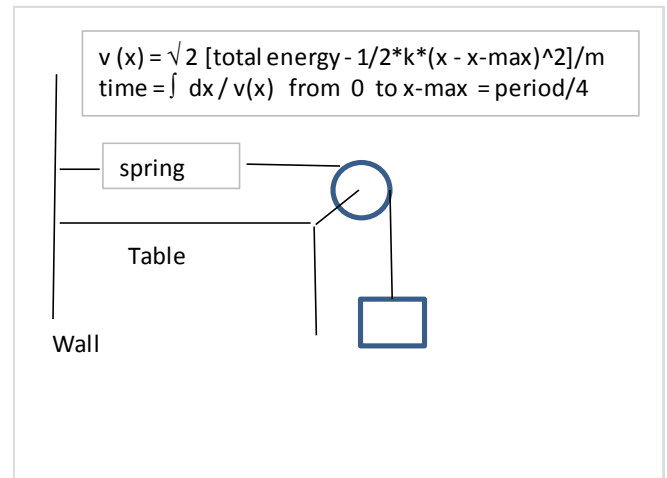


FIG. 6: A schematic view of the simple harmonic motion system used in the simulation with spring constant = 500 N/m, block mass = 40 kg, and pulley has negligible mass.

The simple harmonic motion of a spring-mass system simulation, with period $T = 2 \pi \sqrt{\text{mass}/\text{spring constant}}$, was based on dividing the amplitude into small distance increments. An application of the energy conservation principle for a small distance would give the velocity or speed, as illustrated in Figure 6. The time for that small distance interval was then obtained by dividing the distance by the calculated speed from energy conservation principle. The total time would be obtained by summing all the small distance increment durations numerically such that π can be computed. The number of iterations would be the number of distance intervals used in the simulation. In fact, an approximation of π can be computed using this energy conservation principle simulation, which is similar to the polynomial expansion of π in calculus, as illustrated in Figure 7. We know that $\text{Arc-tan}(1) = \pi/4$. In Calculus the $\text{Arc-tan}(1)$ value can be computed with $\int dx / (1 + x^2)$ with x from 0 to 1, and that is also equal to the infinite series of $\sum 1 - 1/3 + 1/5 - 1/7 + 1/9 \dots\dots\dots$ via the Leibniz formula for π computation. Whether the Leibniz formula or energy conservation principle is more

computational efficient would be a good Excel exercise for software engineering majors.

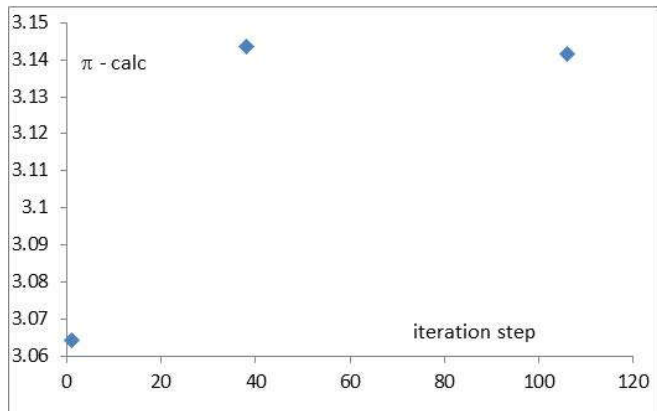


FIG. 7: A graphical illustration of the π calculation versus the number of iterations in the simple harmonic motion simulation.

Note that the capacitor-pulley simulation used a non-linear voltage variation along the gap of the capacitor (Figure 8). The voltage sources are constant and the simulation assumed that the charge transfer needed negligible time. The electrostatic force supplied by the 4,000 Volt constant voltage source plus the weight of the 2.7 kg electrode on the pulley right side would exceed the weight of the 4 kg block on the pulley left side initially. When the 2.7 kg electrode passes the 10 Volt source, charge transfer would diminish the electrostatic force such that the pulley left side effective weight would be heavier and stop the 2.7 kg electrode from falling. Similarly when the 2.7 kg electrode passes the upper 5,000 Volt constant voltage source, the charge transfer would increase the electrostatic force such that the pulley right side effective weight would be heavier and stop the 2.7 kg electrode from raising. This alternating effective weight scheme would result in an oscillatory phenomenon until the 2.7 kg electrode touches the bottom electrode eventually.

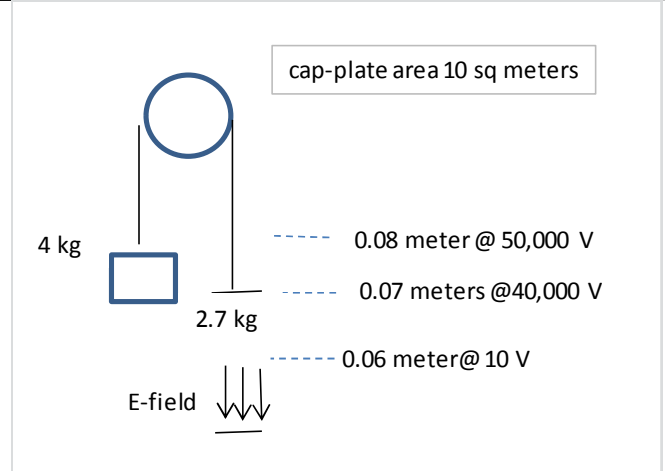


FIG. 8: A schematic view of the parameters used in the simulation.

The result showed an oscillation with increasing amplitude since the mechanical work by the (4 – 2.7) kg mass difference would exceed the electrical energy gain. The displayed cycle between the time intervals from 2 sec to 5 sec in Figure 9 carries a mechanical work of 2.578 Joules and an electrical energy gain of 2.433 Joules. The final situation where the upper capacitor plate will eventually reach the lower plate with zero gap distance will stop the oscillation when the charges become neutralized. Then the 4 kg block will fall and the 2.7 kg electrode with no charge will rise. The expected Casimir effect for the sub-micron gap parallel plate geometry with no charge could be mentioned briefly. Anyway the changing dipole field would still generate a radiation field, though extremely weak and was not included in the simulation.

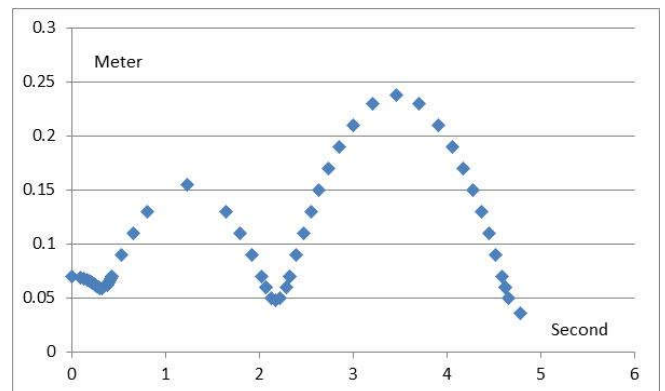


FIG. 9: Upper plate position versus time

4. Discussion

Good Physics Education delivery would be vital for doing productive Physics Education Research with the collected student performance data to assess the use of discovery strategy in teaching physics. The understanding of the reciprocal relationship in capacitor gap distance and the compensation of a faster growing function in voltage such as quadratic feature would generate multiple numerical examples for students to engage in designing different situations. The numerical simulation example in using the capacitor-pulley system is just one example among many others. For example two capacitors connected in series could be configured as an uplift device as shown in Figure 10. This engineering physics model would help students to think about the energy storage issue for wind and solar power alternatives without the electric power grid. The force and electric field application details are also available in the open literature.

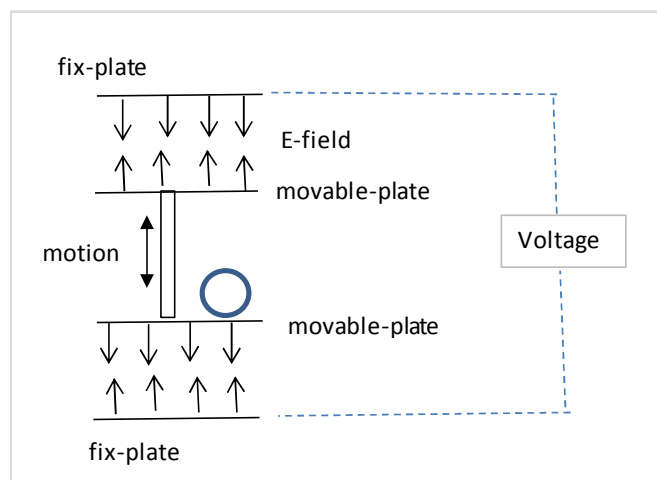


FIG. 10: A schematic view of an uplift device.

The engineering physics example illustrates the importance of hinting/pointing to higher physics class materials, and help students to decide if they are ready as electrical engineering majors when transferring to a 4-year college from our

community college pre-engineering program. When in doubt, a student with a discovery spirit usually would appreciate an instructor's guidance and search the web for ideas. For example, the Townsend Brown work on capacitor is available on popular media [2], and Wikipedia also has an explanation on the Biefeld-Brown Effect [3]. Technical sites like NASA has a publication on propulsion using asymmetrical capacitor design [4], and that US Army Research Laboratory also has a related article in archive [5]. Recent research for space propulsion system via the Biefeld-Brown Effect is also available in pen literature [6]. An instructor knowledgeable with these information resources would be able to sustain the discovery spirit of a student with various problem solving skills linking Physics II explicitly to Physics I; and be vital to providing a good physics education.

5. Conclusions

We have demonstrated the charge movement concept in teaching capacitor related problems, and capacitor-pulley system oscillation with numerical simulation was found to be successful to encourage student discovery spirit.

Acknowledgements

The authors thank all those who put their research results on the web for open access. The project was partially supported by several CUNY internal funding sources.

References:

- [1] MIT Visualizing E&M (2015) Chapter 5: Capacitor Connected to a Spring
<http://web.mit.edu/viz/EM/visualizations/coursenotes/modules/guide05.pdf>
- [2] Nils Rognerud (2011) Townsend Brown and Capacitors.
<http://electrogravityphysics.com/townsend-brown-capacitors/>

[3] Wikipedia: Biefeld–Brown effect.
https://en.wikipedia.org/wiki/Biefeld%E2%80%93Brown_effect

[4] Francis X. Canning, Cory Melcher, and Edwin Winet (2004). Asymmetrical Capacitors for Propulsion.
<http://ntrs.nasa.gov/archive/nasa/casi.ntrs.nasa.gov/20040171929.pdf>

[5] Thomas B. Bahder & Chris Fazi (2002). Force on an Asymmetric Capacitor.
<http://arxiv.org/abs/physics/0211001>

[6] Mario J. Pinheiro (2015) Dimensional Analysis of Thrusting by Electromagnetic Inertia.
<http://arxiv.org/abs/1502.01917>

Rutherford's Scattering: A Fortran Simulation

Antonio Ortiz Castro

Department of Physics
Universidad Anahuac
Huixquilucan 52786, Mexico.
antorca59@gmail.com

keywords: Rutherford scattering, Fortran
PACS: 34.50.Cx

(Submitted 16 Nov 2015)

Abstract

A simulation of Rutherford's experiments of 1911 about the scattering of α particles is presented using Fortran. The number of collisions (number of particles scattered) were considered per unit solid angle and the curve obtained was fitted with a new function.

1 Introduction

A hundred years ago Lord Ernest Rutherford conducted a series of experiments performed by Geiger and his student Marsden that lead him to discover atomic nucleus[1]. Bombarding a thin Au foil with α -particles emitted by RaC (Bi^{214}), they measured the scattering angle, and Rutherford deduced an expression for a coulomb field that was later confirmed quantum mechanically by N. Bohr. Rutherford recognized that the energy and direc-

tion of the emitted particle was a random event and a consequence of a single encounter particle-nucleus and not a result of multiple scatterings. The formula he deduced for the differential scattering cross section $\sigma(\theta)$ is well known and can be found in any Classical Mechanics text book [2, 3]. The α -particle is subject to a coulombian central force field whose potential is

$$V(r) = \frac{K}{r}, \quad K = \frac{1}{4\pi\epsilon_0}q_1q_2 \quad (1)$$

The impact parameter s and the scattering angle θ are related by:

$$s = \kappa \cot\left(\frac{\theta}{2}\right) \quad (2)$$

where $\kappa = K/(2T'_0)$, and T'_0 is the α -particle's energy in the center of mass system [2, 3]. Goldstein [3] defines the differential scattering cross section as

$$\sigma(\theta)d\Omega = \frac{n}{I} = \frac{s}{\sin\theta} \left| \frac{ds}{d\theta} \right|$$

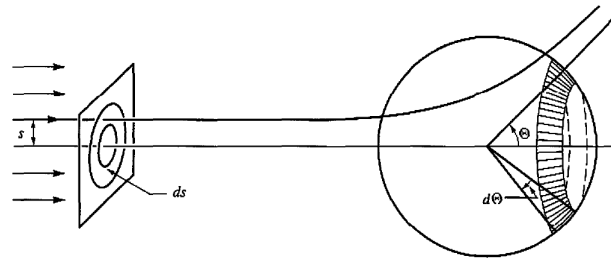
where n is the number of particles scattered within the solid angle $d\Omega$ per unit time and I is the intensity of the incident particles. Substituting s from eq (2) we obtain Rutherford's law:

$$\sigma(\theta) = \left(\frac{K}{4T'_0}\right)^2 \cdot \sin\left(\frac{\theta}{2}\right)^{-4} \quad (3)$$

2 Particle count

The number of particles scattered within unit solid angle $d\Omega$, that is, between θ and $\theta + d\theta$, is determined by[3]:

$$\sigma(\theta)Id\Omega = 2\pi\sigma(\theta)I \sin\theta|d\theta| \quad (4)$$



The area of the shaded region is $2\pi s \cdot \Delta\theta$. The total area is obtained considering the whole range of θ values which is π rad or 180° ; that is, $\text{area} = 2\pi^2 s \cdot 180/\pi = 360\pi s$. ([3], p. 107)

The absolute value is taken because to an increase of θ corresponds a decrease in the scattering angle. The intensity of the incident beam I is calculated as the number of particles per unit area per unit time:

$$I = \frac{\text{number of particles/sec}}{\text{area}} = \frac{N}{2\pi R^2 \sin\theta \Delta\theta} = \frac{N}{90sr^2}$$

Integrating eq (4)

$$n = 4\pi I \sigma_0 \sin\left(\frac{\theta}{2}\right)^{-2} = \frac{N\sigma_0}{90sr^2} \sin\left(\frac{\pi\theta}{360}\right)^{-2} \quad (5)$$

because θ is expressed in degrees. We found that this new function fits the data of the simulation.

3 Data

The next table shows the energies of the α -particles emitted by Bi^{214} and their relative intensities [4]:

Energy (keV)	Intensity
4941	5.3E-5
5023	4.4E-5
5184	1.28E-4
5273	0.00122
5452	0.0113
5516	0.0082

T_0' was taken as the expected value of these energies:

$$\text{Total Energy} = \text{Energy}_1 \cdot p_1 + \text{Energy}_2 \cdot p_2 + \dots = 5.4628 \text{ MeV}$$

where p_i = relative intensity. Nuclear radius was calculated according to[5]:

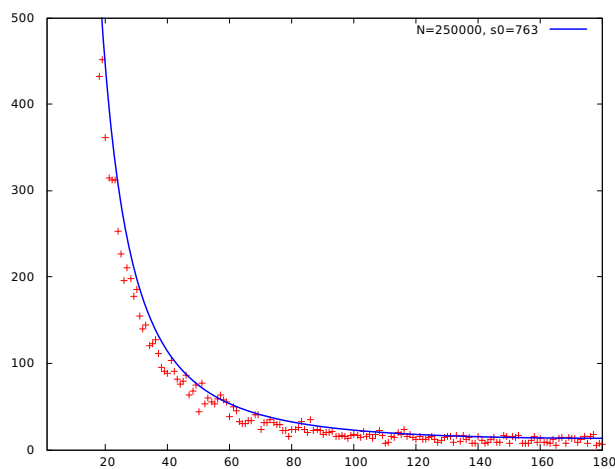
$$r = \left(r_0 + \frac{r_1}{A^{2/3}} + \frac{r_2}{A^{4/3}} \right) \cdot A^{1/3} = 5.4499 \times 10^{-15} \text{ m}$$

being A the atomic number and the parameters take the values: $r_0 = 0.9071$ fm, $r_1 = 1.105$ fm y $r_2 = -0.548$ fm, and $1 \text{ fm} = 10^{-15}$ m. κ and s in ec(2) are expressed as multiples of the nuclear radius r ($\kappa = 3.8210 r = 2.0824 \times 10^{-14}$ m).

4 Fortran

We vary two quantities: l_0 and N . The impact parameter s is generated at random between 0 and l_0 , being l_0 an arbitrary value (l_0 = distance from the scattering nucleus expressed as a multiple of the nuclear radius). Rutherford reports that Geiger made some $N = 250\,000$ counts at each measurement session, so we decided to generate this number of

“events”. Next, the scattering angle θ given in eq (2) is generated, and then, expressed in degrees (the factor 2 in eq (2) becomes: $2 \cdot 180 / \pi = 114.59$.) Each scattering angle is rounded to the nearest integer because we are interested in the number of particles scattered degree by degree. Afterwards we count the particles scattered in each degree. Note that since $s < l_0$, the scattered angles satisfy: $\theta > 2 \cdot \arctan[\kappa / l_0] \cdot 180 / \pi$. The data is dumped in the file “dataC.dat” and read by Gnuplot to obtain the plot shown in fig 4. The code of the Fortran program is in appendix A.



Graph of n vs θ made with Gnuplot of the data generated by Fortran. θ is expressed in degrees and in the vertical axis is n . The continuous line corresponds to eq (5) while the data generated with Fortran are represented with crosses. In this case, $s_0 = 763$ nuclear radii, and 250 000 events were simulated. The code of this graph is in appendix B.

5 Conclusions

According to the results, the new expression eq (5), correctly explains the number of particles found in each degree, since, as we can see, it fits well the data generated. The results also show that it is possible to use Fortran to reproduce Rutherford's experiments of the

scattering of α -particles by a nucleus, by a simple-code program. We would like to add that the random number generator[6] can be considered a good generator because it permitted us to obtain data that resembles the data observed of a phenomenon (emission of particles) which, by its very nature, we know it is completely aleatory.

A Fortran Code

Program scattering

```

implicit none
integer, dimension(180) :: counter
      real(8) :: e, epsilon0, k
      real(8) :: r0, r1, r2, AA, r
      real(8) :: s0
      real(8) :: T0, kappa, sigma0
      real(8) :: rand
      real(8) :: s, theta, sigma
      real(8), parameter :: pi = 3.141592653589793d0
      integer :: error, i, n, v, d, Z

!-----[ Parameters of the problem ]-----80
e          = 1.6022d-19
epsilon0   = 8.8542d-12
Z          = 79.
k          = .5 * Z * e / (pi * epsilon0)

AA        = 1.9697d2
r         = (0.898 + 1.376/AA**(.6666666) - 2.262/AA**(1.333333) ) * 10 **(-15.) &
           * AA**(.3333333)

```

```

T0      = 5.4628d6
kappa   = .5 * k / (T0 * r)
sigma0  = ( .25 * k / T0 )**2.0

!-----[ data ]-----80
print*, "# of events 'N':"
read*,  n
print*, "Choose a value 's0':"
read*,  s0

open(unit=20,file="dataC.dat",status="replace",action="write")

write(unit=20,fmt="(i8)")      n      !
write(unit=20,fmt="(f6.0)")    s0      ! Write these values
write(unit=20,fmt="(es13.6)")  sigma0  ! for Gnuplot
write(unit=20,fmt="(es13.6)")  r      !

!-----[ Initializing the counter ]-----80

counter = 0

!-----[ loop ]-----80

call init_random_seed()

do i = 1, n

call random_number(rand)

s = s0 * rand
theta = 2.0 * atan( kappa / s )

d = nint(theta * 180.0 / pi)
if ( d <= 1.0 ) then      !
counter(1) = counter(1) + 1.0      !
else                      !-----[ counter ]-----80
counter(d) = counter(d) + 1.0      !
endif                      !

```

```
enddo

!-----[ save the counter ]-----80
do i = 1, 180

    write(unit=20,fmt="(i3,i8)",iostat=errorC) i, counter(i)

enddo

close(unit=20)

!-----[ messages ]-----80
print"(a,i4)", "error in 'counter' = ", error

                !*****
                contains
                !*****

!-----[ subroutine init_random_seed ]-----80
subroutine init_random_seed()
!    implicit none
    integer, allocatable :: seed(:)
    integer :: i, n, un, istat, dt(8), pid, t(2), s
    integer(8) :: count, tms

    call random_seed(size = n)
    allocate(seed(n))
    ! First try if the OS provides a random number generator
    open(newunit=un, file="/dev/urandom", access="stream", &
        form="unformatted", action="read", status="old", iostat=istat)
    if (istat == 0) then
        read(un) seed
        close(un)
    else
        ! Fallback to XOR:ing the current time and pid. The PID is
        ! useful in case one launches multiple instances of the same
        ! program in parallel.
```

```
call system_clock(count)
if (count /= 0) then
  t = transfer(count, t)
else
  call date_and_time(values=dt)
  tms = (dt(1) - 1970) * 365_8 * 24 * 60 * 60 * 1000 &
    + dt(2) * 31_8 * 24 * 60 * 60 * 1000 &
    + dt(3) * 24 * 60 * 60 * 60 * 1000 &
    + dt(5) * 60 * 60 * 1000 &
    + dt(6) * 60 * 1000 + dt(7) * 1000 &
    + dt(8)
  t = transfer(tms, t)
end if
s = ieor(t(1), t(2))
pid = getpid() + 1099279 ! Add a prime
s = ieor(s, pid)
if (n >= 3) then
  seed(1) = t(1) + 36269
  seed(2) = t(2) + 72551
  seed(3) = pid
  if (n > 3) then
    seed(4:) = s + 37 * (/ (i, i = 0, n - 4) /)
  end if
else
  seed = s + 37 * (/ (i, i = 0, n - 1) /)
end if
end if
call random_seed(put=seed)
end subroutine init_random_seed
endprogram scattering
```

B Gnuplot Code

```
reset
N      = system("awk NR==1 dataC.dat")
s0     = system("awk NR==2 dataC.dat")
sigma0 = system("awk NR==3 dataC.dat")
```

```
r      =  system("awk NR==4 dataC.dat")

f(x)   =  N * sigma0 / (90 * s0 * r**2.) * sin(x*pi/360.0)**-2.

plot [1.:180.][0.:500.] 'dataC.dat' every ::6 notitle, \
      f(x) title sprintf("N=%.0f, s0=%.0f", N+0, s0+0) \
      lw 1.5 lc 3
```

References

- Brookhaven National Laboratory*, 2014.
- [1] E. Rutherford, *Philosophical Magazine*, Series 6, No. **21**, 669 (1911)
 - [2] J.B. Marion, *Classical Dynamics of Particles and Systems*, (Academic Press, 1970), pp. 302-309.
 - [3] H. Goldstein, Ch. Poole, J. Safko, *Classical Mechanics*, (Addison-Wesley, 3rd Ed, 2000), pp. 106-110.
 - [4] National Nuclear Data Center (Nuclear structure & decay data),
 - [5] I. Angeli, K.P. Marinova, *Table of experimental nuclear ground state charge radii: An update*, Atomic Data and Nuclear Data Tables (Elsevier) **99** (2013) 69-95
 - [6] random_seed, Intrinsic Procedures, *The Gnu Fortran Compiler*.

Nature of Legendre foretold by Pascal

P. R. Subramanian¹, B. V. Jenisha², and A. Jestin Lenus³

¹Central Instrumentation and Service Laboratory, University of Madras,
Guindy Campus, Chennai 600 025, India,
hermite137@yahoo.com

²Department of Theoretical Physics, University of Madras,
Guindy Campus, Chennai 600 025, India,
elizy.jeni@gmail.com

³Department of Physics, College of Engineering, Guindy,
Anna University, Chennai 600 025, India,
justinl137@gmail.com

(Submitted 11-08-2015)

Abstract

Divisibility of a non-zero coefficient of an integer polynomial, by the binomial coefficient associated with the degree of the polynomial and the corresponding index of the power of the argument, is established for a Legendre Polynomial, multiplied by the exact power of 2 which divides the factorial of its degree, and a *modified* Hermite polynomial. These two coefficients have the same parity and their ratio is always an odd integer. Together the coefficients of each one of these two integer polynomials produce a perfect palindrome with respect to their parity. In spite of divisibility, the parity of a coefficient of a Laguerre polynomial, multiplied by the factorial of its degree, and the parity of a coefficient of a Hermite polynomial, cannot be predicted perfectly by the associated binomial coefficient.

1 Introduction

$$n!/2^B = \text{odd } \#, \tag{2}$$

The Legendre polynomials are extremely useful in Special Functions, Mathematical Physics, Numerical Methods, Electromagnetic Theory, Quantum Mechanics, Quantum Theory of Angular Momentum, and Nuclear Physics [1, 2, 3, 4]. The power series expansion of the Legendre polynomial of degree n in x is given by [1, 2, 3]

$$P_n(x) = \sum_{s=0}^{\lfloor n/2 \rfloor} \frac{(-1)^s (2n - 2s)! x^{n-2s}}{2^n s! (n - s)! (n - 2s)!}. \tag{1}$$

Here $\lfloor \rho \rfloor$ is the greatest integer $\leq \rho$. The common denominator of all the coefficients of $P_n(x)$, when reduced to their lowest terms, is 2^B , the greatest power of 2 which divides $n!$ [5, p. 352] (Pearl # 1). Our Legendre polynomial, *from now onwards*, is a rational function (the symbol “ \triangleq ” standing for “is equal to by definition”),

$$P_n(x) \triangleq K_n(x)/2^B, \quad n + 1 \in \mathbb{N},$$

such that all the coefficients of $K_n(x)$, a polynomial of degree n in x , are integers. Thus, by the numerator of $P_n(x)$ we always mean $K_n(x)$, and the denominator of $P_n(x)$ is always 2^B . The coefficients of $K_n(x)$ are 2^B times the Legendre coefficients. It is nice to note that $K_n(x)$ is an *integer polynomial*, i.e., a polynomial whose coefficients are integers [6]. Let us remember that $K_n(x)$ has a definite parity $(-1)^n$ [1, 2, 3]. It is an even (odd) polynomial when the degree n is even (odd). See Eqs. (1) and (2). Focussing on x^{n-2s} in Eq. (1), let us note that both $n - 2s$ and n have the same parity: odd (even) when n is odd (even), since our $2s$ is an even integer.

The purpose of our paper is to show that the coefficient of x^{n-2s} , $0 \leq s \leq \lfloor n/2 \rfloor$, $n + 1 \in \mathbb{N}$, in $K_n(x)$, is always divisible by the associated binomial coefficient $\binom{n}{n-2s}$ (Pearl # 2), and that the ratio of these two coefficients is an odd integer forever (Pearl # 3):

$$\binom{n}{n-2s} \mid \text{coefficient of } x^{n-2s} \text{ in } K_n(x), \tag{3}$$

$$\begin{aligned} (-1)^s \times \text{coefficient of } x^{n-2s} \text{ in } K_n(x) \\ = \text{odd positive integer} \times \binom{n}{n-2s}. \end{aligned} \tag{4}$$

We also establish the *parity-palindromic* nature of the coefficients of $K_n(x)$ (Pearl # 4).

Our paper is organized as follows: Section 2 deals with the contributions of Legendre and Kummer [7, 8, 9] on the *p*-adic valua-

tion of certain interesting integers. In Section 3, we prove Holt's result [5, p. 352] (Pearl # 1) concerning the common denominator of the Legendre coefficients, when reduced to their lowest terms. That Pascal (binomial coefficient) is able to predict perfectly the parity of Legendre (coefficient multiplied by 2^B), is established. We show that each coefficient in the numerator of a Legendre polynomial is divisible by the associated binomial coefficient, *DegreePower*, always resulting in an odd integer upon division. We also prove that the coefficients in the numerator of $P_n(x)$ produce a palindrome with respect to their parity (parity-palindrome) perfectly. Section 4 contains other lovely and pleasant results concerning the Legendre coefficients. In Section 5, we appreciate the beauty of the Pascal's Triangle and consider its application to the Legendre polynomials. Dealing with the Laguerre, Hermite, and *modified* Hermite polynomials [1, 2, 3, 10] in Section 6, we prove that the (non-zero) coefficient of x^s in $\Phi_n(x)$, an integer polynomial [6], is divisible by the binomial coefficient ns , when $\Phi_n(x) = n!L_n(x), H_n(x), He_n(x); n + 1, s + 1 \in \mathbb{N}, 0 \leq s \leq n$. Here $He_n(x), n \geq 0$, are the *modified* Hermite Polynomials [1, p. 189], [10].

2 Remembering and Honouring Legendre and Kummer

Let \mathbb{P} be the set of prime numbers, $p \in \mathbb{P}$, and μ be an integer ≥ 2 . Then $\nu_p(\mu)$, the p -adic

valuation of μ , is the exponent of p in the canonical decomposition in prime factors of μ . It has been elegantly shown by Legendre [7, 8, 9] that

$$\nu_p(n!) = (n - \sigma_p(n))/(p - 1),$$

$$n \geq 2, n \in \mathbb{N}, p \in \mathbb{P}, \quad (5)$$

where $\sigma_p(n)$ is the sum of the digits in the base- p expansion of n , with

$$\sigma_p(np) = \sigma_p(n), n \in \mathbb{N}, p \in \mathbb{P}. \quad (6)$$

Example # 1: Since $2015 = 5 \times 13 \times 31$ and since 5, 13, and 31 are prime numbers, $\nu_5(2015) = 1 = \nu_{13}(2015) = \nu_{31}(2015)$; $\nu_3(2015) = 0 = \nu_{11}(2015) = \nu_{23}(2015)$. *✓cfc (=Checked and found correct!!)*. We are extremely grateful to our revered Guruji, Prof. Dr V Devanathan [4], who always insists: "*Check, Recheck, Cross-Check, Double-Check, Multi-Check!!*" Let us develop the culture of checking the correctness of whatever we do [11]!! As his faithful students, we always ask our students *to check the correctness of their own calculations* in various ways.

Let a be a positive integer and let a_k, a_{k-1}, \dots, a_0 be the digits of a , when written in base p . Hence the base- p expansion of a is

$$a \triangleq (a_k a_{k-1} \dots a_0)_p$$

$$= \sum_{s=0}^k a_{k-s} p^{k-s},$$

$$0 \leq a_{k-s} \leq p - 1, p \in \mathbb{P}. \quad (7)$$

Similarly, let $b \in \mathbb{N}$ with $b \triangleq (b_k b_{k-1} \dots b_0)_p$ and let $\epsilon_q = 1$ if there is a carry-over in the

q^{th} digit when a and b are added; otherwise $\epsilon_q = 0$. Then (see [8, p. 1113], [9, p. 7])

$$c = a + b = p^{k+1} \epsilon_k + p^k c_k + \dots + p c_1 + c_0, \quad (8)$$

with

$$c_0 = a_0 + b_0 - p \epsilon_0, \quad (9)$$

$$c_t = a_t + b_t + \epsilon_{t-1} - p \epsilon_t, \quad (10)$$

$$1 \leq t \leq k,$$

$$\sigma_p(a) + \sigma_p(b) - \sigma_p(a+b) = (p-1) \sum_{r=0}^k \epsilon_r. \quad (11)$$

When we perform the addition of a and b (in base $p \geq 3$), let us remember that $a_r, b_r \geq (p+1)/2$ leads to $\epsilon_r = 1$ (i.e., a carry-over, irrespective of whether there is a carry-over in the previous digit or not (see Eqs. (7) – (10))); $a_r, b_r \leq (p-3)/2$ leads to no carry-over (i.e., $\epsilon_r = 0$), even if there is a carry-over

in the previous digit; $a_r, b_r = (p-1)/2$ leads to $\epsilon_r = 1$, only when there is a carry-over in the previous digit (i.e., $\epsilon_{r-1} = 1$; a conditional carry-over).

Kummer (1852) [7, 8, 9] beautifully and cheerfully unveiled the following result for the binomial coefficient: $\nu_p(nm)$ is equal to the number of carry-overs when m and $n-m$ are added in base p .

Example # 2: We want to establish that the number 9060 is *not* divisible by 5. Now the representation of 60 in base 5 is $(220)_5$; that of 30 is $(110)_5$. Since no carry-over occurs when we add 220 and 110 (in base 5), Kummer [7, 8, 9] is pleased to tell us that the exponent of 5 in 9060, a 24-digit number ending in 4, is just zero. See also [8, p. 1114] and **Example # 5**.

3 Pascal predicts the parity of Legendre perfectly!

It follows from Eqs. (5) and (6) that

$$\nu_2(2n - 2sn \times ns) = \sigma_2(n) + \nu_2(nn - 2s). \quad (12)$$

Since a factor $2^{\sigma_2(n)}$ is common to all $2n - 2sn \times ns$, $0 \leq s \leq [n/2]$, $n-1 \in \mathbb{N}$, we have

$$\begin{aligned} (2n - 2s)! / \{2^n s! (n-s)! (n-2s)!\} &= 2n - 2sn \times ns / 2^n \\ &= 2^{\sigma_2(n)} \times \text{Integer} / 2^n = \text{Integer} / 2^{n-\sigma_2(n)} = A_{n-2s} / 2^B, \end{aligned} \quad (13)$$

where (see Eqs. (5), (12), and (13))

$$B \triangleq n - \sigma_2(n) \equiv \nu_2(n!), \quad (14)$$

$$A_{n-2s} \triangleq (2n - 2s)! / \{2^{\sigma_2(n)} s! (n-s)! (n-2s)!\}, \quad (15)$$

$$\nu_2(A_{n-2s}) = \nu_2(nn - 2s). \quad (16)$$

Equations (1), (2), (13), and (14) demand that the denominator of $P_n(x)$ is $2^B = 2^{\nu_2(n!)}$. Thus, we have proved Holt's result [5, p. 352; Pearl # 1]. It is clear from Eqs. (1), (2), and (13)–(15) that $(-1)^s A_{n-2s}$ is the coefficient of x^{n-2s} in $K_n(x)$. Equation (16) shows that the (non-zero) coefficient of x^{Power} in $K_{Degree}(x)$ and the corresponding binomial coefficient $DegreePower$ have the *same* parity!! These nice results lead to more such nice results, as shown below. The *same* exponent of 2 appears in the canonical decomposition in prime factors of the coefficient of x^{n-2s} in $K_n(x)$ and that of the corresponding bino-

mial coefficient $nn - 2s$. We will not forget that in the case of this binomial coefficient, both *Degree* and *Power* have the same parity ($\because n - (n - 2s) = 2s = \text{even} \# \geq 0$).

It follows from Eqs. (15) and (16) that

$$\begin{aligned} L(n, s) &\triangleq A_{n-2s} / nn - 2s \\ &= \frac{2n - 2sn - s \times 2ss}{2^{\sigma_2(n)} \times ns} \\ &= L(n, n - s), \end{aligned} \tag{17}$$

$$\nu_2(L(n, s)) = 0. \tag{18}$$

Equation (17) exhibits a nice symmetry with respect to an interchange of s and $n - s$.

From Eqs. (5) and (17), we have

$$\begin{aligned} (p - 1) \nu_p(L(n, s)) &= \sigma_p(n) + \sigma_p(n - s) + \sigma_p(s) \\ &\quad - \{ \sigma_p(2n - 2s) + \sigma_p(2s) \} \\ &\quad - (p - 1) \nu_p(2^{\sigma_2(n)}), \quad p \in \mathbb{P}. \end{aligned} \tag{19}$$

Application of Kummer's Theorem [7, 8, 9] to Eq. (17) leads to the following result (p is an odd prime; $\epsilon_r^{\beta, \eta} = 0, 1$; see also Eqs. (11) and (19)):

$$\nu_p(L(n, s)) = \sum_{r=0}^{r_{max}} \{ (\epsilon_r^{n-s, n-s} + \epsilon_r^{s, s}) - \epsilon_r^{n-s, s} \} \in \mathbb{Z}, \quad p \geq 3, \quad p \in \mathbb{P}. \tag{20}$$

Equations (19) and (20) reveal a nice symmetry: $\nu_p(L(n, s)) = \nu_p(L(n, n - s))$. See Eq. (17).

In Eq. (20) $\epsilon_r^{n-s, n-s}$, $\epsilon_r^{s, s}$, and $\epsilon_r^{n-s, s}$ are respectively the number of carry-overs (zero or one, in the r^{th} digit), when $n - s$ and $n - s$ are added, s and s are added, $n - s$

and s are added (see [7, pp. 63–65], [8, p. 1113], [9, p. 7]), all additions done in base p . Using Eqs. (7) – (10) and the discussions following Eq. (11), we can show that

there can be a carry-over in $n - s$ added to s , only if there is a carry-over either from $n - s$ added to itself or from s added to itself (or from both). It is now clear that the right-hand side of Eq. (20), an integer, is never negative for all values of $p \in \mathbb{P}$. Hence $\nu_p(L(n, s)) + 1 \in \mathbb{N}, p \in \mathbb{P}$, and thus the coefficient of $x^{n-2s}, 0 \leq s \leq [n/2], n + 1 \in \mathbb{N}$, in $K_n(x)$, is an integer divisible by $nn - 2s$ (Pearl # 2). As $\nu_2(L(n, s)) = 0$ (see Eq. (18)), $L(n, s)$ is now an odd integer (Pearl # 3). Both 2^B times a Legendre coefficient and the associated binomial coefficient, *DegreePower*, sing joyfully in unison thus: “You are an integer, so am I! If you are odd, I am also odd!! (The contrapositive [12] of this true statement is also true: If I am even, you are also even!!) When I am odd, you too are odd! Truly, we are lovingly made for each other!! Whether we are odd or even, our ratio (“*Legendre / Pascal*”) is always odd! Are we not the Adam and Eve of the Paradise of the Legendre Polynomials!?” Yes, Pascal (*1623, †1662) predicts the nature of Legendre (*1752, †1833)!! “*Tell me who your friends are and I’ll tell you who you are.*” So goes a Mexican Proverb. Ask any coefficient of $P_n(x)$. The reply will be the (corresponding) Binomial Coefficient (Pascal) and the Largest Power of 2 which divides the factorial of the degree n (Holt [5, p. 352])!! (*LP* for Legendre Polynomial, *LP* for Largest Power, *P* for Pascal.) See Eqs. (2) – (4).

Example # 3: $p = 3, n = 10 = (101)_3, s = 4 = (11)_3. \therefore n - s = 6 = (20)_3, 2(n - s) = 12 = (110)_3, 2s = 8 = (22)_3.$ Now $\sigma_3(n) + \sigma_3(n - s) + \sigma_3(s) = 2 + 2 + 2 = 6, \sigma_3(2n - 2s) + \sigma_3(2s) = 2 + 4 = 6,$

$\therefore \nu_3(L(10, 4)) = (6 - 6)/2 = 0.$ See Eq. (19). Moreover, $\sum_r \epsilon_r^{n-s, n-s}, \sum_r \epsilon_r^{s, s}, \sum_r \epsilon_r^{n-s, s}$ are respectively 1, 0, 1. $\therefore \sum_r (\epsilon_r^{n-s, n-s} + \epsilon_r^{s, s} - \epsilon_r^{n-s, s}) = 0.$ These two numbers must be equal. *✓ cfc.* Therefore, 3 cannot be a factor of $L(10, 4)$. *Mathematica* says (see also Table 2) that the coefficient of x^2 in $K_{10}(x)$ is 3465. $\therefore 102 = 45, L(10, 4) = 3465/45 = 77,$ an odd integer. Lo! Behold! $3 \nmid 77.$ *✓ cfc.* Yes, 3 does not divide $L(10, 4)$. Since $104 = 210 = \text{even},$ the coefficient of x^4 must be even and divisible by this binomial coefficient, the quotient being an odd integer. Actually (see Table 2), $-30030/210 = -143,$ an odd integer. *✓ cfc.*

Example # 4: $p = 5, n = 13 = (23)_5, s = 3 = (3)_5. \therefore n - s = 10 = (20)_5, 2(n - s) = 20 = (40)_5, 2s = 6 = (11)_5.$ Now $\sigma_5(n) + \sigma_5(n - s) + \sigma_5(s) = 5 + 2 + 3 = 10, \sigma_5(2n - 2s) + \sigma_5(2s) = 4 + 2 = 6. \therefore \nu_5(L(13, 3)) = (10 - 6)/4 = 1.$ See Eq. (19). Moreover, $\sum_r \epsilon_r^{n-s, n-s}, \sum_r \epsilon_r^{s, s}, \sum_r \epsilon_r^{n-s, s}$ are respectively 0, 1, 0. $\therefore \sum_r (\epsilon_r^{n-s, n-s} + \epsilon_r^{s, s} - \epsilon_r^{n-s, s}) = 1.$ These two numbers must be equal. *✓ cfc.* Using *Mathematica*, we have found that the coefficient of x^7 in the numerator of $P_{13}(x)$ is $-2771340. \therefore 137 = 1716, L(13, 3) = 2771340/1716 = 1615 = 5 \times 17 \times 19 \rightarrow \nu_5(L(13, 3)) = 1. \checkmark cfc.$ Yes, the exponent of 5, in the canonical decomposition in prime factors of $L(13, 3)$, an odd integer (Pearl # 3), is unity! One of its factors is 5.

Example # 5: Consider the binomial coefficient 2311. Kummer [7, 8, 9] gently reminds us that there is only one carry-over when we add 12 and 11 in base 2, since $12 = (1100)_2, 11 = (1011)_2.$ Therefore, the

exponent of 2 in the canonical decomposition in prime factors of this binomial coefficient is simply unity. (See also **Example # 2.**) It is just even, not even divisible by 4. Hence the coefficient of x^{11} in the numerator of $P_{23}(x)$ must be simply even, not at all divisible by 4. *Mathematica* tells us that this coefficient, the above binomial coefficient, and their ratio are respectively 1 805 044 411 170 (a 13-digit number; even, but not divisible by 4 since the last two digits are 70), 1 352 078 (7-digits; not divisible by 4, though even, because of the last two digits: 78), and 1 335 015. Hence their structure is: (Even, Even, Odd)!!. ✓*cfc*.

Using the elementary result,

$$nr = n! / \{r!(n-r)!\} = nn - r, \quad (21)$$

and Eq. (5), we have

$$\begin{aligned} \nu_2(2n + 12n + 1 - 2s) &= \nu_2(2n + 12s) \\ &= \nu_2(2n + 12s + 1) \end{aligned}$$

Hence, due to the (odd or even) *parity* of the binomial coefficients (see [13, p. 156], [14, pp. 18–19]), the coefficients of $x^{2n+1-2s}$ and x^{2s+1} in $K_{2n+1}(x)$ have the *same* parity (Sum of Powers = Degree + 1; remember *DegreePower*). Similarly, since $2n2s = 2n2n - 2s$, the coefficient of x^{2s} in $K_{2n}(x)$ has the *same* parity as that of the coefficient of x^{2n-2s} (Sum of Powers = Degree). This then is the reason for the *palindromic* behaviour of the coefficients of $K_n(x)$ with respect to their (odd or even) parity (Pearl

4). The coefficients of $K_n(x)$ nicely produce a parity–palindrome!! Together the coefficients in the numerator of $P_n(x)$ generate a perfect *parity–palindrome* (*P* for *Pascal*, *P_n(x)*, *p – adic*, *Parity*, *Palindrome*, *Polynomial*, *Power*, *Prime*, *Pearl*, *Product*, *Play*)!! When we play with the number of letters in the words in the title, we get the *palindromic* number 628826, pointing at the *palindromic* behaviour of the coefficients of $K_n(x)$, with respect to their parity (odd or even).

4 More Pearls

As $nn = 1 = odd$, the leading coefficient of $K_n(x)$ is always *odd*, irrespective of the degree n . When n is odd, $K_n(x)$ is an odd polynomial in x [1, 2, 3]. Since the coefficient of x corresponds to $n - 2s = 1$ (see Eq. (1)) and since $n1 = n = odd$, this coefficient is also odd. If n is even, $K_n(x)$ has an even parity [1, 2, 3]. As the constant term comes from (22) the constant term of $K_n(x)$ is also odd. Not only the leading coefficient but also the last coefficient of $K_n(x)$ are always *odd*, independent of the (odd or even) nature of n (Pearl # 5). Since the denominator of $P_n(x)$ is $2^{\nu_2(n!)}$ (see Eqs. (2) and (14)), you can now prove that $P_{2k}(x)$ and $P_{2k+1}(x)$, $k \in \mathbb{N}$, have the *same* denominator (Pearl # 6; see Eq. (2)). As $P_n(1) = 1$ [1, 2, 3], the sum of the coefficients of $K_n(x)$, $n \geq 2$, is exactly the denominator of $P_n(x)$ (Pearl # 7; see Eq. (2)). As this sum is even when $n \geq 2$ (see Eq. (5)), the odd-valued coefficients in the numerator of $P_n(x)$, $n \geq 2$, must occur an even number

of times (Pearl # 8; see Eq. (2))!

5 Beauty of the Pascal’s Triangle and Binomial Coefficients

In 1899 Glaisher [13, p. 156] proved the following very interesting result (see also [8, Corollary 2.8, p. 1118], [9, p. 4], [14, p. 24]): *Each one of the Binomial Coefficients $n0, n1, n2, \dots, nn$ is odd iff n has the form $2^Q - 1, Q \in \mathbb{N}$. Thus we have four “lovely lines” from Pascal’s Poem / Triangle (see Table 1)!! It follows from Table 1 that when $n = 2^Q, Q - 1 \in \mathbb{N}$, but for the leading coefficient and the constant term of $K_n(x)$, all the other coefficients (consistent with parity and degree) must be even only (Pearl # 9). In the case of $K_L(x), L = 2^Q - 2, 2^Q - 1, Q \geq 2, Q \in \mathbb{N}$, all the non-zero coefficients of $K_L(x)$ must be odd only (Pearl # 10)!*

Table 1. The structure of the beautiful binomial coefficients nr [8, 9, 13, 14], with

$Q \geq 2, Q \in \mathbb{N}$, belonging to $n = 2^Q - 2$ is: (1, even, odd, ..., even, 1). Alternately, odd and even! The form of the pleasing binomial coefficients corresponding to $n = 2^Q - 1$ is (thanks to Glaisher [13, p. 156]): (1, odd odd, ..., odd, 1). Always odd!! The arrangement of the nice binomial coefficients corresponding to $n = 2^Q$ is: (1, even, even, ..., even, 1). They are even when they are greater than unity. These results follow from the way the Pascal’s Triangle is constructed (3^{rd} Column onwards; $r \geq 1$), “Down (Bottom Row) = (Immediate Up + Immediate Left) (Immediate Top Row)” ($n + 1r = nr + nr - 1$) and the elementary fact that odd \neq + even \neq = odd \neq . Since the binomial coefficient $nn - 2s = nn - (n - 2s) = n2s$, with $2s = \text{even } \# \geq 0$, divides the coefficient of x^{n-2s} in $K_n(x)$, yielding an odd integer upon division, Pascal’s prediction of the parity of Legendre is perfect!! Note: *G* for Glaisher’s result [13, p. 156]; *I* for *Inference* from *G*; *C* for *Corollary* to *G*; *E* for *Even* #; Φ for *Odd* #; $Q \geq 2; Q, n - 1, r + 1 \in \mathbb{N}; 0 \leq r \leq n$.

$n \downarrow \setminus r \Rightarrow$	0	1	2
(I) $2^Q - 2$	1	<i>E</i>	Φ	...	<i>E</i>	1		
($\downarrow G \uparrow$) $2^Q - 1$	1	$\downarrow \Phi \uparrow$	$\downarrow \Phi \uparrow$...	$\downarrow \Phi \uparrow$	$\downarrow \Phi$	$\downarrow 1$	
(C) 2^Q	1	<i>E</i>	<i>E</i>	...	<i>E</i>	<i>E</i>	<i>E</i>	1

Example # 6: Let us gladly check [11] Glaisher’s beautiful result [13, p. 156] by playing with $Q = 3, n = 2^Q - 1 = 7$. The eight binomial coefficients in this case are

1, 7, 21, 35, 35, 21, 7, 1, and all of them are odd, honouring Glaisher! *✓ cfc*. Let us next check our inference from Glaisher (see Table 1). In the case of $n = 2^Q - 2 = 6$, the seven

binomial coefficients are 1, 6, 15, 20, 15, 6, 1. They are alternately odd, even!! Once again Glaisher is honoured!! ✓*cfc*. As far as our Corollary is concerned (see Table 1), in the

case of $n = 2^Q = 8$, the nine binomial coefficients are 1, 8, 28, 56, 70, 56, 28, 8, 1. As long as they are not unity, they are even only. ✓*cfc*. Hail Glaisher [13, p. 156]!!

6 Divisibility by the Binomial Coefficient extended to Laguerre, Hermite, and *modified* Hermite Polynomials!

In the case of the Laguerre Polynomials [1, 2, 3], we have

$$L_n(x) = \sum_{r=0}^n \frac{(-1)^{n-r} n! x^{n-r}}{r! (n-r)! (n-r)!}, \tag{23}$$

$$n! L_n(x) = \sum_{s=0}^n (-1)^s n! s! (n-s)! x^s. \tag{24}$$

Hence the coefficient of $x^s, 0 \leq s \leq n, n+1 \in \mathbb{N}$, in $n!L_n(x)$, is an integer divisible by ns . Let us not forget that our binomial coefficients and factorials are positive integers (see Eqs. (24), (25), (27), (28)). Remember that $n!L_n(x)$ is an integer polynomial [6].

Since the power series expansion of the Hermite polynomials is given by [1, 2, 3]

$$\begin{aligned} H_n(x) &= \sum_{s=0}^{[n/2]} \frac{(-1)^s n! (2x)^{n-2s}}{s! (n-2s)!} \\ &= \sum_{s=0}^{[n/2]} (-1)^s 2^{n-2s} n! (n-2s)! x^{n-2s}, \end{aligned} \tag{25}$$

it is clear that the coefficient of $x^{n-2s}, 0 \leq s \leq [n/2], n+1 \in \mathbb{N}$, in $H_n(x)$, is an integer divisible by the binomial coefficient $n! (n-2s)$. All the Hermite coefficients are *even* when $n \geq 1$.

However, Pascal cannot predict the parity of Laguerre (coefficient multiplied by $n!$) and Hermite (coefficient) perfectly!

By playing with the *modified* Hermite Polynomials [1, p. 189], [10], we have

$$He_n(x) \triangleq 2^{-n/2} H_n(x/\sqrt{2}). \quad (26)$$

Using Eqs. (25) and (26), we find that

$$He_n(x) = \sum_{s=0}^{[n/2]} (-1)^s \times nn - 2s \times \Psi_s \times x^{n-2s}, \quad (27)$$

where

$$\Psi_s \triangleq (2s)!/(2^s s!) = \begin{cases} 1 = \text{odd } \#, & s = 0, 1, \\ 1 \times 3 \times 5 \times \dots \times (2s - 1) = \text{odd } \#, & s - 1 \in \mathbb{N}. \end{cases} \quad (28)$$

As a simple check on Eq. (28) (for $s \geq 2$), $\nu_2(\Psi_s) = 0 \Rightarrow \Psi_s$ is odd. See Eqs. (5) and (6). It follows from Eqs. (27) and (28) that (a) the *modified* Hermite polynomials are integer polynomials [6], (b) the coefficient of x^{n-2s} in $He_n(x)$, an integer, is divisible by the binomial coefficient $nn - 2s$, (c) both of them (*modified* Hermite and Pascal) have the same parity, (d) their ratio is always odd; for $s \geq 2$, this ratio is a product of s consecutive odd positive integers, starting from 1 (multiplied by a phase factor, ± 1), and (e) the nature of the *modified* Hermite is predicted by Pascal as in the case of Legendre!! Hence Legendre too can predict the nature of *modified* Hermite (*1822, †1901)!! Pascal is equally friendly with Legendre and *modified* Hermite!! Let us not fail to note the *French Connection*: French by birth, Pascal, Legendre, Hermite, and Laguerre are world citizens / world-class mathematicians!! Know Pascal (Legendre), know Legendre (*modified* Hermite)!! What Pascal can do for Legendre,

Legendre can do for *modified* Hermite!! Even though Pa (pascal) is a unit of pressure in Physics, Pascal is unable to put pressure on Laguerre and Hermite mathematically!!

7 Completeness can come with a Table

For the sake of completeness, we present a Table of $K_n(x)$, the numerator of the Legendre Polynomial $P_n(x)$, for $2 \leq n \leq 11$ (see Eq. (2); Table 2). Let us note the following: (a) $K_0(x) = 1, K_1(x) = x$, (b) the adjacent coefficients of $P_n(x), n \geq 2$, alternate in sign [15] (Pearl # 11), (c) there are no missing powers [15], consistent with the degree and definite parity of $P_n(x)$ [1, 2, 3] (Pearl # 12). Here is a nice chance for you to enjoy the beauty of our 12 Pearls and check the correctness of our results [11]!! Since the nature of Legendre is predicted by Pascal, we can confidently conclude, from $K_{11}(x)$, that 119 is odd, but

not divisible by 3, nor by 5^2 , nor by 7; 117 is even, but not divisible by 4. *Mnemonic: Legendre by Pascal is always odd!!* The nature (odd or even) of the coefficients of $K_{10}(x)$ and $K_{11}(x)$ is *palindromic* (Pearl # 4): (*Odd, Odd, Even, Even, Odd, Odd*). *✓cfc*. $P_8(x)$ and $P_9(x)$ have the *same* denominator (Pearl # 1, Pearl # 6; see Eq. (2)). *✓cfc*. The sum of the coefficients of $K_8(x)$ is exactly the denominator of $P_8(x)$ (Pearl # 1, Pearl # 7; see Eq. (2)). *✓cfc*. The odd-valued coefficients

of $K_6(x)$, $K_7(x)$, $K_{10}(x)$, and $K_{11}(x)$ are even (= 4) in number (Pearl # 8). *✓cfc*. But for the last and the leading coefficients, all the coefficients of $K_2(x)$, $K_4(x)$, and $K_8(x)$ are even (Pearl # 9), thanks to Glaisher (1899) [13, p. 156]! *✓cfc*. All the coefficients of $K_2(x)$, $K_3(x)$, $K_6(x)$, and $K_7(x)$ are odd (Pearl # 10); thank you Glaisher!! *✓cfc*. The adjacent coefficients of $P_{10}(x)$ alternate in sign (Pearl # 11) [15]. *✓cfc*. All the odd powers of x , right from 1 up to 11, are present in $P_{11}(x)$ (Pearl # 12) [15]. *✓cfc*.

Table 2. Table of the Polynomials $K_n(x) = 2^{\nu_2(n!)}P_n(x)$, $2 \leq n \leq 11$. $K_n(x)$ is the numerator of $P_n(x)$. Column 2 is the ratio $K_n(x)/P_n(x)$, the denominator of $P_n(x)$ (see Eq. (2)).

n	$2^{\nu_2(n!)}$	Integer Polynomial $K_n(x)$, the numerator of $P_n(x)$
2	2	$3x^2 - 1$
3	2	$5x^3 - 3x$
4	8	$35x^4 - 30x^2 + 3$
5	8	$63x^5 - 70x^3 + 15x$
6	16	$231x^6 - 315x^4 + 105x^2 - 5$
7	16	$429x^7 - 693x^5 + 315x^3 - 35x$
8	128	$6435x^8 - 12012x^6 + 6930x^4 - 1260x^2 + 35$
9	128	$12155x^9 - 25740x^7 + 18018x^5 - 4620x^3 + 315x$
10	256	$46189x^{10} - 109395x^8 + 90090x^6 - 30030x^4 + 3465x^2 - 63$
11	256	$88179x^{11} - 230945x^9 + 218790x^7 - 90090x^5 + 15015x^3 - 693x$

You can also nicely play similarly with a Table of the *modified* Hermite Polynomials [10]. You can definitely enjoy how *modified* Hermite follows *Legendre* faithfully!! Thus, the nature (odd or even) of the coefficients of $He_{10}(x)$ and $He_{11}(x)$ is *palindromic* (Pearl # 4): (*Odd, Odd, Even, Even, Odd, Odd*). *✓cfc*. The odd-valued coefficients of $He_6(x)$,

$He_7(x)$, $He_{10}(x)$, and $He_{11}(x)$ are even (= 4) in number (Pearl # 8). As a simple corollary, $He_n(1), n \geq 2$, is *even!!* *Mathematica* says:

$$\begin{aligned}
 He_{10}(x) = & x^{10} - 45x^8 \\
 & + 630x^6 - 3150x^4 \\
 & + 4725x^2 - 945. \quad (29)
 \end{aligned}$$

Example # 7: $He_{10}(1) = 1216 =$

even. ✓ *cfc*. With $n = 10$ and $n - 2s = 2$, coefficient of $x^2/102 = 4725/45 = 105 = 1 \times 3 \times 5 \times 7$, a product of $s (= 4)$ consecutive odd integers. ✓ *cfc*. See Eqs. (28) and (29). *Modified Hermite by Pascal is always odd!!*

Using the Differential Recurrence Relation, $DHe_m(x) = m He_{m-1}(x)$, $D \triangleq d/dx$, $m \in \mathbb{N}$, you can generate, from Eq. (29), a Table of $He_n(x)$, $0 \leq n \leq 9$, and enjoy the beauty of our Pearls. Thus, all the even powers of x , right from 0 up to 8, are present in $He_8(x)$ (Pearl # 12). All the coefficients of $He_7(x)$ are odd (Pearl # 10), thanks to Glaisher [13].

8 Conclusion

The (non-zero) coefficient of x^s in $\Phi_n(x)$, an integer polynomial [6], is divisible by the associated binomial coefficient, ns , when $\Phi_n(x) = 2^{\nu_2(n!)} P_n(x), n! L_n(x), H_n(x), He_n(x)$. The Chebyshev Polynomials [2, 3], $T_n(x)$, $n \geq 4$, do *not* satisfy this divisibility property in general. If you want to search for more pearls, you have to dive below the (common) denominator and the divisibility of (common denominator times) Legendre (coefficient) by Pascal (binomial coefficient)!! *D* for *Dive*, *D* for *Denominator*, *D* for *Divisibility*!! We have checked the correctness of our results [11] for $P_n(x)$, using *Mathematica* (for $2 \leq n \leq 150$; $2 \leq p \leq 97$); in the case of $He_n(x)$, we have checked [11] the divisibility for $2 \leq n \leq 150$. We can relish Legendre (Polynomials) with Legendre (Eq. (5)), Pascal, Kummer, Holt [5], and Glaisher [13]!! *Blessed are those who are friendly with the Legendre Polynomials and the modified Hermite Polynomials!!*

Acknowledgment

BVJ would like to thank the UGC for the award of a Maulana Azad National Fellowship. This work has been classroom tested and we are extremely grateful to our nice M. Sc. (Physics) and M. Phil. (Computer Science) Students, University of Madras, for their encouraging response. We thank Prof. Dr Rita John, Dr D. Nedumaran, and Prof. Dr P. Thangavel, University of Madras, and Prof. Dr Ranabir Chakrabarti, Chennai Mathematical Institute, for their constant support. It is a pleasure for PRS and AJL to thank Ms. M. Sumathi for her kind help, support, and valuable suggestions. With all humility, we would like to dedicate this work to Dr J. W. L. Glaisher [13], J. B. Holt [5], Prof. Dr E. E. Kummer, A. M. Legendre, B. Pascal, and Prof. Dr Stephen Wolfram (*Mathematica*).

References

- [1] E. D. Rainville, *Special Functions*, Macmillan, New York, 1960.
- [2] W. W. Bell, *Special Functions for Scientists and Engineers*, Van Nostrand, London, 1968; Dover, New York, 2004.
- [3] G. B. Arfken and H. J. Weber, *Mathematical Methods for Physicists*, 5th Edition, Harcourt (India), New Delhi, 2001.
- [4] V. Devanathan, *Angular Momentum Techniques in Quantum Mechanics*

- (Kluwer, Dordrecht, 1999); *Quantum Mechanics*, 2nd Edition (Narosa, New Delhi, 2012); *Nuclear Physics*, 2nd Edition (Narosa, New Delhi, 2013).
- [5] J. B. Holt, On the irreducibility of Legendre polynomials I, *Proc. London. Math. Soc.* **11** ser. 2 (1912) 351–356. For Errata, see *ibid.* **12** ser. 2 (1912) 126–132.
<http://plms.oxfordjournals.org/content/s2-11/1/351.full.pdf>
<http://plms.oxfordjournals.org/content/s2-12/1/126.full.pdf>
- [6] E. W. Weisstein, “*Integer Polynomial.*” From *MathWorld—A Wolfram Web Resource.*
<http://mathworld.wolfram.com/IntegerPolynomial.html>
- [7] B. Sury, Revisiting Kummer’s and Legendre’s formulae, *Resonance* **10** (2005) 62–66.
<http://www.ias.ac.in/article/fulltext/reso/010/02/0062-0071>
- [8] D. Mihet, Legendre’s and Kummer’s theorems again, *Resonance* **15** (2010) 1111–1121.
<http://www.ias.ac.in/article/fulltext/reso/015/12/1111-1121>
- [9] A. Granville, Binomial coefficients modulo prime powers, pp. 1–24.
<http://www.dms.umontreal.ca/~andrew/PDF/BinCoeff.pdf>
- [10] E. W. Weisstein, “*Hermite Polynomial.*” From *MathWorld—A Wolfram Web Resource.*
<http://mathworld.wolfram.com/HermitePolynomial.html>
- [11] P. R. Subramanian, Culture of checking the correctness of calculations, *Phys. Educ. (India)* **8** (1992) 387.
- [12] See, for example, B. Kolman, R. C. Busby, and S. C. Ross, *Discrete Mathematical Structures*, 6th Edition (Pearson Prentice–Hall, New Delhi, 2009).
- [13] J. W. L. Glaisher, On the residue of a binomial–theorem coefficient with respect to a prime modulus, *Quart. J. Pure Appl. Math.* **30** (1899) 150–156. Thanks to *Niedersaechsische Staats- und Universitaetsbibliothek Digitalisierungszentrum, 37070 Goettingen, Germany.* Email: gdz@www.sub.uni-goettingen.de
http://gdz.sub.uni-goettingen.de/dms/load/pdf/?PPN=PPN600494829_0030&DMDID=DMDLOG_0007
- [14] Chapter 4, Binomial Coefficients, October 6, 2009, pp. 1–61.
<http://www.cs.columbia.edu/~cs4205/files/CM4.pdf>
- [15] P. R. Subramanian, On the adjacent coefficients of certain real orthogonal polynomials, *Eur. J. Phys.* **8** (1987) 149–150.
http://www.iopscience.iop.org/0143-0807/8/2/116/pdf/0143-0807_8_2_116.pdf

Comparative Analysis of M 3 and NGC 2420 using SDSS Data

Shishir Khandelwal and Saurabh Nangia

Department of Physics and Astrophysics
University of Delhi,
New Delhi-110007

(Submitted : 10-08-2015)

Abstract

The Sloan Digital Sky Survey (SDSS) is an ambitious astrophysical survey that has obtained photometric and spectroscopic data for millions of objects in the universe. In this article we explain the use of SDSS to obtain astrophysical data. We also introduce an indispensable tool for astronomers – H-R Diagrams, in particular, Colour-Magnitude Diagrams (CMDs). Using SDSS data, we plot three CMDs each for star clusters Messier 3 and NGC 2420 and qualitatively analyse their properties. The entire process of our analysis is explained in this article. We hope it will interest undergraduate students particularly the ones interested in astronomy and astrophysics.

1. Introduction

The Sloan Digital Sky Survey (SDSS) is one of the largest astronomical surveys ever undertaken. Photometric and spectroscopic observations were made over a period of eight years using a 2.5 metre wide-angle telescope along with an array of CCDs and a pair of spectrographs, at the Apache Point Observatory in New Mexico, United States. The CCDs captured high resolution images in 5 different colours, while the spectrographs allowed the spectra of 640 objects to be studied simultaneously.

Though the survey obtained individual astrophysical data on millions of objects including stars, galaxies and quasars, the ultimate task of the survey was to connect this data and create a 3D map of a part of the universe. An advanced image processing software was used to analyse the properties of hundreds of millions of objects to provide insights into the large scale structure of

the universe. This is necessary to understand the evolution of the universe over billions of years since the big bang.

SDSS has made all collected astrophysical data public via the internet and data from their newer projects is being released till date. It is free to use for non-commercial purposes by anyone from school students to scientists and is accessible through a variety of tools including an internal SQL server. SDSS has also provided a variety of suggested research projects for interested students. As a demonstration, in this paper we use SDSS data to plot CMDs for two well-known star clusters - Messier 3 and NGC 2420. The entire process of acquisition of data from the SDSS database is explained. A brief qualitative analysis of the CMDs is also included.

2. Hertzsprung-Russell Diagrams

Astronomers have speculated about the life cycle of a star since centuries. Despite having access to

large amounts of meticulously recorded data, the first real progress in our understanding of the nature of the life processes of a star came only in the early parts of the 20th century when *Ejnar Hertzsprung* and *Henry Norris Russell* independently devised what are today known as Hertzsprung-Russell Diagrams (H-R Diagrams). These diagrams are powerful tools and remain to be one of the most widely employed devices in modern astronomy for understanding stellar evolution.

An H-R Diagram, in essence, is a 2-dimensional plot of temperature and luminosity for a group of stars. An individual star is represented as a point in the diagram. However, every star is a dynamic object and undergoes significant changes in its lifetime. As it does so, the point moves around in the diagram. By observing these changes, there is a lot that can be understood about the internal mechanisms of a star. Such processes, however, happen over billions of years and hence, instead of plotting a single star and studying its evolution, several hundreds of stars at different stages in their life cycles are plotted on the same diagram and analysed.

To plot the position of a star on an H-R Diagram, its temperature and luminosity need to be measured. However, the temperature cannot be measured directly. Instead, the spectrum of the star is first obtained by measuring the flux at each particular wavelength. Then by approximating the star to be a blackbody, its effective temperature can be determined. For measuring the luminosity, the combined flux received by us on the earth for all the wavelengths is measured to determine the star's apparent brightness. This is combined with the distance measured to the star, through parallax measurements, to get its true luminosity.

In practice, it is easier to obtain the flux for only a few wavelengths rather than for the entire spectrum. The SDSS, for instance, employs only 5 filters: two in visible; g(4770Å) and r(6231Å), two in infrared; i(7625 Å) and z(9134 Å) and one in

ultraviolet; u(3543 Å). The data obtained can be used to prepare a variant of an H-R Diagram. On the luminosity axis, the Magnitude¹(represented by capital letters; for example G for filter g) associated with an individual filter is taken and on the temperature axis, the Colour Index². The diagram obtained, though not exactly the same, is equivalent to an H-R Diagram and is called a Colour-Magnitude Diagram (CMD). Similarly, other variants of H-R Diagrams exist too and are widely employed.

H-R Diagrams find their greatest utility when used for studying star clusters. Several factors contribute to this. Firstly, all the stars in a cluster are assumed to be formed from the same interstellar gas cloud and thus are assumed to have the same chemical composition. Further, they are all formed within a few million years (an insignificant period at the time scales involved) of each other and hence can be assumed to be of the same age. Thus, stars in a cluster differ significantly in only one aspect: their mass. Thus, an H-R Diagram for a cluster can help astronomers understand how the mass of a star affects its life processes. Another factor that makes H-R Diagrams of star clusters so important is the fact that all the clusters in the galaxy seem to have the same relative distribution of stellar masses described by the stellar Initial Mass Function (IMF). Thus, by studying one star cluster, we gain insight about others as well. This can be used to determine important information about a given cluster such as its age, its distance, etc. Finally, from a practical viewpoint, star clusters are useful because all the stars in a cluster are roughly at the same distance from us. This eliminates the need to determine the absolute magnitude of brightness for the stars. Instead, the apparent magnitudes may directly be used. Thus, there is no need to measure the distance to a particular star which often proves to be the most difficult quantity to obtain. In this paper, we shall be studying two star clusters: Messier 3 and NGC 2420.

Having seen why star clusters are so important, we briefly digress from our discussion about H-R Diagrams to discuss certain important points about such clusters. From observations, it is found that there are broadly two categories of star clusters - globular clusters and open clusters. The members of each category are held together through their mutual gravitational attractions. However, significant differences exist. Messier 3 represents

a typical globular cluster and NGC 2420 belongs to the class of open clusters. Given below are inverted colour images³ obtained from the SDSS Navigation Tool of the two clusters for comparison.

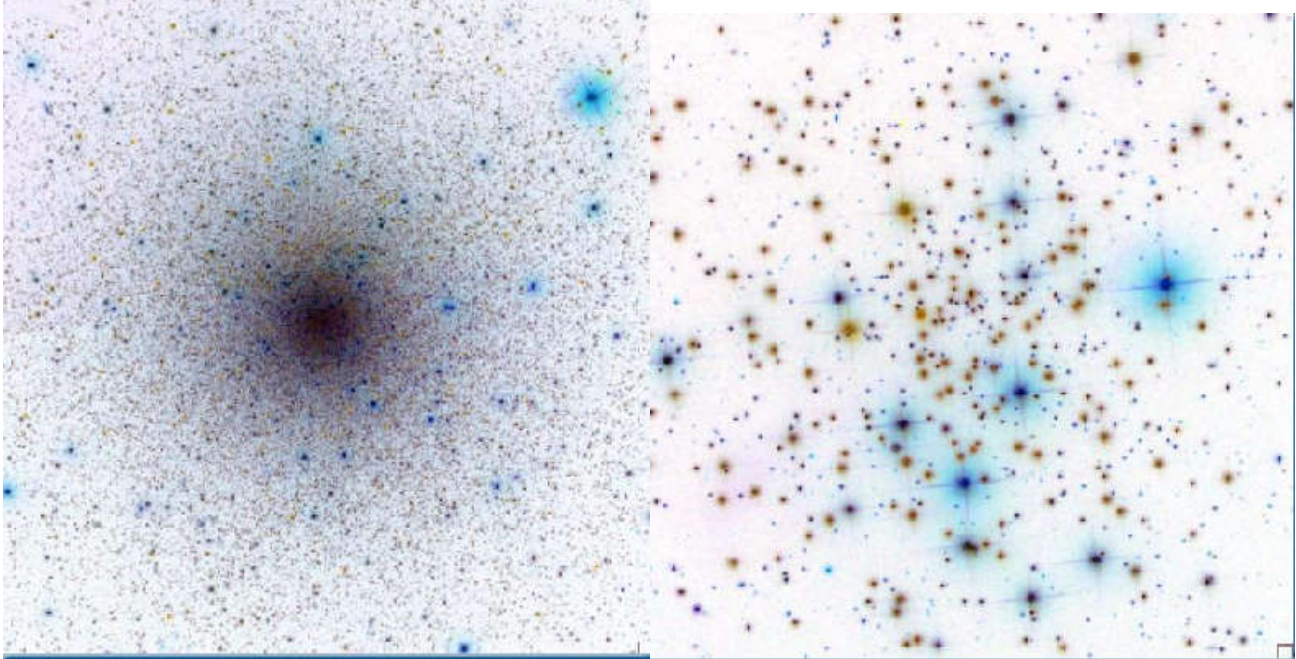


Figure 1: Inverted Colour Images of Messier 3 (left) and NGC 2420 (right) obtained using SDSS Navigation Tool

A typical globular cluster is massive, containing hundreds of thousands of stars tightly bound together forming a relatively dense spherical distribution as can be seen in the image for Messier 3 in Figure 1. An important feature of globular clusters is their age. From spectroscopic analysis it is observed that the members of a globular cluster have a low abundance of heavy elements. In its early stages the universe was mostly made up of Hydrogen and Helium (it still is dominated by them) and so the earliest stars were mainly composed of only these elements; the heavy elements were only formed later through fusion reactions in the cores of stars. Therefore, the low abundance of metals in stars in globular clusters

suggests that these stars were formed when the universe was relatively young. In fact, globular clusters are believed to be amongst the oldest observable structures of the universe. For a typical globular cluster, an age of at least 10 billion years is estimated.

Open clusters differ in several important ways. Typically they only contain a few thousand stars and do not possess any definite shape. They are only loosely held together and hence as they get older, the members tend to drift apart and the cluster “dissolves”. Thus, an open cluster is not expected to be too old. This is confirmed by spectroscopic studies which show that the

members of these clusters are vastly richer in heavier element abundances. These stars could not have been formed along with the earliest generations of stars. Typically, an open cluster is estimated to be only a few hundred million years old, though some have been shown to be a few billion years old.

These differences between the two clusters lead to interesting characteristic features in the H-R

Diagrams for each. We shall see this clearly once we have plotted our diagrams.

We now return to our general discussion about H-R Diagrams. In Figures 2(a) and 2(b), we represent broadly the important features of a typical H-R Diagram. Figure 2(a) labels the most important regions and Figure 2(b) depicts how the H-R Diagram of a given cluster evolves with time.

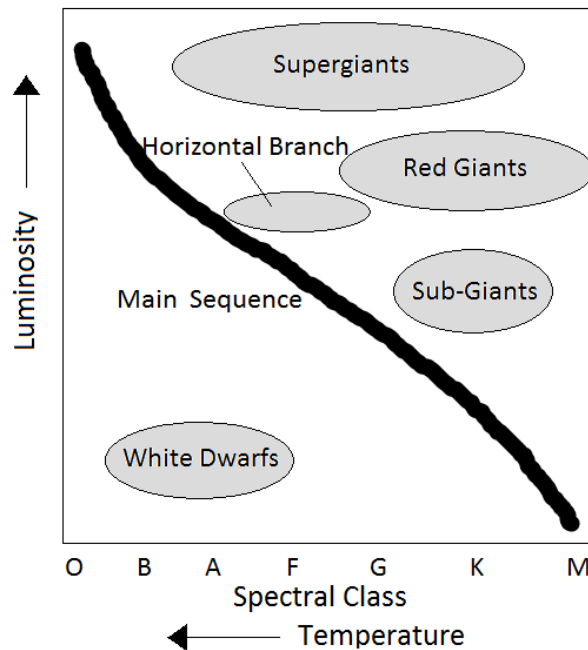


Figure 2(a): Important Regions of an H-R Diagram⁴

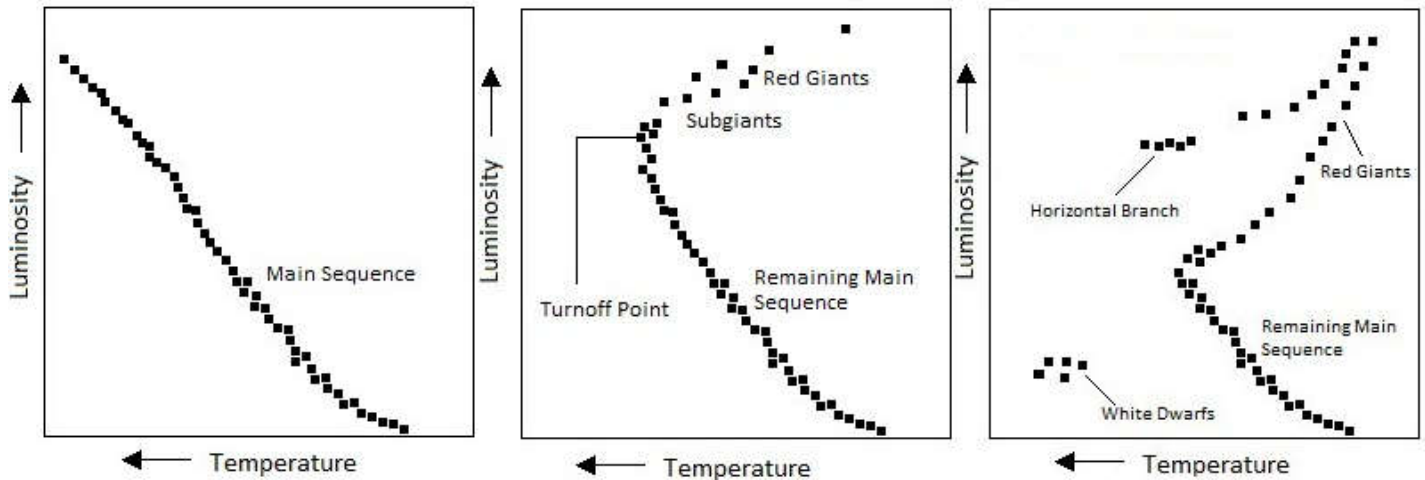


Figure 2(b): Evolution of the H-R Diagram of a cluster (time evolves as we go from left to right)

1. The most noticeable feature of any H-R Diagram is that a large number of the stars seem to be located on a diagonal curve across the graph. This region is called the main sequence. There are steady and continuous nuclear reactions in the main sequence stars and energy is produced by conversion of hydrogen into helium. The radiation pressure so generated prevents the star from collapsing under its own gravity. Along the main sequence, the position of a star depends mostly on its initial mass with the more massive ones lying higher up the diagonal. Also, the position of an individual star changes only negligibly during this stage. So, as long as a star is on the main sequence (a period that constitutes a majority of its lifetime), it remains practically stationary on the H-R Diagram. However, this cannot carry on forever - stars evolve and the details depend mainly on the initial mass M of the star. The energy stored in a star is roughly proportional to M and the rate at which it expels this energy is roughly proportional to M^4 . This means that the time a heavy star would spend on the main sequence is much less than time a light star would (the approximate variation is $t \propto M^{-3}$). The M^4 variation breaks down for extremely massive or

extremely light stars but the general rule that more massive stars evolve more rapidly still stands. Depending on the initial mass of the star, its main sequence lifetime can vary from just a few million years to hundreds of billions of years.

2. When hydrogen is depleted in the stellar core, because of the reduced nuclear fusion, the internal production of thermal energy can no longer balance the gravitational interaction and the main sequence star begins to contract. This in turn causes the core to heat up. The increased core temperature causes the outer layers of the star to expand. This leads to the star entering the “Red Giant” phase. As it expands, the temperature drops due to its larger surface area, and thus its peak wavelength shifts towards orange. Despite being cooler than main sequence stars, red giants, due to their greater size, are much more luminous than the red stars on the main sequence. They lie on the upper right corner of the diagram. Compared to the main sequence lifetime of a star, its transition period to the red giant phase is quite small. As we can see in Figure 2(b), as time evolves more and more stars begin to enter this stage and there is an abrupt turning point to the main sequence diagonal leading into the red giant region. After plotting H-

R Diagrams for Messier 3 and NGC 2420, we shall see how the age of a cluster can be estimated by noting the position of this turning point.

3. When nuclear fuel is completely depleted from a star's core, the gravitational attraction is no longer balanced by the production of thermal energy. The star contracts. Since electrons obey the Pauli Exclusion Principle, an electron degeneracy pressure builds. It balances out the gravitational attraction if the mass of the star is less than Chandrasekhar's limit. These stars are much less luminous than the blue stars in the main sequence and thus are much smaller in size. They are called White Dwarfs and lie on the bottom left of Figures 2(a) and 2(b).

We note that apart from these three main stages of stellar evolution, there are several other sub-stages that an individual star may go through. For example, Figure 2(a) shows the Horizontal Branch region and the Supergiant region. Both of these are occupied by stars that are in between the red giant and the white dwarf phases. Similarly, the Subgiant stage occurs just before the red giant phase. Other regions, not shown in Figure 2(a), such as the Planetary Nebula region, Asymptotic Giant Branch, etc. are also of interest. For details, refer to [1].

It is important to mention that our discussion above is only valid for stars with average masses. In massive stars, helium ignition causes them to expand, reducing the temperature. The red supergiant thus formed collapses in a supernova. Depending upon the initial mass of the star, a neutron star or a black hole may be formed.

3. SDSS Search Tools

A variety of tools are available on the SDSS website that allow users to extract data on any of the hundreds of millions of objects that have been covered by the survey. These are:

1. Navigation Tool[10]: It allows users to navigate in the vicinity of a point in the sky by entering its coordinates (RA and Dec⁵). An image of the vicinity of that point is seen on the screen. One can obtain all the available data for any object in the frame by selecting it and clicking on 'explore'. Spectra of select objects are also available. A disadvantage of this tool is that data has to be collected individually for all objects. Figure 3 shows the SDSS Navigation Tool.

2. Radial Search Tool[11]: It allows users to search for data on all objects around a certain point, within a certain radius. A major advantage, of course, is that data for hundreds, even thousands of objects can be obtained through just a single search. Search for data is restricted by setting a particular radius and limiting values of colour magnitudes (U, G, R, I, Z). A major disadvantage of this tool is that it searches for any object in the vicinity of the given point. So, the data it provides may contain unwanted objects. For example, in a search for stars in a cluster, it may add galaxies that appear in the vicinity of the given point. Figure 4 shows the SDSS Radial Search Tool.

3. SDSS SQL Search Tool [13]: It allows the user to write SQL queries to search for the required data. It can be used to make very precise searches that only return the data the user wants without including unwanted results. This is the tool that we used to obtain the data required for the CMDs of Messier 3 and NGC 2420. The details are explained in the next section.

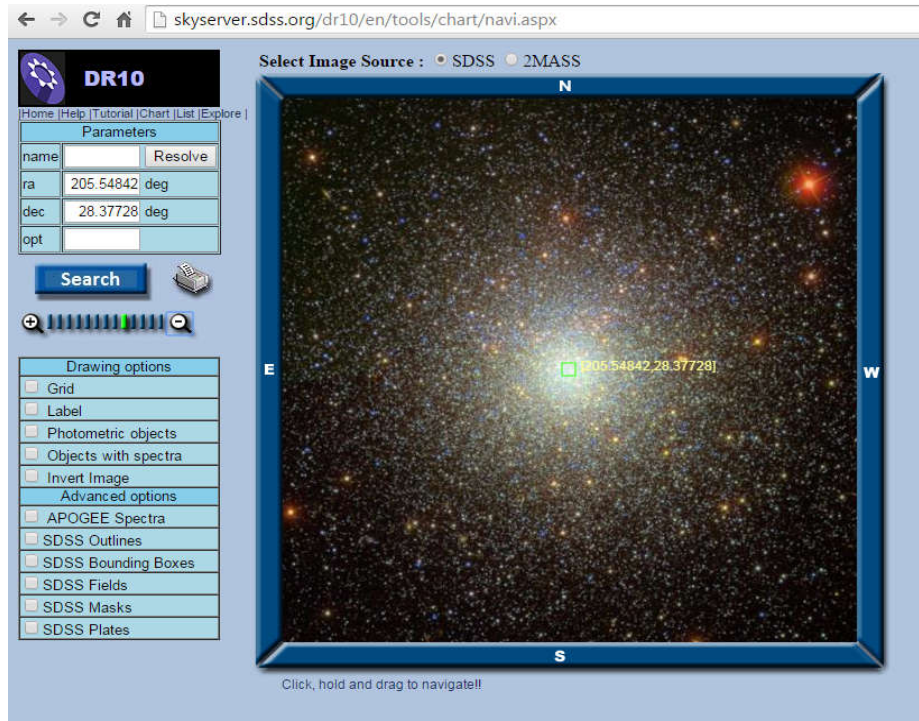


Figure 3: DR10 Navigation Tool Showing M3



Figure 4: DR10 Radial Search Tool with M3 coordinates entered

4. Data for Messier 3 and NGC 2420

For acquiring the data for the clusters, we made use of SDSS's Data Release 10. We first obtained the RA and Dec values for Messier 3 and NGC 2420 which can easily be found from any astronomy catalogue. By entering these values in the SDSS Navigation Tool, we obtained an image for both the clusters. The image was used to obtain an estimate for the apparent diameter of the cluster which is its spatial extension as seen from the earth. The values used are:

Messier 3:

Right Ascension = 205.54842°

Declination = 28.37728°

Apparent Radius = 9 arcmin

NGC 2420:

Right Ascension = 114.59958°

Declination = 21.57409°

Apparent Radius = 6 arcmin

The SDSS database contains information on millions of objects and has been organised into tables, each dedicated to data of a specific type. The data can be accessed by writing SQL queries. A complete description of the various tables and their contents can be found at[12]. Once the data required has been identified, the query may be written in the SDSS SQL Search Tool provided at[13]. We used two SQL queries, one for extracting the data for Messier 3 and the second one for extracting the data for NGC 2420.

Query for Messier 3

```
select
s.objid, s.ra, s.dec, s.u, s.g, s.r, s.i, s.z
```

```
from
star s,
dbo.fGetNearbyObjEq(205.54842, 28.37728,9) n
```

```
where
s.objid = n.objid
```

Query for NGC 2420

```
select
s.objid, s.ra, s.dec, s.u, s.g, s.r, s.i, s.z
```

```
from
star s,
dbo.fGetNearbyObjEq(114.59958,21.57409,6) n
```

```
where
s.objid = n.objid
```

The SQL queries have three parts:

1. Under 'select', we specified the data that we wanted the particular query to return. In the above queries, we instructed the system to return the following information: object ID (objid), Right Ascension (RA), Declination (Dec), and magnitudes.
2. Under 'from', we specified the tables that contain the data to be returned. In the above queries, we instructed the system to search in the table called 'star'. This ensured that only data for stars is returned and not for other objects. We also employed the function `dbo.fGetNearbyObjEq` which accepts three arguments (a, b, c). It works by creating a temporary table based on the arguments entered and can be used to return the required data for all stars within a radius of 'c' arcmin around the point with RA 'a' and Dec 'b'. For example, in the Query for Messier 3, we specified the region within a radius=9 arcmin around the point with RA=205.54842° and Dec=28.37728°. All the stars (not other objects) within this region were thus returned by the query.
3. Under 'where', we specified the constraints that we wished to impose on the returned data. For the above queries, the condition imposed ensured

that both the table ‘star’ and the one generated by the function `dbo.fGetNearbyObjEq` contained the same data.

A comprehensive tutorial for writing SQL queries on SDSS may be found at [14].

The data for the analysis was obtained in CSV format and analysis was done in Excel®.

5. Results

Shown in the following pages are the CMDs for NGC 2420 and Messier 3 obtained using the data extracted from SDSS. We plotted three diagrams for each cluster: R vs $G-R$, G vs $R-Z$ and U vs $G-I$. These quantities simply represent the luminosity vs temperature variation with temperature decreasing along the positive direction of X-axis (increasing $G-R$, $R-Z$ and $G-I$) and luminosity increasing along the positive direction of Y-axis (decreasing R , G and U).

The screenshot shows the SkyServer DR10 SQL Search interface. The browser address bar displays `skyserver.sdss.org/dr10/en/tools/search/sql.aspx`. The page header includes the Sloan Digital Sky Survey III logo and navigation links: Home, Data, Schema, Education, Astronomy, SDSS, Contact Us, Download, Site Search, and Help. The main content area is titled 'SQL Search' and contains a text input field with the following SQL query:

```
select
s.objid, s.ra, s.dec, s.u, s.g, s.r, s.i, s.z
from
star s,
dbo.fGetNearbyObjEq(205.54842, 28.37728, 9) n
where
s.objid = n.objid
```

Below the query input, there is a 'Submit' button, a 'Check Syntax Only?' checkbox, and an 'Output Format' section with radio buttons for HTML, XML, CSV (selected), JSON, VOTable, and FITS. A 'Reset' button is also present. The page includes several informational paragraphs and links to help pages.

Figure 5: DR10 SQL Search with Query for M3 (Output format CSV is selected)

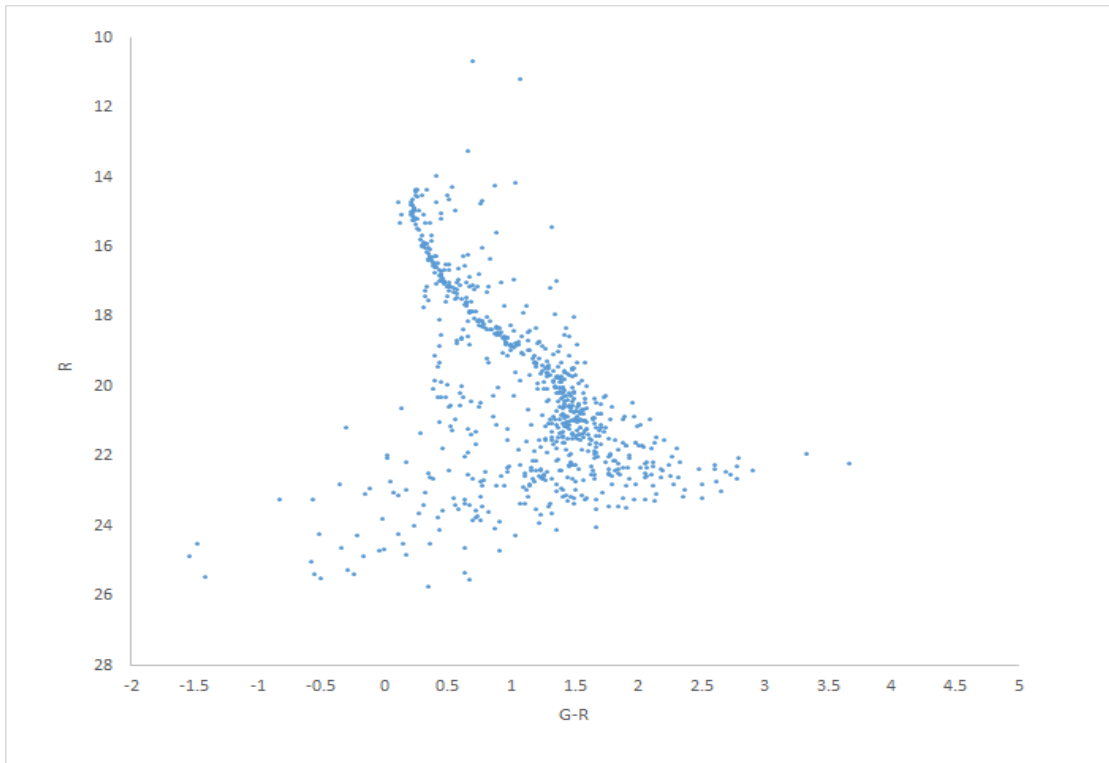


Figure 6: R vs G-R CMD for NGC 2420

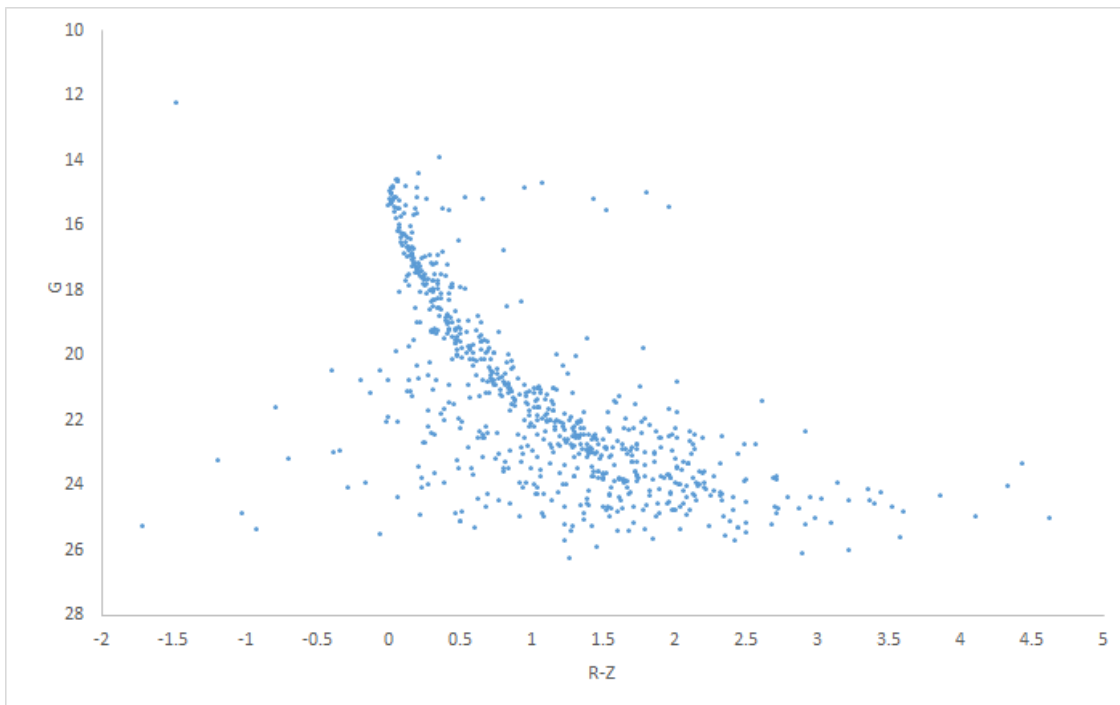


Figure 7: G vs R-Z CMD for NGC 2420

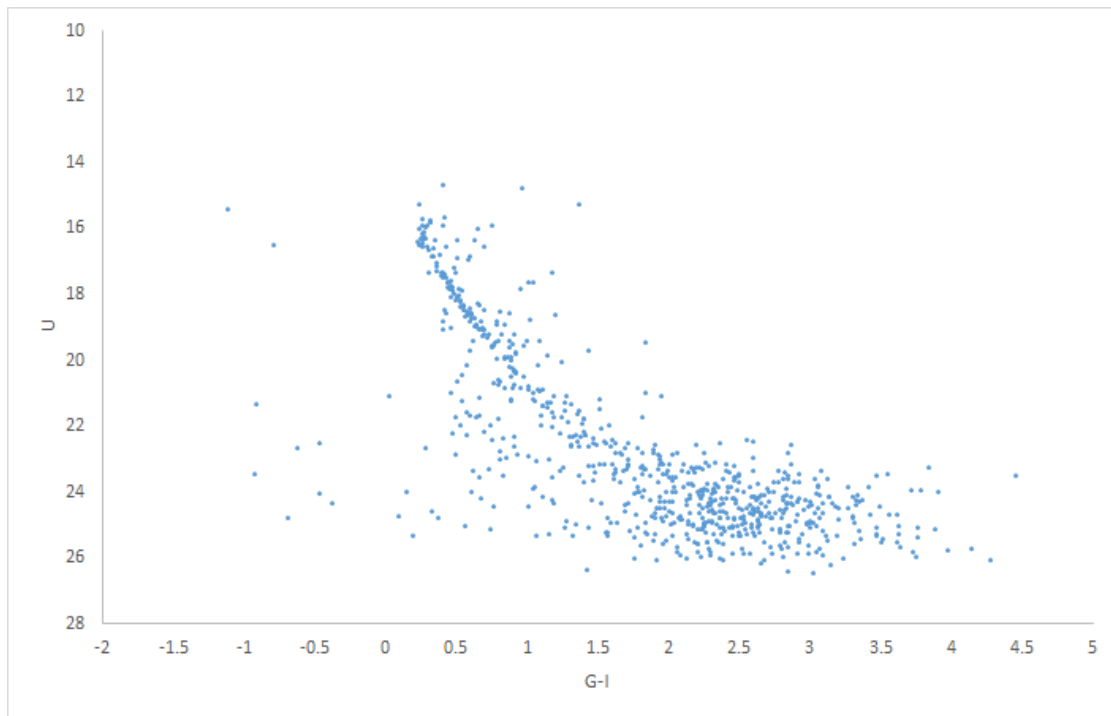


Figure 8: U vs G-I CMD for NGC 2420

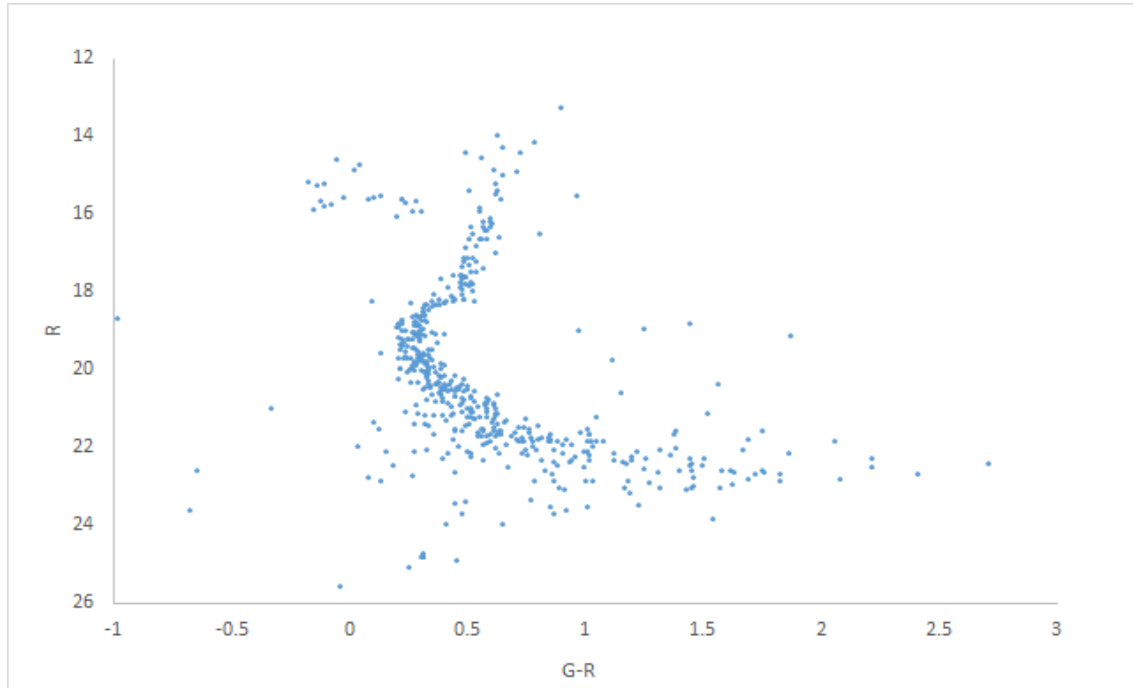


Figure 9: R vs G-R CMD for Messier 3

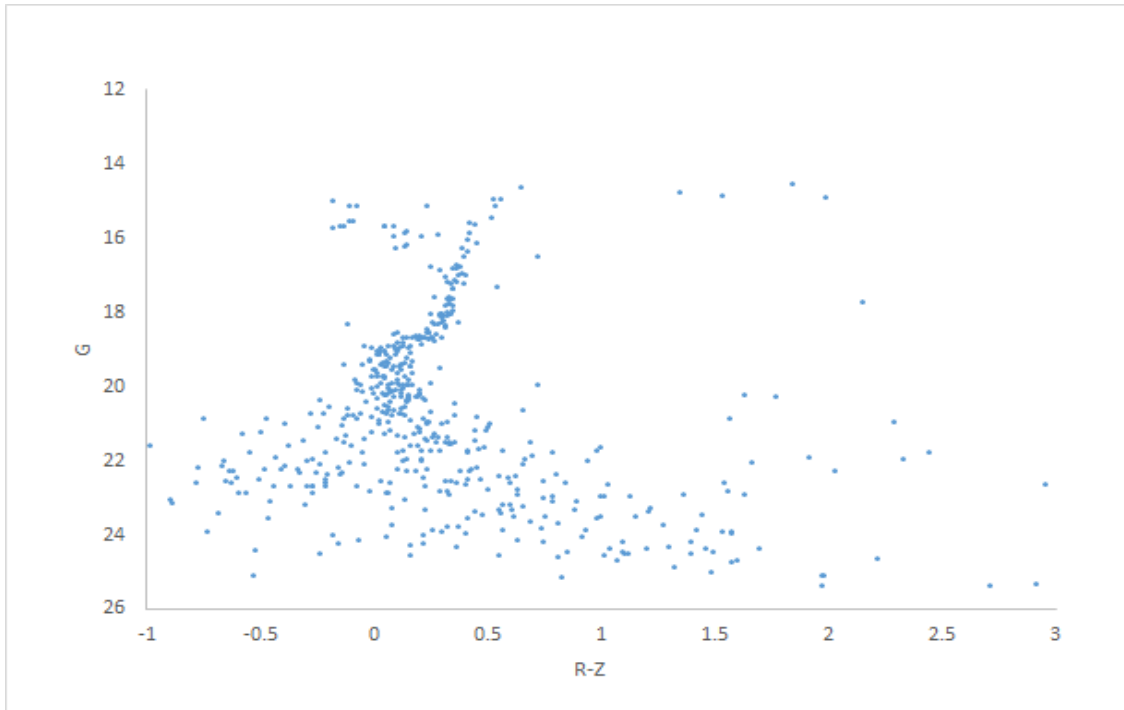


Figure 10: G vs R-Z CMD for Messier 3

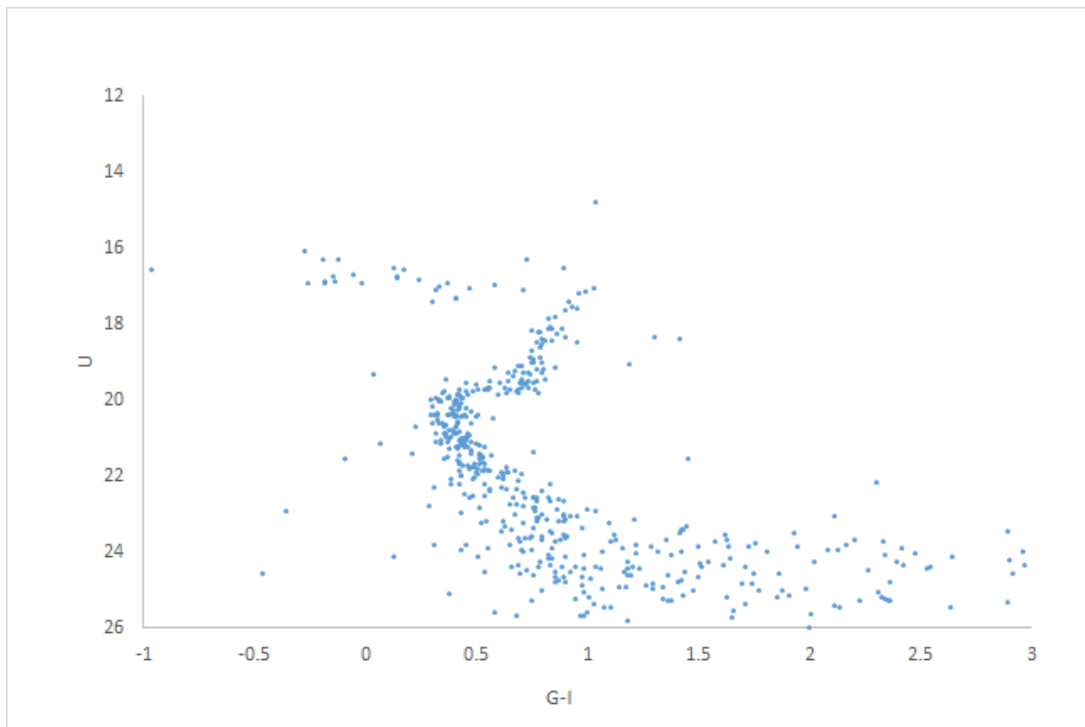


Figure 11: U vs G-I CMD for Messier 3

6. Analysis

Our diagrams clearly show the main sequence for both the clusters. For NGC 2420, it is the most prominent feature with almost the entire population occupying it, from the more massive stars to the lesser ones. For Messier 3, however, the more massive stars seem to be missing and the main sequence region only seems to extend up to the stars with lesser mass.

The diagrams represent typical features to be expected in the CMD of an open and a globular cluster respectively. To see why, we need to consider what we had discussed above. NGC 2420, and open clusters in general, are young. Most of their stars are still in their Hydrogen-burning stage in which they spend the major part of their lives. These stars are found along the main sequence band. In fact, the young age of the cluster means that some of the least massive stars of the cluster are yet to even enter the main sequence region and are called Pre-Main Sequence stars (PMS stars). It is only the most massive stars that have had enough time to evolve out of the main sequence as they have burned up all their Hydrogen (the fate that awaits these is a catastrophic one - a supernova explosion; however, for this discussion we are more interested in the evolution of the cluster as a whole, rather than that of individual stars). Now, as time progresses, the CMD for a cluster undergoes changes. The PMS stars also enter the main sequence region but more prominently, more and more stars begin to leave it and enter the red giant region. The point on the CMD at which the stars just begin to leave the main sequence is called the turn-off point. For older clusters, this point corresponds to successively lower mass stars.

We can clearly see the turn-off point in the CMD for Messier 3. Also, the red giant region is significantly populated. These are features that are missing from the CMD of NGC 2420. This can again be understood by considering the age of Messier 3. Because globular clusters are quite old, many of their stars have used up all their Hydrogen and moved out of the main sequence region. Indeed, the most massive ones evolved first and underwent supernovae explosions, but with time stars with lower masses too have burned through their hydrogen reserves. These stars don't possess enough mass to undergo violent explosions; rather they enter a new phase of generating energy through Helium-burning and become red giants. Eventually, these stars will end up as white dwarfs - their final evolutionary state.

There are two more important features that may be seen in the CMD of Messier 3. One is the presence of the horizontal branch region. This region is occupied by stars not having too high masses immediately after they evolve out of the red giant phase. Again, this represents aging and it is a characteristic feature of old clusters and hence, we cannot find it in the CMD for NGC 2420. Finally, there is the white dwarf region. Globular clusters such as Messier 3 contain several white dwarfs.

As we mentioned before, CMDs can be used to determine important information about a cluster. Before concluding, we briefly mention one such possible extension to this work - using a CMD to determine a cluster's age. Through the knowledge of internal stellar mechanisms of energy generation, observations of metallicity for the cluster whose age is to be found, the stellar initial mass function, etc. astrophysicists can generate theoretical CMDs corresponding to different ages using computer simulations. These are known as isochrones. By comparing these isochrones to the

observed data, the best fit can be determined. This gives an estimate of the age. From such estimates (as well as other techniques), the age of NGC 2420 is estimated to be about 2 billion years [8], whereas that for Messier 3 is estimated to be about 11.39 billion years [9].

7. Conclusion

We have prepared and analysed Colour-Magnitude Diagrams for Messier 3 and NGC 2420 and used them to illustrate the differences between globular and open clusters. We have demonstrated how the data was obtained from SDSS; one important point to note is that our method of data acquisition cannot differentiate between stars that are actually members of a particular cluster and stars that just happen to be in the same field of view. This can lead to some non-member stars being plotted in the CMDs. Perhaps this explains why we see certain unexpected features such as the presence of some stars in the white dwarf region for NGC 2420. However, the diagrams still bring out the most important features for each cluster. We hope our work shows how SDSS can be an extremely useful resource, particularly for undergraduate students who can use the platform to pursue a number of independent research projects.

8. Acknowledgements

Funding for SDSS-III has been provided by the Alfred P. Sloan Foundation, the participating institutions, the National Science Foundation, and the U.S. Department of Energy Office of Science. The SDSS-III web site is <http://www.sdss3.org/>. SDSS-III is managed by the Astrophysical Research Consortium for the participating institutions of the SDSS-III Collaboration including the University of Arizona, the Brazilian Participation Group, Brookhaven National

Laboratory, Carnegie Mellon University, University of Florida, the French Participation Group, the German Participation Group, Harvard University, the Instituto de Astrofísica de Canarias, the Michigan State/Notre Dame/JINA Participation Group, Johns Hopkins University, Lawrence Berkeley National Laboratory, Max Planck Institute for Astrophysics, Max Planck Institute for Extraterrestrial Physics, New Mexico State University, New York University, Ohio State University, Pennsylvania State University, University of Portsmouth, Princeton University, the Spanish Participation Group, University of Tokyo, University of Utah, Vanderbilt University, University of Virginia, University of Washington, and Yale University.

We would also like to thank the referee for his/her valuable comments and advice.

9. References

- [1] F. H. Shu, *The Physical Universe: An Introduction to Astronomy*, (University Science Books, 1982)
- [2] A. R. Choudhury, *Astrophysics for Physicists*, (Cambridge University Press, 2010)
- [3] D. Eisenstein et al., *The Astronomical Journal*, **142** (Issue 3), 72.24 (2011)
- [4] J. Gunn et al., *The Astronomical Journal*, **131** (Issue 4) (2006)
- [5] C. Ahn et al., *The Astrophysical Journal Supplement*, **211** (Issue 2), 17 (2014)
- [6] J. Gunn et al., *The Astronomical Journal*, **116** (Issue 6) (1998)
- [7] M. Doi et al., *The Astronomical Journal*, **139** (Issue 4) (2010)

[8] T. von Hippel, G. Gilmore, arXiv:astro-ph/0006033v1, [http://arxiv.org/abs/astro-ph/0006033]

[9] D. A. Forbes, T. Bridges, arXiv:1001.4289 [http://arxiv.org/abs/1001.4289]

[10] <http://skyserver.sdss.org/dr10/en/tools/chart/navi.aspx>

[11] <http://skyserver.sdss.org/dr10/en/tools/search/radial.aspx>

[12] <http://skyserver.sdss.org/dr1/en/help/browser/browser.asp>

[13] <http://skyserver.sdss.org/dr10/en/tools/search/sql.aspx>

[14] <http://skyserver.sdss.org/dr1/en/help/howto/search/>

10. Glossary

¹Magnitude: It is a logarithmic scale that measures the brightness of an astronomical object either at a particular wavelength or as a composite quantity. The scale is defined so that a lower magnitude object is brighter than a higher magnitude one. For example, an object with R magnitude = -7 is brighter than an object with R magnitude = -6 (by roughly 2.5 times) at wavelengths centred around red.

²Colour Index: In astronomy, colour is assigned a numerical value, called Colour Index, by calculating the difference between magnitudes at two different wavelengths. For example, G-R represents a particular colour. An object with a higher value of G-R is redder than one with a

lower value. An important point to note is that Colour Index provides a measure of the temperature of a star. This is because a star can be approximately considered to be a Blackbody and hence the ratio of luminosities at two different wavelengths (magnitudes form a logarithmic scale and hence G-R actually corresponds to a ratio of luminosities at green and red) is only a function of the temperature.

³Inverted colour image: An inverted colour image is one in which the colours and brightness values are reversed so that the bright areas appear dark and vice versa, just as in a negative. We have used inverted colour images for M 3 and NGC 2420 as they help emphasise the differences in the structures of the two clusters.

⁴Spectral class: It is an alternative method to Colour Index for specifying stellar temperatures. The spectrum of a star is obtained and the absorption lines it contains give information about the relative abundance of ions of various chemical elements in the star's outer surface. By assuming that temperature is the main factor for determining these ratios and by using our knowledge of the atomic energy levels, the surface temperature can be calculated. Accordingly, there are 7 main classes (and several sub-classes) into which stars are classified (in decreasing order of temperature): O, B, A, F, G, K, M. For more details, consult [1].

⁵RA and Dec: Right ascension and declination form a system of coordinates widely employed in astronomy to specify the location of objects in the night sky. For details, consult any resource on introductory astronomy.

NIM BASED MUON TELESCOPE – AN EDUCATIONAL EXPERIMENT FOR POST GRADUATE STUDENTS

S.N.L Sirisha¹, Kajal Garg² and Sonali Bhatnagar³

^{1,2}Research Scholar
Dayalbagh Educational Institute
Agra282110, India.

³Department of Physics and Computer Science
Dayalbagh Educational Institute
Agra282110, India.

(Submitted: 04-12-2014)

Abstract

Cosmic rays offer an outstanding educational platform involving a free source of high energy subatomic particles. In continuation of the preliminary studies [1] presented at 31st National Conference of Indian Association for Radiation Protection at BARC, the paper demonstrates the fundamental properties of cosmic rays and also exposes the post graduate (PG) students to particle detection techniques, advanced nuclear electronics and data analysis. A review on several possible studies using plastic scintillator such as time characteristics of PMT which includes rise time, fall time, amplitude dependence on high voltage, jitter and walk effects of PMT pulse, coincidence, horizontal and vertical separation between detectors, dependence of cosmic ray flux with respect to temperature, pressure, humidity will be discussed.

1. Introduction

In recent years, a numerous number of high schools and universities are forming collaborations (for e.g.: CROP (Cosmic Ray Observatory Project)[2], CHICOS (California High School Cosmic ray ObServatory)[3], SEASA (Stockholm Educational Air Shower Array)[4], ALTA (Alberta Large Area Time-Coincidence Array)[5]) for performing the cosmic ray studies all over the world. Many educational aspects tend to characterize the experiments using different detection techniques for study of fundamental properties of high energy particles. This has also

offered a possible usage of the advanced nuclear laboratory which involves construction of apparatus, use of different detectors, physical measurements, muon monitoring, data analysis and interpretation for students in field of high energy physics.

In the past few years there have been some impressive advances in our understanding of Ultra High Energy Cosmic Rays (UHECR's). The origin of UHECR's is a challenge for observational/experimental studies of particle acceleration and its propagation which provides

information on the spectrum, chemical composition and anisotropy.

Cosmic rays (CRs) are particles originating from space which bombard the Earth's atmosphere. The spectrum of relativistic particles has been observed ranging from 10^6 eV to 10^{19} eV [6]. It is described by a power law which slightly steepens at 3×10^{15} eV which is termed as 'knee' and the spectrum flattens down at the ankle near 3×10^{18} eV. The knee may be the result of limitations on particle acceleration at typical supernovae, whereas the ankle may indicate a transition to particles of extragalactic origin. HiRes (High Resolution Fly Eye's) [7] and Telescope Array [8] claim the detection of the GZK feature and is consistent with the value of $E_{1/2}$, i.e. the energy at which the modification factor in the flux of UHECRs is reduced to $\frac{1}{2}$ of the value inferred from the lower energy extrapolation, can be used as a powerful indicator of the presence of GZK feature and its association to photo-pion production. It measured the quantity and found its value to be $10^{19.73 \pm 0.07}$ eV. The chemical composition measured by HiRes by using elongation rate is consistent with a proton dominated composition at energies above 10^{18} eV. Pierre Auger Observatory [10] measured and observed a gradual change in composition at higher energies which is dominated by iron at 50 EeV. It also found the correlation of the arrival direction of UHECRs above 57 EeV. But it is difficult to infer the flux reduction at 10^{19} eV. Overview of the cosmic ray spectrum obtained from various observatories such as LEAP [11], AKENO [12], AUGER [13], KASCADE [14], AGASA [15], HiRes and Proton is shown in Figure 1.

The quest of UHECRs is related to the issue of transition from Galactic cosmic rays to CRs generated in extragalactic sources. It has been considered that the ankle in the CR spectrum, at $\sim 10^{19}$ eV, is the spectral signature of the transition from a steep Galactic spectrum to a flatter extragalactic spectrum. The nature of the ankle is the consequence of three models developed. The *dip model* [16] explains the spectrum of cosmic

rays propagating on cosmological scales due to Bethe-Heitler pair production. The *mixed composition model* [17] describes that larger abundances of nuclei is heavier than hydrogen. The maximum energy of protons is relatively low at $\sim 4 \times 10^{18}$ eV and for iron it extends to 10^{20} eV. This is considered as disappointing fit due to flux suppression at 10^{20} eV with intrinsic cutoff at source spectrum and no correlation due to heavy composition at highest energy. Both these models i.e. *dip and mixed composition* lead us to expect that galactic cosmic ray ends in EeV region rather than ankle. This is even supported from the cosmic anisotropy studies. This is due to the supernovae remnant (SNR) [18] paradigm which is based on non-linear theory of particle acceleration at supernova shocks where cosmic ray acceleration in SNRs may reach a maximum rigidity $\sim 10^{16}$ GeV. The main discrimination among these models is based on the measurement of chemical composition especially in transition region.

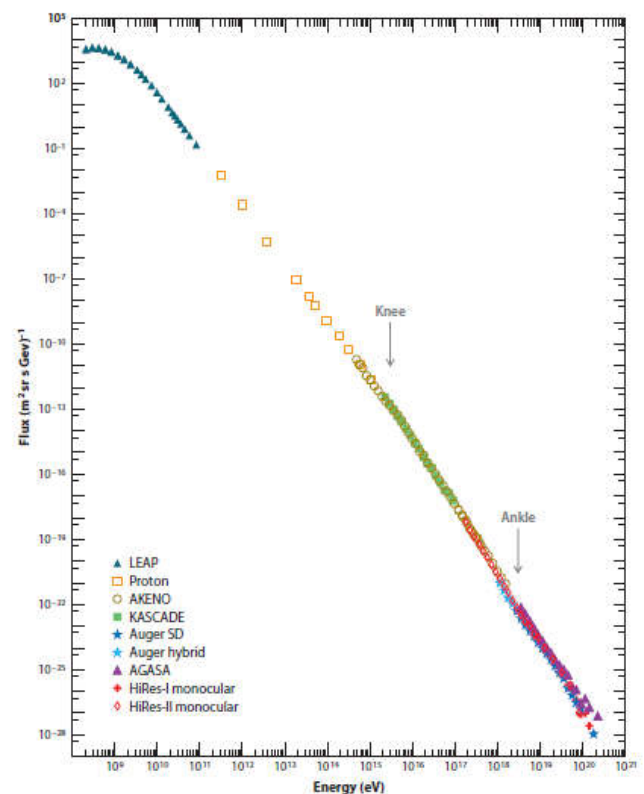
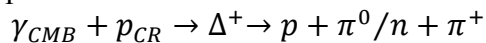


Figure 1: Cosmic Ray Spectrum [18]

The study of arrival distribution of the high energy cosmic rays is the most useful method for identifying the sources. This forms different categories: a) search for source of galactic central region, b) significant correlation of cosmic ray arrival direction with astrophysical objects, c) Cosmic ray arrival direction distribution for its anisotropy search.

At energies below 10^{14} eV, the spectrum can be measured directly by balloon and satellite-borne experiments. These experiments generally have an area of less than 1 m^2 . Above this energy, the flux is generally too small to make direct measurements. Ground-based experiments are used, where the energy of the primary cosmic ray must be inferred from its secondary's which are produced after the interaction of primary source with the Earth's atmosphere. The high energy primary cosmic rays are protons. These protons interact through the cosmic microwave background (CMB) [19] photons on their way to the earth. Above threshold energy, the following photo-production interaction is allowed:



where the number of protons should significantly decrease. This energy is referred to as the Greisen-Zapsepin-Kuzmin (GZK) cut-off and corresponds to proton energy of $\sim 4 \times 10^{19}$ eV. Protons above this range will interact with the CMB photons and have their energy degraded while producing an air shower cascade which is mostly of charged and neutral pions. These particles will subsequently decay or interact with other nuclei. The air shower has three components: electromagnetic (80%), muonic (1.7%) and hadronic (0.3%) [20]. Neutrinos are not counted, although they are abundantly produced in weak decays. Relativistic charged particles will produce Cerenkov light as they propagate through the atmosphere. Finally, excitations of nitrogen molecules in the atmosphere will generate fluorescence light.

Measurements of multiparticle production in fixed target experiments at low energy and in collider experiments at high energy are suitable to verify model assumptions and to limit their extrapolations

to cosmic ray energies. The data which reaches upto 10^{17} eV [21] equivalent energy of cosmic ray protons obtained from LHC is of more important. The high energy secondary particles are more relevant to interpretation of cosmic ray data. Muon detection is an essential part in the Large Hadron Collider (LHC) experiments. It helps in understanding the background of the underground detectors and to simulate the atmospheric showers induced by muons. At super high energies, these are also considered for exploration of primary cosmic rays, neutrino studies in different arrays like Super-Kamiokande [22], GRAPES-3 (Gamma Ray Astronomy at PeV Energies) [23] and for numerous environmental experiments like the solar activity characterization or climate change observations [24]. Also, it has successfully been used as muon tomography technique in the search for hidden rooms in pyramids or in volcanology [25]. There are other possible applications to increase the safety procedures in mining excavations, oil industry as an easy way to search for oil bags or at the customs checkpoints, to scan the passing vehicles [26]. In many applications such as industry and academia, an accurate determination of the direction from where gamma rays are emitted is either needed or desirable. Radiation therapy treatments, the search for unknown sources, and homeland security applications are few of the fields that can benefit from directional sensitivity to gamma-radiation [27].

This paper is extension of the previous work done on "Preliminary Studies of Muon Telescope" [1]. We discussed till now the fundamental properties of cosmic ray spectrum, its chemical composition and anisotropy. In section II, we present a brief description of on-going experiments in our laboratory where the PG students get an exposure to advanced nuclear electronics. The feedback of the students who did the lab course work is discussed in section III. An overview of various methods that can be implemented for study of time characteristics of photomultiplier tube, obtain the efficiency of detector system through coincidence techniques, calibrate the TDC and obtain the

energy deposited from CAMAC modules (ADC, TDC), angular dependence of cosmic ray flux and finally ends with atmospheric parameters such as temperature, pressure, solar activity and their effect on cosmic ray flux are presented in Section IV. The future aspects of our laboratory are given in Section V.

2. Experiments conducted with Post Graduate Students:

In the preceding work, we performed basic pre-preliminary studies of our telescope. It includes light leakage testing from detectors and optimized the discriminator threshold voltage. Counting statistics was applied to determine the error flexibility within the data range. The experimental studies conducted with the students for understanding the concept of scintillation, signal transmission, electronics used to suppress the noise, logical conversion of pulse to acquire data in optimizing PMT operating voltage and the correlation between count rate and accidentals will be discussed in this section. Two polystyrene (PS) based scintillators i.e. Double Fiber Detector (DFD) and Single Fiber Detector (SFD) with dimension $24 \times 23.5 \times 2 \text{ cm}^3$ are presently in use in the laboratory. These were assembled at Cosmic Ray laboratory, Ooty; a field station of T.I.F.R, Mumbai. Polystyrene (PS) with a photon emission at 300 nm is doped with a two stage phosphor wavelength shifter composed of 0.5% p-terphenyl (absorbs photon at 300 nm and emits at 350 nm) and 0.02% POPOP (absorbs photon at 350 nm and emits at 410 nm). The response peak of the organic scintillator is shown in figure 2.

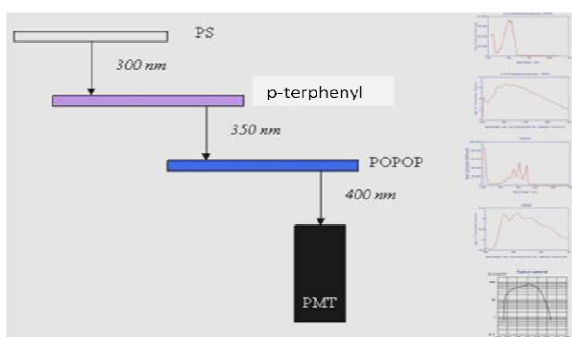


Figure 2: Organic Scintillator Mechanism [8].

During the process of polymerization the temperature should be controlled at 70°C for at least 60-72 hours. Polymerization is a highly exothermic process (165 cal/gm) and the temperature control is mandatory when dealing with large volumes. Rising polymerization temperature may produce bubbles and cracks. The fabricated scintillator is shown in figure 3 (a).



Figure 3(a): Plastic Scintillator used in Experiment.

After cleaning the scintillator with isopropanol liquid and polish on both extremes with sandpaper, the scintillator is grooved all over. Wave length shifting (WLS) fiber of Kuraray Y-11 manufacture (refractive index, $n=1.59$, inner clad, $n=1.42$, outer clad, $n=1.49$) with double-clad of 1.2 mm diameter is inserted into the groove. This absorbs the primary scintillation light ($\sim 410 \text{ nm}$) and reradiates the energy at a longer wavelength ($\sim 550 \text{ nm}$) [4]. It helps to match the emission spectrum of scintillator with the response peak of a photomultiplier tube. They also increase the decay time, improve the resolution and decrease the self-absorption of the detector. The scintillation detectors embedded with wavelength shifting fibers are optically coupled to photomultiplier tube (ET Enterprises, Type 9807B), a regular 12-stage linear focused dynode structure and highly efficient at 550 nm. An aluminum box with volume 55 cm^3 (length) \times 25 cm (width) \times 10 cm (height) and 1.2 mm in thickness is designed to place the entire setup i.e. scintillator coupled to a photomultiplier tube using a cookie (figure 3(b)). The whole setup of detector is shown in figure 3(c).

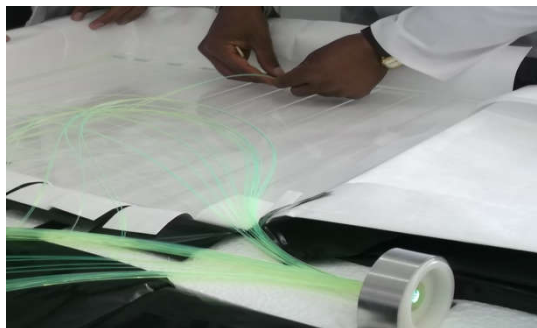


Figure 3(b): Optical coupling of scintillator to PMT with a cookie.



Figure 3(c): Detector Setup

The information provided by the detectors from the emitted radiations is in the form of electrical signals. This is processed by a signal processing electronics using Nuclear Instrumentation Module (NIM) which can sort out various unwanted signals from detectors to extract energy information and determine the relative timing between the two signals. It generates a fast negative logic with a rise time of the order ~ 1 ns. The corresponding voltage levels are thus 0V and -0.8V for logic 0 or 1 respectively. These fast NIM signals can be transmitted through coaxial cables. Students have studied the characteristics of pulse, coaxial cables, impedance matching, inhibiting discriminator pulse from veto functioning, versatile functions of logic unit such as AND, OR and anti-coincidence. Correlation between detector count rate and its accidental rate is also observed. These are briefly described along with the results in the following exercises given below:

Exercise 1: Study the pulse characteristics

In any pulse processing system, it is important to distinguish between two types of signal pulses i.e. linear and logic. A linear pulse carries information through its amplitude or shape. A sequence of these pulses differs widely by its size and shape characteristics. Logic pulse has a standard size and shape that carries information only by its presence or absence or by precise time of its appearance. Initially all radiation detector signal starts out with linear pulses and at some point, a conversion is made to logic pulses based on some pre-determined criteria.

A fast linear pulse collects the output current of radiation detector using a collection circuit whose time constant is small. The signal-to-noise ratio properties of fast linear pulses are always much less than a corresponding tail pulse which is derived by integrating the charge output of the detector across a large time constant [28]. The rapid rise and fall time overcome this outcome when timing information and high counting rates are more important than amplitude resolution. Its polarity depends on the bias voltage applied to the detector. The basic pulse characteristics associated with its polarity, amplitude, shape and its occurrence in relative time are explained here for a linear and NIM logic pulse to study its voltage/current as function of time. Figures 4(a) and 4(b) demonstrate these parameters obtained for double and single fiber detector configurations.



Figure 4(a): Linear pulse characteristics obtained for double fiber detector.



Figure 4(b): Linear pulse characteristics obtained for single fiber detector

Both the configurations are compared in order to understand the amplitude difference where a 350 mV amplitude pulse generated for double fiber, 200 mV in case of single fiber detector. This depends on the number of photoelectrons that reach the anode of the PMT where these fiber configurations may give a possible impact.

Exercise 2:(a) Check the reflections in a cable by using a 50Ω impedance terminator.

Signal transmission is transfer of a signal from point A to B and also to preserve the information in the signal. These cables should be capable of transmitting an infinite frequency range over a certain distance in uniform and coherent manner. But stray capacitances, inductance or resistance will invariably results in distortion of the pulse at receiving end. When a fast pulse signal is transmitted through simple wire connections, it attenuates and dies down after few cm. It is necessary to transmit infinite range of frequencies in laboratory. A basic concept in processing of pulses from radiation detectors is the impedance of the devices that comprise the signal processing chain. High input impedance usually has a less load [29]. For example, the input impedance of an oscilloscope is always high to avoid excessive loading.

The device impedance also should be in match with the cable impedance to avoid signal distortion from reflection. When a fast signal is viewed on an oscilloscope, it undergoes an

impedance mismatch due to high impedance of oscilloscope. In such cases, the cable can be terminated with an appropriate value so as to adjust the total load impedance seen by cable. This is done by placing a resistance of 50Ω in parallel with device. The signal seen by the oscilloscope for DFD and SFD are shown in figure 5. The signal is reflection free on terminating with 50Ω load impedance.

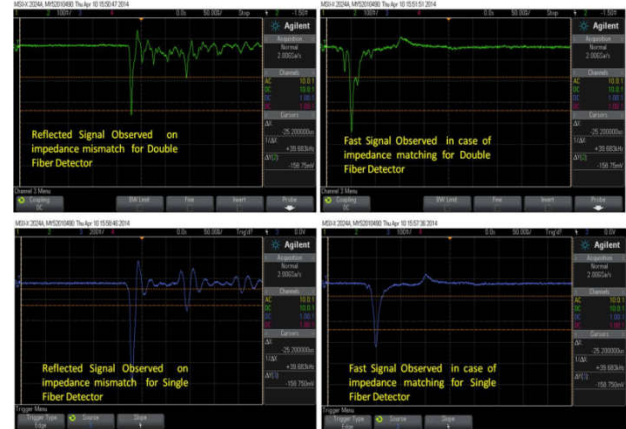


Figure 5: Analog Signal Transmission Observed using with and without 50 Ω terminating.

We can observe from figure 5, that the signal distortion from reflection can be avoided by matching device impedance with cable impedance. Direct transmit of fast NIM signal will result in impedance mismatch and fast signal reading. But slow signal can be transmitted and also compatible as cables are not too long. So cable should be terminated for fast NIM pulse.

(b) To compute the characteristic impedance, velocity propagation, time delay and reflection coefficient of coaxial cables RG 59/U, 5D2V.

Coaxial cables are used for standard transmission of signals. It consists of two concentric cylindrical conductors separated by a dielectric material. The outer conductor serves as a ground and also shields the central wire from stray electromagnetic fields. Frequencies ≤ 100 kHz are efficiently attenuated in most standard cables [28]. The line constituents of coaxial cables generally contain a self-capacitance and inductance. Using EM theory

for two concentric cylinders, they can be represented as:

$$L = \frac{\mu \ln\left(\frac{b}{a}\right)}{2\pi} (H/m) = 0.2k_m \ln\left(\frac{b}{a}\right) \mu H/m$$

$$C = \frac{2\pi\epsilon}{\ln\left(\frac{b}{a}\right)} F/m = \frac{55.6k_e}{\ln\left(\frac{b}{a}\right)} pF/m$$

Where a,b are radii of inner and outer cylinders; μ , ϵ are permeability and permittivity of insulating dielectric; $k_e = \epsilon/\epsilon_0$, $k_m = \mu/\mu_0$ permittivity and permeability relative to vacuum. For non-ferromagnetic materials, $k_m=1$. L and C are on the order of 100 pF/m and few tenth $\mu H/m$. Coaxial cables with air or other gas as a dielectric have a propagation velocity very close to the velocity of light in a vacuum (3.00×10^8 m/s).

General wave equation for a coaxial cable in terms of transmission line can be represented as

$$\frac{\partial^2 V}{\partial z^2} = LC \frac{\partial^2 V}{\partial t^2} + (LG + RC) \frac{\partial V}{\partial t} + RGV$$

Let us consider an ideal loss less cable where R and G are zero

$$\frac{\partial^2 V}{\partial z^2} = LC \frac{\partial^2 V}{\partial t^2}$$

For a sinusoidal voltage in time

$$V = V(z) \exp(i\omega t)$$

$$\frac{\partial^2 V}{\partial z^2} = -\omega^2 LC V = -k^2 V$$

$$k^2 = \omega^2 LC$$

The space solutions to represent the two waves which are travelling in +z and opposite -z direction are

$$V(z, t) = V_1 \exp(i(\omega t - kz)) + V_2 \exp(i(\omega t + kz))$$

Here second wave corresponds to a reflection and its presence or absence depends on the boundary

for the cable. From the above equation, k is considered as wave number and velocity of propagation is

$$v = \frac{\omega}{k} = \frac{1}{\sqrt{LC}}$$

As long as the cable is constant in cross-section, the product LC is independent of length and $LC = \mu\epsilon$, where ϵ permittivity is and μ is permeability of dielectric. Thus for a cable with free space as dielectric velocity of propagation = $\frac{1}{\mu_0\epsilon_0} = c$ = speed of light in vacuum. Speed of signal propagation is also reciprocal of time of propagation per unit length which is also known as $T = v^{-1} = \sqrt{LC}$. Here is T is time delay of the cable per unit length of the order 5 ns for 50 Ω cable.

All signal cables generally utilize polyethylene for dielectric in which the velocity of propagation is about 66% of that of light in vacuum. In some delay cables it is reduced by a factor of 100 [29]. Pulse transmission through coaxial cable is in two extremes i.e. low frequency and slow pulses, high frequency and fast pulses. The application of fast and slow pulses depends on the comparison of fastest pulse component (rise time) with the transit time of the pulse. For dielectric material such as polyethylene, the transit time is about 5.1 ns/m [29]. Similarly a pulse through 15 m of RG 59/U coaxial cable has a transit time of 76.5 ns/15m. Pulsethrough high rise time compared with the transit time is considered as slow pulse. In this case, cable acts much like simple conductor. The resistance of central conductor is very small for cables less than 100 m length. When a 20 m RG-59/U cable have 0.5 μs rise time, the resultant pulse can be considered as a slow pulse. This is due to the transit time of the cable i.e. 102 ns/20m being less than the rise time. Thus, for a signal transmission of slow pulse through a cable does not any termination as the resistance of central conductor is very small which result in negligible signal loss. Characteristic Impedance is another important property of transmission cable which is ratio of the voltage to the current in the cable.

$$Z_o = \frac{V}{I} = \sqrt{\frac{L}{C}}$$

In fast nuclear electronics applications, cables have a standard characteristic impedance of 50 Ω and for slower spectroscopy pulse the characteristic impedance is 93Ω. These cables are limited to a range of 50-200 Ω of characteristic impedance. The ratio $\frac{b}{a}$ should be a factor of 3.6 to minimize losses. For all these cables, dielectric is Polyethylene whose relative permittivity is 2.29. The observations are given in the table 1 and

When reflections overlap with original signal, then interference or distortion will result. Reflections occur when a travelling wave encounters a new medium in which the speed of propagation is different. In transmission lines, these reflections occur when characteristic impedance of the line is suddenly changed. These reflections are calculated by considering boundary conditions at interface. Consider a cable of characteristic impedance Z terminated with an impedance R. As the signal travels, the ratio of voltage to current must be equal to Z. When the interface encounters reflections, it must be compatible with original characteristic impedance since they travel back in opposite direction. Thus

$$Z = \frac{V_o}{I_o}, R = \frac{V_o + V_r}{I_o + I_r} \Rightarrow Z = \frac{V_R}{-I_R}$$

V_o, I_o are voltage and current of original signal and V_R, I_R are voltage and current of reflected signal. From these equations, Reflection coefficient

$$\Gamma = \frac{V_R}{V_o} = \frac{-I_R}{I_o} = \frac{R + Z}{R - Z}$$

If $R > Z$, the reflection will be of same polarity, but with amplitude between 0 and original pulse height. For infinite load impedance, reflected amplitude is equal to incident amplitude. The reflection is in opposite polarity when $R < Z$. For zero load impedance, reflection is equal and opposite in polarity to incident amplitude. If $R = Z$, No reflection takes place where the load and cable impedance gets matched.

Exercise 3: Study the specifications of the Phillips 704 Discriminator: VETO, OUT.

Discriminator is a device that responds only to input signals with a pulse height greater than a certain threshold value. It gives a standard logic signal when the criterion gets satisfied. It blocks out low amplitude noise pulse from PMT and other detectors. Time arrival between input and output is constant where as an important aspect of

Table 1: Characteristic Impedance

Coaxial Cable	Outer diameter (mm)	Inner diameter (mm)	log (D/d)	ϵ_r	$Z_o(\Omega)$
Manufacturer Values RG59/U	4.95	0.8	0.79	2.29	75
RG 59/U	4.40	0.63	0.84	2.29	76.6 (2.3% error)
Manufacturer Values 5D2V	7.3	1.4	0.71	2.29	50
Coaxial Cables	5.01	0.79	0.75	2.29	50.1 (0.2% error)
Manufacturer RG 59/U		69	5.14		0.89
RG 59/U		73 (5% error)	5.18 (0.7% error)		0.92 (0.3% error)
Manufacturer 5D2V		65	5.06		0.78
5D2V		68 (4% error)	5.09 (0.5% error)		0.81 (0.3% error)

Signal in a coaxial cable is sum of original and reflected signal travelling in opposite direction. It is represented in arbitrary signal form as

$$V = f(x - vt) + g(x + vt)$$

discriminator is the method of triggering which is a leading edge triggering. It occurs the moment pulse crosses the threshold value. Double pulse resolution and continuous pulse train are two parameters of this module which measures the smallest time separation between two pulses and the highest frequency of equally spaced pulses [30]. A standardized NIM logic level (-800mV) pulse is delivered while suppressing the unwanted stray radiations arriving along with analog signal. Inhibiting the discriminator pulse can be accomplished by fast vetoing. This VETO function is shown in figure 6.



Figure 6: VETO Function in Model 704 Quad four channels Discriminator.

Although the main use of a discriminator is to turn a variable-height input pulse into a standard logic pulse, there are additional features of this unit that can be used. Each discriminator channel has a “complementary” output, noted as \overline{OUT} . This output is always opposite to the regular outputs as shown in Figure 7.

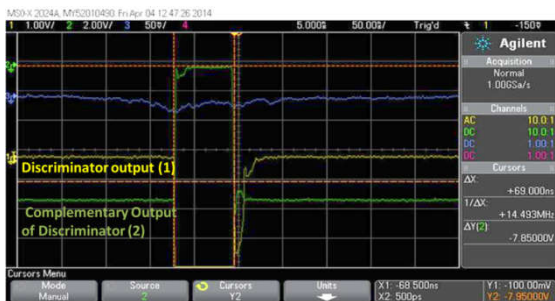


Figure 7: Discriminator Specification Study from Oscilloscope.

Exercise 4: Study the 2 input AND, OR logics using Phillips Quad Four fold logic unit.

The coincidence unit determines if two or more logic signals are coincident in time and generates a logic signal if **true (1)** and no signal if **false (0)**. Versatile functions of this module [31] with the selection of Logic AND, OR and Anti-coincidence are observed in figure 8(a), (b), (c).

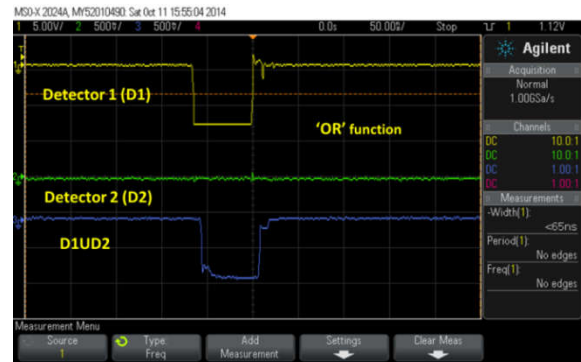


Figure 8(a): Logic OR function

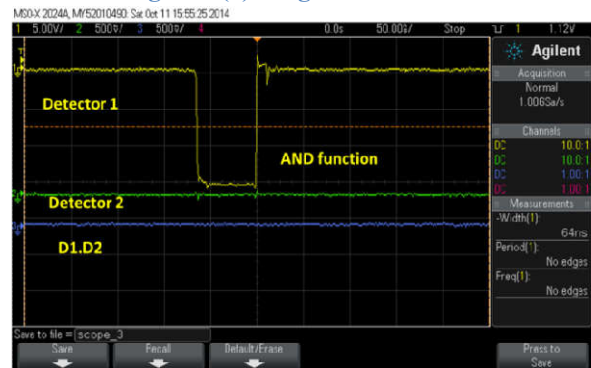


Figure 8(b): Logic AND function

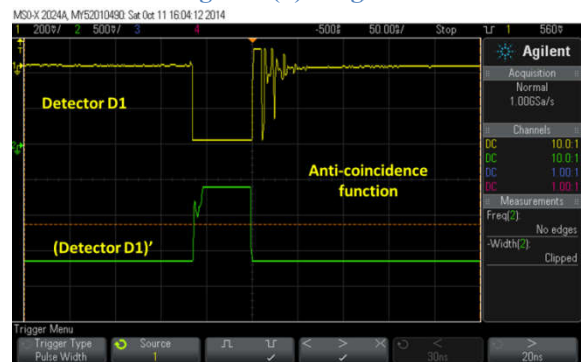


Figure 8(c): Anti-coincidence function

Figure 8(a) demonstrates the OR function where the status of detector D1 is 1 and D2 is 0 which results in an output as 1. This proves that the module performs OR logic. Similarly in figure

8(b), we can observe the AND logic i.e. when D1 is 1 and D2 is 0, the final output gives 0. Figure 8(c) shows the Anti-coincidence function when input (D1) is given.

Exercise 5: Determine the PMT (photo-multiplier tube) operating voltage and the count rate correlation with accidental counts in the detector.

To improve the acceptance value of plastic scintillator while suppressing the lower energy signals from PMT, the operating voltage for each detector i.e. (Double Fiber Detector, DFD and Single Fiber Detector, SFD) is determined. The experimental setup is shown in figure 9. Two plastic scintillation detectors are placed in coincidence. The threshold voltage of Quad 300 MHz discriminator (model number 708 [30]) was fixed at – 20 mV with a pulse width of 60 ns.

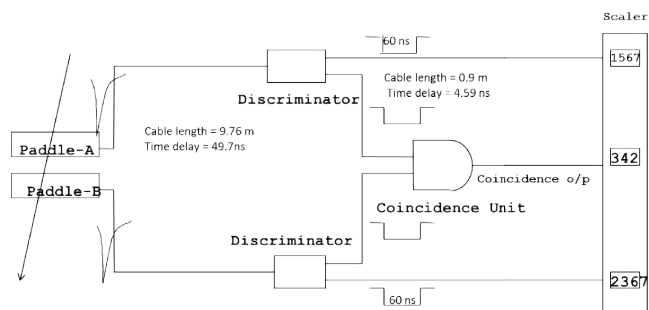


Figure 9: Experimental setup

The high voltage of one detector is fixed at 1700V whereas the high voltage of the other is varied from 1200 – 1800 V with 50V interval. To obtain a coincidence among the pulse the logic switch of Phillips Quad four fold logic unit (model number 756 [31]) is set at level 2. The counts were taken using the CAEN Quad Scaler and Preset Counter Timer (model number N1145 [32]). The coincidence rate/sec with respect to high voltage (H.V.) is observed for each PMT of the detector in order to determine its operating voltage.

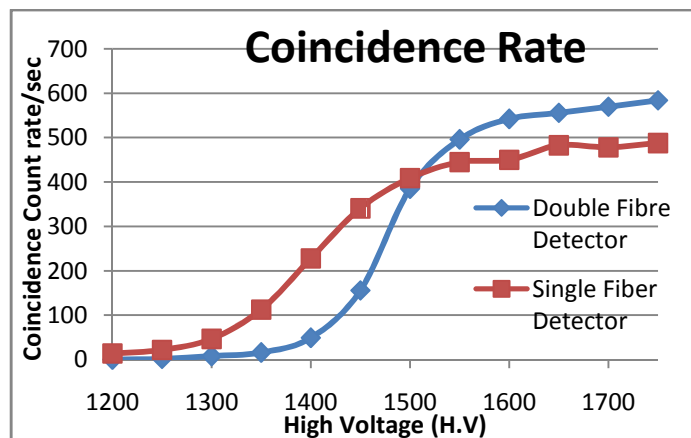


Figure 10: Operating voltage of PMT in DFD and SFD

From the plot (Figure 10), the operating voltage for each detector is observed at the point of inflexion for single fiber detector it is observed to be 1500V and for double fiber detector at 1550V. While making the coincidence measurement, we should consider the uncorrelated background events in the detector. They may arrive within the resolving time of the circuit or through random noise which triggers the discriminator. We can overcome this disadvantage by measuring the accidental coincidences that occur in circuit which must be kept to a minimum. The rate of accidentals can be estimated from the singles rate in each detector and the time resolution of the circuit. Consider n_1 and n_2 are the individual count rate for detector 1 and 2 respectively and τ is the resolution time which is set to trigger the circuit. Total number of accidentals per unit time,

$$A = 2\tau n_1 n_2,$$

Where τ is 60 ns. Correlation of detector count rate with accidental is shown in figures 11 (a), (b).

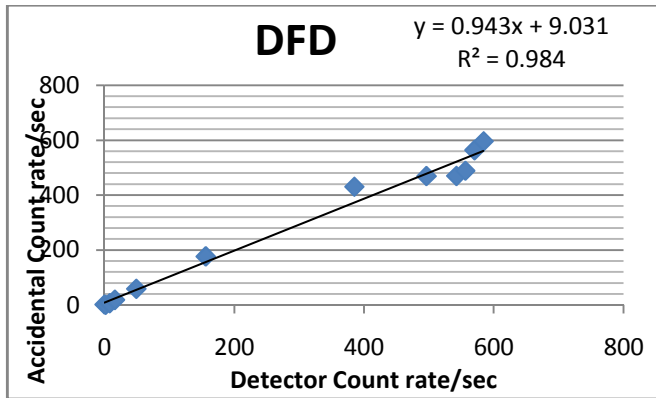


Figure 11(a): Correlation between detector count rate and accidentals in double fiber detector

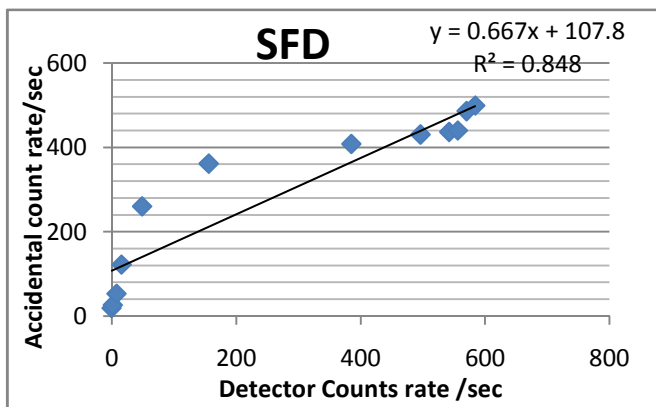


Figure rate single

a	To a great extent
b.	Sufficient
c.	A bit
d.	Nothing

11(b): Correlation between detector count and accidentals in fiber detector

From figure 11 (a), (b); we can observe a linear relation with in the detector count rate and its accidentals. This is due to the noise which gradually increases with count rate on increasing the high voltage (H.V) of the PMT.

3. QUESTIONNAIRE FOR LABORATORY STUDENTS

After evaluation of the results we conducted an analysis through questionnaire regarding understanding capability of the students in

performing the experiment. The questionnaire helped us to understand the basic conceptual problems and evaluating the misunderstandings. At that point of view we prepared the following for students:

1. Did you understand the scintillation mechanism after doing the experiment?
2. Did you understand the main significance of PMT which is used in the experiment?
3. At PG level do you understand the working of this experiment?
4. Is the theoretical concept of coaxial cables clear which are used for transmission of fast pulse in the experiment?
5. Discriminator is used to suppress noise and give a standard logic signal. Do you think it acts as main source in experiment?
6. Did you understand why the signals are transmitted through Logic unit in experiment?
7. Interaction of radiation with matter. Is this concept which you studied in the graduation clear after performing the experiments in this laboratory?

The rating of the students opinion is taken through the following multiple choice options regarding their understanding capability in scintillation mechanism, PMT significance, coaxial cable transmission, discriminator, logic unit and experiment working with its concept clarity.

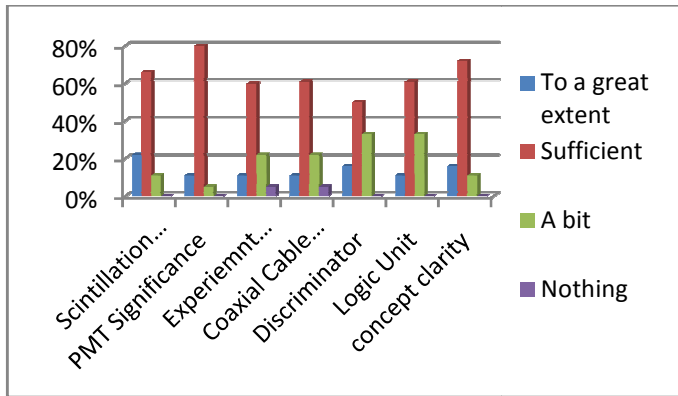


Figure 12: Students feedback in understanding the concepts of the experiemnt

Taking into account the students responses we concluded from graph (figure 12): 66% of students understood the scintillation mechanism, 83% got the significance of PMT, 61% understood the transmission concept in coaxial cables, 50% understood the working of discriminator where as 61% understood about logic gate usage in experiment and it is remarkable that 72% of the class got the clarity of working principle of experiment and its concept.

8. Among the experiments which is more user friendly

- a. GM counter
- b. NaI - Gamma ray spectroscopy
- c. NaI - Multichannel analyzer
- d. Plastic scintillator – Nuclear Instrumentation Module

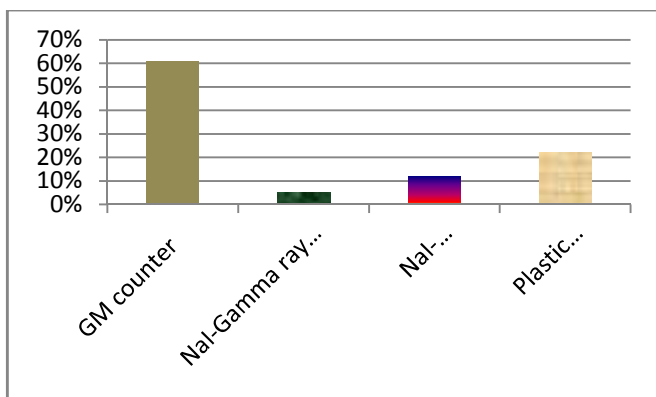


Figure 13: Students feedback after performing the experiments in the laboratory

Among the experiments which are performed by students in the laboratory, as shown in graph (figure 13), 61% of the students felt GM counter is more userfriendly where as it is remarkable that 22% of the class are comfort with the usage of NIM based plastic scintillator experiment which is presently studied in this paper.

9. Which one do you think is more preferable for study of cosmic rays?

- a. NaI
- b. Plastic Scintillator

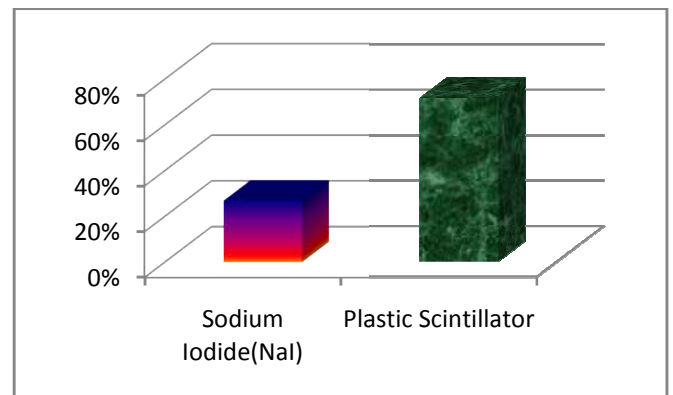


Figure 14: The feedback of students in using the plastic scintillator and Sodium Iodide (NaI) for study of cosmic rays

While comparing the organic and inorganic detectors (as shown in graph (figure 14)) which are present in laboratory for study of cosmic rays, 72% of the students opted for plastic scintillator which is suitable got cosmic ray study.

10. Among the techniques used, which is preferable for studying the efficiency of detectors

- a. Pulse Height Discrimination
- b. Coincidence Technique

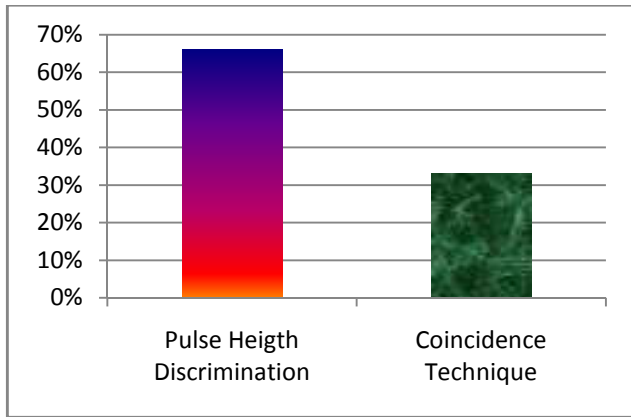


Figure 15: The technique suitable to determine efficiency of detectors from students rating of their opinion

The two techniques i.e. pulse height discrimination and coincidence technique when compared for determining the efficiency of detectors (as shown in graph (figure 15)), 66% of the students opted for pulse height discrimination where as 33% opted for coincidence technique.

11. Among the equipments given, which can cause main source for errors/noise in the experiment?

- a. Scintillator
- b. Coaxial Cables
- c. PMT
- d. Discriminator

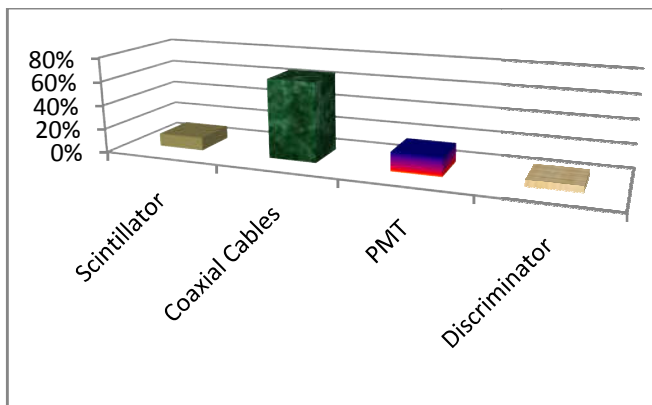


Figure 16: Students feedback regarding the noise/error source in experiment within the equipments

When discussed for possible error/noise source in experiment as shown in graph (figure 16)), 66% of the students gave their feedback for coaxial cables and 16% opted for PMT as a main source of noise in experiment.

4. Review on Previous Studies Done:

4.1 Time Characteristics studies of PMT:

The dynode voltage drops in different Photo Multiplier Tubes with respect to PIN number have been tested on fixing H.V of PMT for long time. The most important factor in any timing system is its resolution. One method is to measure the resolution i.e. to measure the time difference of two exactly coincident signals [33]. The *walk* effect occurs due to variations in the amplitude and/or rise time of the incoming signals. For example, even though if two signals of different pulse amplitude is in coincident, then the two signals will trigger the discriminator at different position. The second cause of walk effect is the charge required to trigger the leading edge of the pulse. Noise and statistical fluctuations also result in a time variation of signals generally termed as time jitter.

4.2 Efficiency Studies of Scintillation Counters:

Instead of measuring the number of particles passing through the detector, efficiency of the entire system can be determined from the coincidence measurement. The ratio of coincidence counters to optimized counters allows to study the number of particles in a particular counter detects relative to the others.

The efficiency is calculated from the plateau region of third paddle (3F/2F) (Detector dimension is $60 \times 20 \times 1 \text{ cm}^3$, $45 \times 3 \times 1 \text{ cm}^3$, $45 \times 2 \times 1 \text{ cm}^3$). It is studied as function of longitudinal length of the detector and also with respect to varying distance from PMT (Detector dimension is $199 \times 19.5 \times 0.9 \text{ cm}^3$) [34]. The Plateau region of the test paddle determined from the efficiency (3F) (1st paddle = $200 \times 165 \times 10 \text{ mm}^3$, 2nd paddle = $200 \times 165 \times 10 \text{ mm}^3$, Test paddle = $340 \times 200 \times 10 \text{ mm}^3$) [35]. Probability at a certain time instant where all four paddles record a signal was

calculated from the individual count rate per 100 sec, 4-fold trigger rate per 600 sec and average frequency (Hz). Here the chance coincidence in which a muon passes through paddles 1, 3, 4 and paddle 2 records any signal (noise/muon) also determined along with actual chance coincidence rate, actual cosmic ray muon rate and average muon flux (P1 – $30 \times 2 \times 1 \text{ cm}^3$, P2 – $30 \times 3 \times 1 \text{ cm}^3$, P3 – $40 \times 20 \times 1 \text{ cm}^3$, P4 – $40 \times 20 \times 1 \text{ cm}^3$)[36]. Efficiency (counts/hr) rate taken for two weeks where the correlation between count rate and atmospheric pressure, temperature, barometric coefficient within 2 weeks observed. The statistics such as chi-square test, p-value, correlation coefficient, slope of the correlation was also determined ($1000 \times 200 \times 10 \text{ mm}^3$ with $2 \times 2 \text{ mm}^3$ square type WLS fibre)[37].

4.3 Calibration of TDC:

The time scale of TDC was calibrated in work conducted from reference [38]. Distance between the peaks produced by different delays and the time resolution of the paddles ($60 \times 20 \times 1 \text{ cm}^3$, $45 \times 3 \times 1 \text{ cm}^3$, $45 \times 2 \times 1 \text{ cm}^3$) were measured.

4.4 Calibration of ADC:

In the report [38], number of photoelectrons produced at the PMT photocathode from scintillator paddle for cosmic ray muon ($60 \times 20 \times 1 \text{ cm}^3$, $45 \times 3 \times 1 \text{ cm}^3$, $45 \times 2 \times 1 \text{ cm}^3$) was measured. Muon energy was determined (P1 – $30 \times 2 \times 1 \text{ cm}^3$, P2 – $30 \times 3 \times 1 \text{ cm}^3$, P3 – $40 \times 20 \times 1 \text{ cm}^3$, P4 – $40 \times 20 \times 1 \text{ cm}^3$). Response spectrum on changing the coincidence width was also studied for Number of counts v/s ADC channel ($1000 \times 200 \times 10 \text{ mm}^3$ with $2 \times 2 \text{ mm}^3$ square type WLS fibre from).

4.5 Radioactive source:

The isotropic behavior of radiation using two detectors where one is fixed at a position and other is varied at different angles – coincidence counts. Study the inverse square law behavior. Study the dependence of cosmic ray flux on placing different shielding (lead, Al, wood) between

source and PMT (Lead acid battery – 6.35 cm, Al – 0.3175 cm thick, Wood – 5.08 cm) [39].

4.6 Atmospheric parameters:

The correlation between the flux distributions and barometric pressure was studied with variable angular acceptance at the earth's surface of two scintillator paddle muon telescope. A paddle separation of 0, 7, 14 inches conducted for a correlation and anti-correlation analysis of muon count rate with the barometric pressure, surface temperature, stratospheric temperature and solar activity parameters (IMF (nT), plasma speed (km/hr) and Kp index) ($33 \times 7 \times 1 \text{ cm}^2$, $12 \times 12 \text{ cm}^2$) [40]. The dependence of cosmic ray flux over zenith and azimuthal angle observed. Coincidence counts as function of shielding thickness was also determined (Three scintillator – $40 \times 80 \times 3 \text{ cm}^2$, Light guide – $40 \times 40 \text{ cm}^2$, Iron plate – 2cm thick) [40].

5. Conclusion:

Cosmic rays are a prevailing source of information for performing high energy physics experiments. They provide energetic, correlated, particles which arrive on Earth. The detection of such particles and the study of the inclusive and definite properties of secondary cosmic rays may provide basic and advanced educational activities to get involved of undergraduate and post graduate students. The hardware required by such experiments may include the use of scintillators and fast pulse techniques for possible experimental investigations. By such devices we can carry out numerous quantitative experiments, with the prospect to enhance the physics curriculum.

6. Future Plans:

Students are presently performing horizontal coincidence, vertical coincidence and at different elevations. Later they are going to compare the difference among the count rate of horizontal and vertical coincidence. They will also determine the efficiency of detectors from three fold and four fold. The effect of absorbers when placed between

detectors will be observed from their count rate. Future plan is to interface with CAEN C111C Ethernet CAMAC Controller, calibrating Phillips TDC 7187 and Phillips 7164 ADC module to study the resolution which have an impact on range of digitization and time spectrum of the particle. Measure and store the time difference between the two pulses generated in the same detector to visualize the two pulses originating from the muon and the electron. Investigate the cosmic ray muon life time with different counters and absorbers.

7. Acknowledgment:

The authors wish to thank Cosmic Ray Laboratory (CRL), Field Station of Tata Institute of Fundamental Research, Ooty; for its technical assistance in fabricating and designing the plastic scintillation detectors. We want to express special thanks to Prof. Sunil Gupta, Shri K.C Ravindran, Shri. Atul Jain, Shri. C. Ravi and to the staff, management of Cosmic Ray Laboratory, Ooty.

The authors also thank Panjab University, Inter University of Accelerator Center for their technical assistance in setting up data acquisition. We want to express special thanks to Dr. Vipin Bhatnagar, Shri. V.K Bhandari, Shri. Kundan Singh, Mrs. Ruby Santhi and Shri.V.V.V Satyanarayana.

8. References:

- [1] Sonali Bhatnagar et.al, “Preliminary Studies of muon telescope”, 31st National Conference of Indian Association for Radiation Protection on “Advances in Radiation Measurement Systems and Techniques”, March 19-21, 2014, BARC, Mumbai.
- [2] Sonali Bhatnagar, “High Energy Cosmic Rays”, Indian Association of Physics Teachers Bulletin, Vol.24, No.11, pp 336, Nov. 2007.
- [3] Sonali Bhatnagar, “Extensive Air Shower-High Energy Cosmic Rays (II)”, Physics Educational Journal, University of Pune, Oct-Dec 2009.
- [4] Sonali Bhatnagar, “Gamma Ray astronomy at PeV energies”, Current Science, Vol. 97, No 7, 10 October, 2009.
- [5] Bogdanov, A.. “Energy spectrum of cosmic ray muons in ~100 TeV energy region reconstructed from the BUST data”, *Astroparticle physics*, 224, 2012.
- [6] Ralph Engel, “Extensive Air Showers and Hadronic Interactions at High Energy”, *Annu. Rev. Nucl. Part. Sci.* 2011, 61: 467-489.
- [7] Pasquale Blasi, “Theoretical challenges in acceleration and transport of ultra-high energy cosmic rays: A review”, *EDP sciences*, 53, 01002 (2013).
- [8] James J. Beatty, “The Highest Energy Cosmic Rays”, *Ann. Rev. Nucl. Part. Sci.* 59, 319-45, 2009.
- [9] Watson. A. A, “Recent results from the Pierre Auger Observatory—Including comparisons with data from AGASA and HiRes”, *Nuclear Instruments and Methods in Physics Research Section A*, Volume 588, Issue 1-2, p. 221-226.
- [10] Muons in air showers at the Pierre Auger Observatory: Measurement of atmospheric production dept, *Physical Review D*, 90 (2014) 012012arXiv: 1407.5919.
- [11] T. Yamamoto, “Development of Atmospheric Monitoring System at Akeno Observatory for the Telescope Array

- Project”, Nucl.Instrum.Meth. A488 (2002) 191-208.
- [12] Mattia di Mauro, “New evaluation of the antiproton production cross section for cosmic ray studies”, Phys. Rev. D 90, 085017 – Published 20 October 2014
- [13] P. Abru, “The Pierre Auger Observatory II: Studies of Cosmic Ray Composition and Hadronic Interaction models”, arXiv:1107.4804 [astro-ph.HE].
- [14] S Riggi, “A large area cosmic ray detector for the inspection of hidden high-Z materials inside containers”, 2013 *J. Phys.: Conf. Ser.* 409
- [15] D.J Thomson, “Cosmic ray studies with the Fermi Gamma-ray Space Telescope Large Area Telescope”, Cosmic rays topical issue, Volumes 39–40, December 2012, Pages 22–32.
- [16] V. Berezhinsky, “Dip in UHECR spectrum as signature of proton interaction with CMB arXiv:astro-ph/0502550v1 28 Feb 2005
- [17] R. Aloisio, Ultra High Energy Cosmic Rays: The disappointing model, arXiv:0907.5194v2 [astro-ph.HE] 16 Feb 2011
- [18] D. Allard, UHE nuclei propagation and the interpretation of the ankle in the cosmic-ray spectrum, arXiv:astro-ph/0505566v2 4 Jun 2005
- [19] D. Kosenko, “Parametric studies of cosmic ray acceleration in supernova remnants”, MNRAS (September 11, 2014) 443(2): 139 0-1401.
- [20] Lazarian, “Heliotail and anisotropy of cosmic ray flux”, 40th COSPAR Scientific Assembly. Held 2-10 August 2014, in Moscow, Russia, Abstract D1.4-6-14.
- [21] A.A.Petrukhin., “Muon puzzle in cosmic ray experiments and its possible solution.” *Nuclear Instruments and Methods in Physics Research A* , 228-231, 2014.
- [22] Gupta, S, “High Energy Astroparticle Physics at Ooty and the GRAPES-3 Experiment”, *Proc Indian Natn Sci Acad* , 80 No. 4, pp. 827-876, 2014.
- [23] Dayananda, M. A., “Correlation Studies of Cosmic Ray Flux and Atmospheric and Space Weather”. *ScholarWorks @ Georgia State University*, 2013.
- [24] B'en', S., “Air shower simulation for background estimation in muon tomography of volcanoes”. *Geosci. Instrum. Method. Data Syst* , 11-15, 2013.
- [25] Overholt, A. C. “A link between solar events and congenital malformations: Is ionizing radiation??”, 2015.
- [26] Cortes, M. L., BC404 scintillators as gamma locators studied via Geant4 simulations. *Journal of Instrumentation* , JINST 9 C05049, 2014.
- [27] Leo, W.R; (1994) Techniques for Nuclear and Particle Physics Experiments, Second Revised edition, Berlin Heidelberg: Springer-Verlag.
- [28] Glenn F. Knoll, “Light Collection in scintillation detector composites for neutron detection”, IEEE Transactions on Nuclear Science, Vol. 35, No. 1, February 1988
- [29] Data Sheet Manual, Quad 300 MHz Discriminator, Model 704, Phillips Scientific
- [30] Data Sheet Manual, Quad Four Fold Logic Unit, Model 756, Phillips Scientific

-
- [31] Data Sheet Manual, Quad Scaler Preset Counter and Timer, Model N1145, CAEN. Environmental Center”, *Advances in Space Research* 47 (2011) 1140–1146.
- [32] Mitrica, B., “A Mobile Detector for Muon Measurements Based on Two Different Techniques”. *Advances in High Energy Physics*, 1-7, 2013.
- [33] Yun Ho Kim, “Cosmic ray measurement and experimental temperature analysis with a muon detector”, *Journal of Korean Physical Society*, Vol. 64, No:4 August 2012, Pg:647-652.
- [34] Cecchini., “Atmospheric muons: experimental aspects”. *Geosci. Instrum. Method. Data Syst*, 185-196, 2012.
- [35] Riggi, S., “Muon tomography imaging algorithms for nuclear threat detection inside large volume containers with the Muon Portal detector”. *Nuclear Instruments and Methods in Physics Research A*, 59, 2013.
- [36] MAGHRABI., “Future Plans for Cosmic Ray Activities in Saudi Arabia”. *33RD INTERNATIONAL COSMIC RAY CONFERENCE*, 1-3, 2013.
- [37] Hofverberg, P, “Cosmic ray anisotropy studies with the Stockholm Educational 1-5, 2011.
- [38] A.Ollila, “Changes in cosmic ray fluxes improve correlation to global warming”, *International Journal of the Physical Sciences*, 822-826, 2012.
- [39] A. Dragic, “Measurement of cosmic ray muon flux in the Belgrade ground level and underground laboratories”, *Nuclear Instruments and Methods in Physics Research A* 591 (2008) 470–475.
- [40] A. Chilingarian, “Calculation of the barometric coefficients at the start of the 24th solar activity cycle for particle detectors of Aragats”, *Space*
-

Functional differential equations. 6: Quantum Mechanics

C. K. Raju

ckr@ckraju.net

(Submitted 29-03-2016)

Abstract

Reformulating classical physics using functional differential equations (FDEs) is of significant value in itself. But does it lead to quantum mechanics? Formally, the use of mixed-type FDEs leads to a structure of time, and thence to a quantum logic, and the postulates of quantum mechanics. Here, we give a simple and intuitive account of the structured time interpretation of quantum mechanics (STIQM), that quantum mechanics may be due to advanced interactions. We solve the modified Maxwell's equations in a linear approximation, for both retarded and advanced cases. The solutions show that a free electron oscillates under its own self-action. The oscillations are sustained because both damping and anti-damping are present even in the fully retarded case. Quantitative agreement with the de Broglie wavelength is possible with a simple extra hypothesis, though we do not examine it further here. A structure of time corresponds to many logical worlds, which we explain using the close analogy to parallel computing. With STIQM wave-particle duality does not present any conceptual difficulty. If quantum mechanics is indeed due to advanced interactions then a scalable quantum computer must necessarily be an android.

1 Recap

We have seen that if we do the math correctly, functional differential equations arise in the formulation of the two-body problem

of classical electrodynamics. It is invalid to approximate these by ODEs and PDEs as is commonly done, since FDEs lead to fundamental departures from expectations based on ODEs and PDEs.[1] Briefly, FDEs correspond

to a *coupled* systems of ODEs and PDEs. It is hazardous to neglect that coupling, even though it is commonly neglected in everyday physics.[2]

Next we saw that to do the classical hydrogen atom correctly we need to include the radiation reaction. But if we include radiation reaction, even the one body problem of electrodynamics cannot be solved since runaway solutions arise. This state of affairs too needs to be corrected. There is a way to fix those infinities by modifying Maxwell's equations at a microphysical level. (This is similar to the technique used to fix the infinities of quantum electrodynamics.) But this turns even the 1-body equations of motion, with radiation reaction, into FDEs.[3]

Further, FDEs are not restricted to electrodynamics. Compatibility with special relativity requires that Newton's "laws" of motion must be reformulated. But Newton's laws of motion and law of gravitation come as a package deal, so that even gravitation has to be reformulated in a Lorentz covariant way. This leads to the FDEs of retarded gravitation theory (RGT). RGT is theoretically better than Newtonian gravitation (since Lorentz covariant), and practically better than general relativity (since using it makes the many body problem for the galaxy tractable). Even if we accept dark matter as the reason for the failure of Newtonian physics for the galaxy, we must use RGT to calculate its extent, not Newtonian gravitation.[4]

Finally, the existing formulation of physics is not consistent with our everyday experience that *we* create a bit of the future. The easiest way to reformulate physics to allow for the

observed ability of living organisms to create some of the future is to allow advanced interactions, or a tilt in the arrow of time. This is not a new hypothesis, but just drops the usual hypothesis of causality. That leads to mixed-type FDEs.[5]

Thus, we have used FDEs for a series of corrections and "tweaks" which leads to a better mathematical formulation of classical electrodynamics, and gravitation, and to a physics more in accord with the mundane experience of both time asymmetry and creativity. That is of substantial value in itself. But will any of this lead to quantum mechanics?

Now the relation of mixed-type FDEs (MFDEs) to quantum mechanics was pointed out long ago[6] in what is called the structured-time interpretation of quantum mechanics (STIQM). However, that connection was established at a very abstract level, which is hard for most physicists. The present article aims to provide a simpler and more intuitive account of STIQM.

2 The base MFDEs

With the modified Maxwellian electrodynamics, retarded and advanced propagators are defined as before.[7] That is,

$$G_a(\mathbf{x}, \mathbf{y}) = \delta((\mathbf{x} - \mathbf{y})^2 + d^2)\theta(y^0 - x^0), \quad (1)$$

is the advanced Green function, while to obtain the field strength we now need to use the derivatives at advanced time instead of retarded time.

Mixed-type propagators are defined as a convex combination of retarded and advanced propagators

$$G_m = aG_a + (1 - a)G_r \quad 0 < a < 1, \quad (2)$$

so that for the fields we have

$$F_m = aF_{adv} + (1 - a)F_{ret} \quad 0 < a < 1. \quad (3)$$

With this expression for the field, the equations of motion of even a single classical charged particle are MFDEs.

2.1 The locally linear approximation

There are *no* general methods of solving this type of nonlinear MFDE. However, a simple way to obtain an approximate solution, called the locally linear approximation, was suggested long ago.¹ The idea is to approximate the nonlinear MFDE locally by an equation *of the same type*, a linear MFDE with constant coefficients and constant deviation of the argument.

To obtain this linear MFDE the coefficients are frozen in the neighbourhood of a particular point of time, as are the delay and advance. We know how to solve such linear MFDEs with constant coefficients and constant deviation of arguments. We then continue the solution by using this locally linear approximation in neighbourhoods around different

¹C. K. Raju, "Simulating a tilt in the arrow of time", paper presented at the seminar on "Some Aspects of Theoretical Physics", Indian Statistical Institute, Calcutta, 14–15 May 1996 (unpublished).

points of time, and patching together solutions at different times. This may not result in a globally continuous or unique solution, but that is not a requirement.

2.2 A linear approximation: retarded case

Let us start by explicitly working out this linear approximation in the retarded case. It is helpful to convert from proper time to coordinate time, and to use 3 vectors and a 3+1 decomposition.

A straightforward but tedious calculation gives for the electromagnetic field strength \mathbf{E}

$$\mathbf{E} = \frac{qc\tau}{4\pi\epsilon_0(c^2\tau - (\mathbf{v} \cdot \boldsymbol{\chi}))^3} \left(-\mathbf{a}(c^2\tau - (\mathbf{v} \cdot \boldsymbol{\chi})) + \mathbf{u}(c^2 - v^2 + \boldsymbol{\chi} \cdot \mathbf{a}) \right) \quad (4)$$

where \mathbf{v} , \mathbf{a} are the 3 vectors corresponding to velocity and acceleration respectively (both at retarded time), $(\tau, \boldsymbol{\chi}) = \zeta$ is the 3+1 decomposition of the retardation vector ζ . Further, $\mathbf{u} = \frac{1}{\tau}\boldsymbol{\chi} - \mathbf{v}$, is analogous to the vector defined in elementary texts [Griffiths]. However, recall that, unlike the Maxwellian case, ζ is no longer a null vector, since interaction takes place along a hyperboloid. Consequently, $\frac{1}{\tau}\boldsymbol{\chi} \neq \hat{\boldsymbol{\chi}}$. Instead, we now have

$$\chi^2 + d^2 = c^2\tau^2. \quad (5)$$

For the case of self-action, let us approximate the retardation 3-vector $\boldsymbol{\chi}$ as

$$\boldsymbol{\chi} \approx \mathbf{v}\tau. \quad (6)$$

This gives from (5) that

$$\tau = \gamma \frac{d}{c}. \quad (7)$$

Since $\boldsymbol{\chi} \approx \mathbf{v}\tau$ we actually have $\mathbf{u} \approx 0$ for the case of self action, and we can also use (6) to simplify the expression due to the dot product $\boldsymbol{\zeta} \cdot \dot{\boldsymbol{\alpha}}$

$$c^2\tau - \mathbf{v} \cdot \boldsymbol{\chi} = (c^2 - v^2)\tau \quad (8)$$

To derive our approximate linear equation, let us further neglect the force due to the magnetic field. The self-force on the charge due to the electric field is $\mathbf{F} = q\mathbf{E}$, and the equation of motion is

$$\ddot{\mathbf{x}} = \frac{q}{m}\mathbf{E} \quad (9)$$

Recalling that $\mathbf{u} = 0$ for the case of self-action, and recalling that we are neglecting the magnetic field in this approximation, the equation (9) reduces to the simple equation

$$\ddot{\mathbf{x}} = -k_r \mathbf{a} \quad (10)$$

where

$$k_r = \frac{q^2 c \tau}{4\pi\epsilon_0 m (c^2\tau - \mathbf{v} \cdot \boldsymbol{\chi})^2}. \quad (11)$$

Using (8), this simplifies to

$$\begin{aligned} k_r &= \frac{q^2 c}{4\pi\epsilon_0 m \tau (c^2 - v^2)^2} \\ &= \frac{q^2}{4\pi\epsilon_0 m c^3 \tau (1 - \frac{v^2}{c^2})^2} \end{aligned} \quad (12)$$

If the charged particle is an electron so that $m = m_e$, the last equation can be rewritten

$$\begin{aligned} k_r &= \frac{q^2}{4\pi\epsilon_0 m_e c^3 \tau (1 - \frac{v^2}{c^2})^2} \\ &= \frac{r_e}{c} \cdot \frac{1}{\tau} \cdot \gamma^4 \\ &= \frac{\tau_{\text{relax}}}{\tau} \gamma^4 \\ &= \frac{r_e}{d} \gamma^3, \end{aligned} \quad (13)$$

where $r_e = \frac{q^2}{4\pi\epsilon_0 m_e c^2}$ is the classical radius of the electron, $\tau_{\text{relax}} = \frac{r_e}{c}$ is the so-called relaxation time of the electron (time taken by light to travel across the classical electron radius), and d is the separation parameter in the modified Maxwell equations. If $d \approx r_e$, we have $k_r \approx 1$.

3 Oscillatory solutions

For our immediate purpose, we can, without loss of generality, further simplify the above equation to an equation in a single dimension (so that x is a scalar, not a vector). (There is no loss of generality because in the vector case we simply apply the following reasoning to each component of the vector.)

To begin with, since $k_r \approx 1$, we set $k_r = 1$, in (10) and solve the simple equation

$$\ddot{x} = -\ddot{x}(t - \tau) \quad (14)$$

We look for pure imaginary roots of the characteristic quasi-polynomial. That is, we substitute $x = e^{\omega t}$ in (14), to obtain

$$-\omega^2 x = \omega^2 x e^{-\omega\tau}. \quad (15)$$

Cancelling $\omega^2 x$ from both sides, we see that we are seeking a solution of

$$e^{-i\omega\tau} = -1. \quad (16)$$

Such a solution is easily found. Taking real and imaginary parts we see that we need the simultaneous solution of

$$\begin{aligned} \cos \omega\tau &= -1, \\ \sin \omega\tau &= 0. \end{aligned} \quad (17)$$

The solution is evidently given by

$$\begin{aligned} \omega\tau &= \pi + 2n\pi, \quad n = 0, \pm 1, \pm 2, \dots \\ &= (2n + 1)\pi, \quad n = 0, \pm 1, \pm 2, \dots \end{aligned} \quad (18)$$

In general, this equation has an infinity of roots. Each pure imaginary root corresponds to an undamped oscillatory motion of the particle. Thus, the solution of (14) is

$$\begin{aligned} x(t) &= e^{i\omega t} \\ \omega &= (2n + 1)\frac{\pi}{\tau}, \quad n = 0, \pm 1, \pm 2, \dots \end{aligned} \quad (19)$$

Thus, we see that a single free charged particle will, under its own self-action, oscillate. While there is no rest frame for such a particle, we may consider as a “zero” frame a frame where the particle does not drift off, and has zero average velocity. As seen from a frame which it is moving with respect to the zero frame, so that the particle has an average velocity V , the particle will correspond to a travelling wave, say,

$$x = Vt + A \sin(\omega t). \quad (20)$$

However, for the wavelength λ of such a travelling wave we will have

$$\lambda = VT, \quad (21)$$

where $T = \frac{2\pi}{\omega}$ is the time period of the sinusoidal oscillation. Since $T \propto \tau = \frac{\gamma d}{c}$, we see that quantitative agreement with the de Broglie formula requires an additional hypothesis

$$d \propto \frac{1}{E}, \quad (22)$$

where E is the average energy, and we neglect the γ factor, for simplicity. For a free particle $E = \frac{1}{2}mV^2$, so, with this hypothesis, from (21) we get

$$\lambda \propto \frac{1}{mV}. \quad (23)$$

Now the parameter d is not specified by the theory. Roughly speaking, it relates to the “interior” of the electron, where anything at all might happen. The above hypothesis about it looks simple enough. Nevertheless, any attempt to justify it would bring in ramifications far beyond the scope of this article, which aims to give a simple and intuitive account of the structured-time interpretation of quantum mechanics (STIQM). Therefore, for the purposes of this article let us proceed with qualitative agreement alone: some sort of oscillatory or wave motion is naturally associated with a free charged particle.

Note that we have an infinite (discrete) spectrum of possible frequencies *in classical physics*. That is obviously not possible in classical *mechanics* or with ODEs. If we were to do the same for a system of ODEs, no matter how many particles are involved, we would end up with a polynomial with a finite number of roots, never a quasi polynomial with an infinity of roots. On the theory of Fourier series, this means that we are not restricted

to sinusoidal oscillations, and can have any general period function.

4 Damping and anti-damping

The significance of pure imaginary roots of the characteristic quasi-polynomial is that pure imaginary roots correspond to stable or undamped oscillations. However, in arriving at the simplified equation (14) above we assumed that $k_r = 1$, although from the last of the equations (13) it is clear that that can never *exactly* be the case.

So, let us go to the next level of complexity, and solve the equation after putting back the value of k_r but supposing it to be a constant, possibly different from 1. That is, we solve the equation

$$\ddot{x} = -k_r \ddot{x}(t - \tau), \quad (24)$$

obtained by neglecting just the magnetic field, and treating k_r as a constant.

We now take as a trial solution

$$\begin{aligned} x &= e^{zt}, \quad \text{where} \\ z &= u + i\omega. \end{aligned} \quad (25)$$

Substituting in (24), and cancelling $z^2 e^{zt}$ as before, we are led to the characteristic quasi-polynomial equation

$$e^{-z\tau} = -\frac{1}{k_r}, \quad (26)$$

in place of (16). Equating real and imaginary parts as before, we arrive at

$$e^{-u\tau} \cos \omega\tau = -\frac{1}{k_r}, \quad (27)$$

$$\sin \omega\tau = 0. \quad (28)$$

in place of (17). This can be solved by choosing ω as before as a solution of (17) and choosing u as the solution of

$$e^{-u\tau} = \frac{1}{k_r}. \quad (29)$$

That is,

$$u = \frac{1}{\tau} \log k_r \quad (30)$$

Thus, the solution of (24) is given by

$$x(t) = e^{ut} \cdot e^{i\omega t} \quad (31)$$

with ω as before given by (18) and u given by (30).

Thus, we now have oscillations which are damped *or* anti-damped by a factor of e^{ut} where $u = \frac{1}{\tau} \log k_r$. Damping holds if $u < 0$, or $k_r < 1$, that is, for large values of d or τ ($d > \gamma^3 r_e$ or $\tau > \gamma^4 \tau_{\text{relax}}$). If the reverse inequality holds ($k_r > 1$), that is for small values of d or τ ($d < \gamma^3 r_e$ or $\tau < \gamma^4 \tau_{\text{relax}}$) we will have anti-damping. This should be noted, because on intuition built on classical mechanics there is no possibility of anti-damping with purely retarded radiation.

In particular as $d \rightarrow 0$, it is anti-damping which prevails, and we recover the runaway solutions as in the theory with point masses. That is, the method of deriving radiation reaction by a limiting procedure is not valid, because in the process of taking the limit there is an unexpected switch from damping to anti-damping.

4.1 Self-excited oscillations

The existence of both damping and anti-damping raises the possibility of self-excited oscillations. Indeed, $k_r = \frac{r_e}{d} \gamma^3$, is velocity dependent. For constant $\frac{r_e}{d}$, as $v \rightarrow c$ we have $\gamma \rightarrow \infty$, so k_r will increase, and anti-damping will set in. In an oscillatory motion, v will decrease and become zero. During this time, we have $\gamma \rightarrow 1$, so if $\frac{r_e}{d} < 1$, damping will set in. *Thus, both damping and anti-damping may be present in the course of a single oscillation.*

What will be the effect of this? We cannot write down a formula for this case, where the damping factor is velocity dependent, but the numerical solution is given below. The solution is stable, or at least semi-stable, corroborating the possibility of self-excited oscillations, though the frequency of the oscillation is no longer given exactly by (17).

Thirdly, even $\tau = \frac{\gamma d}{c}$ is γ dependent. So long as the values of v are small relative to c this does not seem to make much of a difference, and the numerical solution remains almost the same.

Thus, on classical physics (with FDEs) an electron is not just a mass point which sits idly waiting for an external force to move it as in Newtonian mechanics. Under its own retarded self-action it undergoes a rapid self-excited oscillation, during which its momentum and energy also vary, though there is no net loss or gain of energy due to radiation.

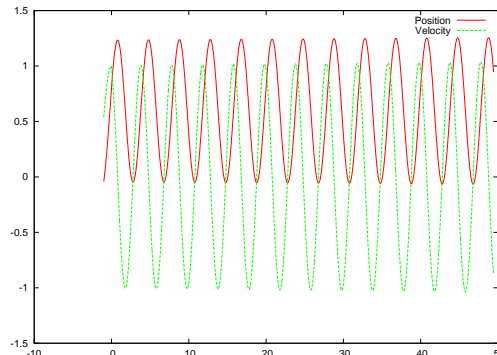


Figure 1: Solution of the retarded equation (24) with the velocity dependence of k_r and τ taken into account. The x -axis is time in units of τ_{relax} (deci-yocto seconds). The y -axis does double duty. For velocity it is in units of $\frac{c}{30}$ (or $\frac{c}{300}$) dfm/dys, for position it is in corresponding units of distance (deci-femto meters).

4.2 The equations of motion for self-action: mixed case

We now take up the mixed-type case, where the propagator is a convex combination of advanced and retarded propagators. Working exactly as above, we arrive at the approximate equations of motion for a charged particle as,

$$\ddot{x} = ak_r \ddot{x}(t + \tau) - bk_r \ddot{x}(t - \tau), \quad a + b = 1, \quad (32)$$

where the weight of the advanced component $a \ll 1$, so that the weight of the retarded component $b \approx 1$. To solve this equation, assuming k_r constant, we proceed as before and take as a trial solution $x = e^{zt}$, with $z = u + i\omega$. Substituting in (32), and cancelling $z^2 e^{zt}$ as

before, we are now led to the characteristic quasi-polynomial equation

$$1 = ak_r e^{z\tau} - bk_r e^{-z\tau}. \quad (33)$$

Taking real and imaginary parts as before, we now obtain

$$ak_r e^{u\tau} \cos \omega\tau - bk_r e^{-u\tau} \cos \omega\tau = 1 \quad (34)$$

$$ak_r e^{u\tau} \sin \omega\tau + bk_r e^{u\tau} \sin \omega\tau = 0. \quad (35)$$

If ω is a solution of (17), then $\sin \omega\tau = 0$ so the equation (35) is satisfied, and, since $\cos \omega\tau = -1$, (34) reduces to

$$ae^{u\tau} - be^{-u\tau} = -\frac{1}{k_r}. \quad (36)$$

This can be solved by setting $y = e^{-u\tau}$ so that $u = -\frac{1}{\tau} \log y$. This leads to the quadratic equation

$$\frac{-1}{k_r} = \frac{a}{y} - by \quad (37)$$

Explicitly the quadratic is $by^2 - \frac{1}{k_r}y - a = 0$ and this has the solution

$$y = \frac{1 \pm \sqrt{1 + 4abk_r^2}}{2bk_r}. \quad (38)$$

We need a positive root since we need the log of y . Approximately, this is given by

$$y \approx \frac{2}{2bk_r} + \frac{2abk_r^2}{2bk_r}, \quad (39)$$

so that

$$y \approx \frac{1}{bk_r} + ak_r. \quad (40)$$

Since $b \approx 1$ we have as before $y \gtrsim 1$ almost according as $k_r \gtrsim 1$. Thus, the solution in the mixed-type case is

$$x(t) = e^{ut} \cdot e^{\omega t} \quad (41)$$

with ω as before given by (18) and $u = -\frac{1}{\tau} \log y$ with y given by (40).

However, in this case there is one more solution. We can choose $\cos(\omega\tau) = 1$ in (34), so that $\omega = \frac{2n\pi}{\tau}$. In this case, instead of (36) we have the equation

$$ae^{u\tau} - be^{-u\tau} = \frac{1}{k_r}. \quad (42)$$

With y defined as before by $y = e^{-u\tau}$ we now get the quadratic $by^2 + \frac{1}{k_r}y - a = 0$, which has the solution

$$y = \frac{-1 \pm \sqrt{1 + 4abk_r^2}}{2bk_r}. \quad (43)$$

Further analysis shows that this solution is unstable since permanently anti-damped (unless some assumptions fail), hence we discard it.

5 STIQM

That brings us to a very fundamental issue, at the core of STIQM.[6] The difference between MFDEs and retarded FDEs is not just a matter of slightly differing rates of damping. With MFDEs past does not determine future. Indeed, the existence of advanced interactions allows the future to communicate with the past, so that even the past is not fully determinate. However, since advanced interactions are rare, the indeterminacy of the past is very small compared to that of the future.

The question now is this: how does one *model* such indeterminacy? A structure of

time helps us to model indeterminacy. In Newtonian mechanics a dynamical variable has a definite value at one instant of time. A structure of time means that it may have more than one value at one instant of time.

Because the structure of time in STIQM arises from the use of MFDEs with only a tiny advanced component, a retarded FDE model still remains a good first approximation. The world is still approximately deterministic, and the indeterminacy relates typically to a microphysical level. That is, STIQM involves a *microphysical structure of time*. We can expect advanced effects to be most readily manifest at the level of single particles.

It may seem illogical to say of a dynamical variable that $q = 3$ is true, and also that $q = 4$ is true, but logic itself depends on the nature and structure of time.[8] A change in logic is a key *required* feature in modeling the indeterminacy of qm; it is well-known that the logic obeyed by quantum mechanics is not Boolean like 2-valued logic.

In terms of probabilities, quantum probabilities are different from classical probabilities, just because quantum probabilities are defined on a different logic, and *hence* do not admit a joint probability distribution of canonically conjugate variables. In the von-Neumann formulation of qm, the representation of dynamical variables by operators may be understood as relating to random variables as measurable functions defined on the non-Boolean lattice or logic of subspaces of a Hilbert space, also called a quantum logic.

The temporal logic corresponding to a structured time is neither 2-valued, nor 3-valued; it is quasi truth-functional. That is we cannot

always assign a truth value to the statement $q = 3$. A subtle but important point here is that this is NOT the same thing as saying that $q = 3$ has the truth value “indeterminate”, as in, say Lukasiewicz’s 3-valued logic.[6, chp. 1] In that 3-valued logic, the logical connectives remain functions of the 3 truth values; that is no longer the case with quasi truth-functional logic.

Roughly speaking, in 3-valued logic we assign *neither* truth value (true, false) to a proposition; in quasi truth-functional logic we may assign *both* truth values (at one “instant” of time). It is not the case that Schrödinger’s cat is either alive or dead, and we don’t know which is the case; rather it is the case that Schrödinger’s cat is both alive and dead (at one “instant” of time). The 3-valued logic used by Reichenbach[9] or Kothari[10] does not lead to a valid interpretation of qm. A key result of STIQM, however, is this: a quasi truth-functional logic is a quantum logic. Though this result is formally proved only in the book[6], and not in the related series of articles in this journal, let us try to understand it here in simple intuitive terms.

As already noted, the key aspect of quantum probabilities is that joint probability distributions do not exist for canonically conjugate variables. This is mathematically linked to the non-commutativity of operators, with dynamical variable defined as random variables, with probability defined on the lattice of subspaces of a separable Hilbert space instead of a usual Boolean algebra. The key requisite feature of the lattice of projections on a Hilbert space is that the distributive law of “and” over “or” fails.

Let us try to understand this in simple and intuitive terms. Consider a two slit experiment with two slits A and B . Consider the two propositions:

1. The electron reached the screen AND passed through slit A OR the electron reached the screen AND passed through slit B.
2. The electron reached the screen AND passed through slit A OR slit B

The two statements are equivalent on a Boolean logic. However, they are *physically* different, since in the first case one observes a mixture of two gaussians, and in the second case one observes an interference pattern. Hence, the distributive law fails, and a quantum logic must be non-Boolean.

The lattice of projections on a Hilbert space is such a non-distributive lattice. If P_1 and P_2 are two projection on subspaces S_1 and S_2 respectively, we define $P_1 \wedge P_2$ as the projection on the intersection $S_1 \cap S_2$, and $P_1 \vee P_2$ as the projection on the span of $S_1 \cup S_2$. If P_x and P_y and P_{xy} are projections on the x -axis, y -axis and the line $x = y$ respectively, then $(P_{xy} \wedge P_x) \vee (P_{xy} \wedge P_y) = 0$, whereas $P_{xy} \wedge (P_x \vee P_y) = P_{xy}$, so that “and” (\wedge) is not distributive over “or” (\vee).

The explanation of non-distributivity with quasi truth-functional logic is much easier to understand. The two statements above are not equivalent because the OR in proposition 1 is exclusive, while the OR in proposition 2 is inclusive. That is, we allow for the possibility that the electron passed through both slits. The electron is a particle, it did not divide

into two halves like a wave; but it is time which split into two threads to allow for both possibilities simultaneously.

The formal mathematical way to make a quasi truth-functional logic meaningful is to interpret it in terms of logical (2-valued) “worlds”. A logical world, in the sense of Wittgenstein, is “all that is the case”. That is, a logical world corresponds to an assignment of binary truth values “true” or “false” to any proposition. This understanding of the word “world” must be clearly distinguished from the loose way in which the word “world” is used in, say, the many-worlds interpretation of quantum mechanics. In STIQM, there is only one physical world. Multiple logical worlds are just a semantic device we use to make its description easily comprehensible in natural languages. In particular, these logical worlds may interact with one another.

Parallel computers provide a concrete model of the use of quasi truth-functional logic. The parallel computer is analogous to the single physical world we have. It, however, consists of multiple processing units, each of which runs a sequential execution “thread” or sequential process,[11] and thus each processor constitutes a logical world. These worlds interact with one another. Each execution thread itself is a thread or branch of structured time. Now suppose we want to debug a parallel program, and break its execution. This would give us the “state” of the physical world at one “instant”. However, it is perfectly possible that we find Schrödinger’s cat is alive in one processor, and dead in another, there is no paradox in that. A quasi truth-

functional logic is needed to understand such debugging.[12]

When the STIQM was developed, almost a quarter century ago, parallel computing was in its infancy, and OCCAM was being used as the language of parallel computing, since there was nothing much then by way of parallel Fortran or parallel C. An example computer program in OCCAM illustrating the above considerations (and using the indeterministic ALT construct of OCCAM) is given in [6].

5.1 Two sources of uncertainty

Thus, the use of FDEs brings in *two* novel sources of uncertainty. First, unlike the case in Newtonian mechanics, a particle such as an electron does not stay at rest. Even with purely retarded FDEs, and under its own self-action the particle oscillates. As such its position and momentum are not fixed, but are constantly varying.

Secondly, with MFDEs the future, and even the present and past really are uncertain at the microphysical level. This corresponds to a microphysical structure of time. While this situation can be described as multiple parallel “worlds”, in STIQM, unlike the many-worlds interpretation, these are only parallel *logical* worlds. There is only one physical world, as in one computer performing concurrent computation.

Note that the existence of these parallel worlds follows from classical physics done correctly, by addressing problems neglected over the last century.

5.2 Wave particle duality

An interesting feature emerges when we combine both sources of uncertainty, or both the features of (a) an oscillating particle which (b) exists in multiple sub-threads of time.

Consider again the classical two-slit experiment with an electron. If the electron behaves as a free particle *before* the slits, then there are two sub-threads of time, one in which the electron comes from slit *A* and another in which it comes from slit *B*. These multiple past possibilities will reflect in multiple future solutions between the slits and screen. It is clear that the two solutions will, in general, travel different distances to reach a given point on the screen. Accordingly, there will be a phase difference between the two oscillations. Since there is only one physical world, what we will observe is a superposition of the two oscillations corresponding to the two sub-threads. Since both solutions concern one and the same electron, this is a *coherent* superposition. Accordingly, we will see an interference pattern.

If, however, we observe which slit an electron goes through (delayed choice is irrelevant) then we destroy the possibility that the electron goes through both slits. That is, we change the past data. Consequently, the solution changes also between the slits and the screen. (Note that STIQM is explicitly non-local, since it is all about advanced effects, and it is not a hidden-variable theory, since the uncertainties in it cannot be eliminated, as the very notion of a structure of time indicates.[6, chp. 6a])

Thus, with a structure of time obtained through the use of MFDEs, wave particle duality does not present any *conceptual* problem. What about quantitative agreement? Will the observed interference pattern correspond to the de Broglie wavelength? To reiterate the answer above, such quantitative agreement can be obtained by supposing that (22) of some equivalent hypothesis holds. But justifying that very simple hypothesis involves ramifications beyond the scope of this article.

6 Schrödinger equation

It has long been known that, using Koopman's formalism, the representation of dynamical variables by operators on a Hilbert space can also be used in classical statistical mechanics. The critical issue related to qm is the non-commutativity of the operators. That, as explained above, connects to a change of logic, which may be understood using the STIQM.

But what about Schrödinger's equation? Now Schrödinger's equation gives us unitary evolution in Hilbert space; this is possible even with Koopman's formalism. Further, Schrödinger's equation holds only in equilibrium, and as pointed out in my first interpretation of quantum mechanics[13] unitary evolution is equivalent to stationarity which corresponds to equilibrium or indifference to the origin of time. Either way, unitary evolution in Hilbert space does not by itself present any fundamental difficulty.

The critical issue is about the Hamiltonian, or the infinitesimal generator of the unitary group. Why is the quantum Hamiltonian the

same function of the dynamical variables as the classical Hamiltonian (when the latter exists)? This indicates that qm and classical physics are not just two different theories; they are closely connected. We will not go further into this question here, except to point out that the STIQM is the best way currently available to connect classical physics to quantum physics.

7 Concluding remarks

Classical physics done correctly, i.e., with MFDEs, exhibits many of the most puzzling conceptual features of quantum mechanics. Those puzzling features are the expected consequences of the existence of advanced interactions.

We emphasize that we have not *derived* qm from classical physics, nor was such derivation ever a goal. At the least some extra phenomenology will be required to obtain the Planck constant or the fine structure constant to obtain quantitative agreement.

We do not claim to have derived qm from classical physics also since classical physics with MFDE's is *not* identical to qm. It is a self-contained theory with many of the features of qm, but distinct from qm. Thus, with MFDEs non-locality central: the theory can be tested by testing for the existence of advanced interactions.

Nevertheless, the understanding acquired above, that key features of qm can be explained as advanced "effects", is important for the technology of quantum computing, considered vital to the future. The key current

problem with that technology is the problem of decoherence or the inability to scale up a quantum computer.

The speed-up provided by a quantum computer is due to parallelism, which on the above understanding relates to a structure of time. And that, according to STIQM is due to advanced effects. So, is there a way to scale up tiny advanced effects to some reasonable macrophysical level? Living organisms (and only living organisms) seem to be able to do that. We do not today understand how that happens. For such understanding we would, at the least, need to simulate the interactions of biological macromolecules using MFDEs in place of the ODEs as is done today.

However, on the structured-time interpretation of quantum mechanics, we can safely conclude that scaling advanced effects would necessarily involve living organisms. (Recall that time travel is *impossible* with machines.[5]) Hence, a (scalable) quantum computer would necessarily be an android (not as in the popular operating system, but as in half-live, half-machine); it would involve at least biological macromolecules.

References

- [1] C. K. Raju. Functional differential equations. 1: A new paradigm in physics. *Physics Education (India)*, 29(3), July-Sep 2013. <http://physedu.in/uploads/publication/11/200/29.3.1FDEs-in-physics-part-1.pdf>.
- [2] C. K. Raju. Functional differential equations. 2: The classical hydrogen atom. *Physics Education (India)*, 29(3), July-Sep 2013. <http://physedu.in/uploads/publication/11/201/29.3.2FDEs-in-physics-part-2.pdf>.
- [3] C. K. Raju. Functional differential equations. 3: Radiative damping. *Physics Education (India)*, 30(3), July-Sep 2014. <http://www.physedu.in/uploads/publication/15/263/7.-Functional-differential-equations.pdf>.
- [4] C. K. Raju. Functional differential equations-4. retarded gravitation. *Physics Education*, 31(2), April-June 2015. [http://www.physedu.in/uploads/publication/19/309/1-Functional-differential-equations-4-Retarded-gravitation-\(2\).pdf](http://www.physedu.in/uploads/publication/19/309/1-Functional-differential-equations-4-Retarded-gravitation-(2).pdf).
- [5] C. K. Raju. Functional differential equations. 5: Time-travel and life. *Physics Education (India)*, 31(4), Oct-Dec 2015.
- [6] C. K. Raju. *Time: Towards a Consistent Theory*, volume 65 of *Fundamental Theories of Physics*. Kluwer Academic, Dordrecht, 1994.
- [7] C. K. Raju. On a method of solving mixed-type functional differential equations. In *Proc. PIERS (Progress in Electromagnetics Research)*, Stockholm, 2013.
- [8] N. Rescher and A. Urquhart. *Temporal Logic*. Springer, 1971.

- [9] H. Reichenbach. *Philosophic Foundations of Quantum Mechanics*. Dover, 1998.
- [10] D. S. Kothari. *Theoretical Fundamentals of Natural Science*, chapter Modern Physics and Syadavada, Appendix IV D, pages 441–48. Firma KLM, Calcutta, 1991.
- [11] C. A. R. Hoare. *Communicating Sequential Processes*. Prentice Hall, 1985.
- [12] K. R. Apt, editor. *Logics and Models of Concurrent Systems*. Springer, 1984.
- [13] C. K. Raju. Interpretation of quantum mechanics as a theory of extended particles. *Int. J. Theor. Phys.*, 20:681–96, 1981.

ANNOUNCEMENT

Gravitational Waves Detected
Laser Interferometric Gravitational Observatory
 GW150914 Event

A animation video for Non-experts
 by
Arvind Gupta Toys, IUCAA, Pune 411007

Abstract

The **first observation of gravitational waves** occurred on 14 September 2015 and was announced by the [LIGO](#) and [Virgo](#) collaborations on 11 February 2016. Previously, gravitational waves had been inferred only indirectly, by observing the decay in the orbit of binary pulsar star systems because of energy loss from gravitational waves. The [waveform](#), detected by both LIGO observatories, matched the predictions of [general relativity](#) for a [gravitational wave](#) emanating from the [inward spiral](#) and [merger](#) of a [pair of black holes](#) of around 36 and 29 [solar masses](#) and the subsequent "ringdown" of the single resulting black hole. The signal was named **GW150914** (from "Gravitational Wave" and the date of observation).

wikipedia

400 years after Galileo's first telescope we are on the verge of new way of looking at space, which will open new frontiers in Astronomy. This will be achieved through the observations of Gravitational-waves (GW), predicted by one of the most revolutionary theories in physical sciences, Einstein's General theory of Relativity, proposed 100 years ago. In this film, we will introduce the basic idea, current developments and highlight the contributions made by Indian scientists. In March, 1944 Einstein had humorously quipped, "Why is it that nobody understands me, yet everybody likes me?". The domain of General Relativity is complex and esoteric however this has become so pedantic that it is literally in the hands of 2.6 billion people in form of smart phones.

Consider the following analogy. Throw a lighter ball at a fast speed- it will roll around the heavier ball due to the curvature in the fabric the latter induced. Analogously, this is why the earth goes in a curved orbit around the sun because according to Einstein's general relativity, the sun curves the space-time around itself. The stretched sheet is 4-dimensional space time fabric of the universe and gravity is the manifestation of curvature of space-time.

If two black holes collide or large twin stars circle around each other, then they would radiate GW which are strong enough to be measured. And by measuring these waves we could see what no man or woman has seen before. Even these "strong" gravitational waves would require extremely sophisticated instruments capable of measuring tiny displacements of test masses to the tune of 10^{-18} m which is much smaller than the size of an atomic nucleus. The GW signal recorded in these instruments is very feeble and is drowned in the detector noise. Seismic noise, Airplanes flying by, traffic noise, even the school band playing nearby can corrupt the data. So to detect and extract just the GW signal from the noisy data, we also need really smart algorithms or methods which can extract the pure Gravitational Wave from the noisy data. This is where Indian scientists figure in. The basic method to detect and extract the in-spiralling binary GW signal from detector data was developed by a team of scientists at IUCAA and is now used universally across the world. Extraction process requires very accurate phase information of the wave which was done by scientists at Raman Research Institute. Indian scientists have made many other significant contributions in gravitational wave research. We list some these below:

1. Developing an understanding of Black

- Holes, their event horizons, their ring down modes or quasi-normal modes.
2. Data analysis strategies to detect and measure GWs from other type of astrophysical sources, such as periodic, stochastic, etc.
 3. Identifying and mitigating instrumental glitches.
 4. Following up potential GW events with electromagnetic telescopes such as optical etc.

We have just detected a candidate GW event with the LIGO detectors of the US. These are laser interferometric detectors placed 2000 miles apart in the US. But the Holy Grail in Gravitational waves is not only to detect a GW but to also locate the astrophysical source of the wave in the sky. Now to accurately locate the source of the wave in the sky, we need to have another detector as far away as possible from existing detectors. By detecting the same wave from three detectors, geographically well separated, we can triangulate the location of the GW source in the sky with far better accuracy. This is very important for the electromagnetic follow up of the GW source, using either optical or other electromagnetic telescopes. India is on the other side of the world in relation to the US. So if we build a LIGO type detector in India we will be able to enormously improve the accuracy of finding the GW source. The improvement can be as large

as an order or two orders of magnitude!

Currently, we are at a very interesting phase in Astronomy where India can play a major role. With some of the most fundamental research in Gravitational Waves, General Relativity supporting us and the geographical advantage of being farthest from existing detectors, we take a lead and pave the way for many fundamental discoveries in our understanding of cosmos and testing basic scientific theories. We hope to get started soon on this massive LIGO-India project in India which will provide a platform for many scientists and youngsters to collaborate together in our quest for beyond.

Story and Animation: Manish Jain, Nidhi Gupta
This work is supported by IUCAA (www.iucaa.in) and TATA Trust
(www.tata.com/aboutus/sub_index/Tata-trusts)

Credits: Ashok Rupner, Manish Jain, Pradnya Pujari, Shivaji Mane, Jyoti Hiremath, Arvind Gupta, Vidula Mhaskar

A brief animation video describing the discovery. Ctrl+Click below to a link for a 7.25 minutes video <https://youtu.be/kM6eVWWFVrM> and other videos on the subject.